UNIVERSITÀ
DEGLI STUDI
FIRENZE

Dottorato di Ricerca in
Ingegneria Industriale

Ciclo XXIX

Radiometric measurements for assessing the performances of high-temperature solar absorbers

Settore Scientifico Disciplinare: ING-IND/09

Dottorando

Dott. Marco Meucci

Tutore

Prof. Maurizio De Lucia

Co-Tutore

Dott. Luca Mercatelli

Co-Tutore

Dott.ssa Elisa Sani

Coordinatore

Prof. Maurizio De Lucia

Anni 2013-2016

Contents

Acronyms (alphabetic order)

BP: bicolor pyroreflectometry

CSP-PT: Concentrating Solar Power, Parabolic Through

CSP-F: Concentrating Solar Power, Linear Fresnel

CSP-T: Concentrating Solar Power, Tower

CSP-D: Concentrating Solar Power, Dish

CVD: Chemical vapor deposition

DIEF: Dipartimento di Energetica, Università di Firenze

FTIR: Fourier Transform InfraRed

HIP: Hot Isostatic Pressing

HP: Hot Pressing

INO-CNR: Istituto Nazionale di Ottica, Consiglio Nazionale delle Ricerche

IR: InfraRed

ISTEC: Institute of science and technology of ceramic materials

MEDIASE: Moyen d'Essai et Diagnostic en Ambiance Spatiale Extreme

MS: Microwave Sintering

NIR: Near Infra-Red

NIST: National Institute of Standards and Technology

PROMES-CNRS: PROcedes, Materiaux et Energie Solaire- Centre National de la Recherche Scientifique, France

PS: Pressureless sintering

PV: PhotoVoltaics

PVD: Plasma or Vapor Deposition techniques

RS: Reaction sintering

RSPS: Reacting Spark Plasma Sintering

UHTCs: Ultra-High Temperature Ceramics

UNICA: Università degli studi di Cagliari

UV: Ultra-Violet

UVA, UVB, UVC: Ultra Violet A, B, and C

SEM-EDS: Scanning Electron Microscopy, Energy Dispersive x-ray Spectrometry

SOFCs: Solid oxide fuel cells

SHS: Self-propagating High-temperature Synthesis

SPS: Spark Plasma Sintering

TPV: Thermo-Photovoltaic

VIS: Visible

List of symbols

h: Plank constant

c: velocity of light

λ: wavelength

Ω: solid angle

T: temperature

b: Wien's displacement constant

k: Boltzmann constant

σ: Stefan-Boltzmann constant

ε: emissivity / emittance

α: absorptance

ρ: reflectance

τ: transmittance

α_{int}: integrated absorptance

$\mathcal{E}_{int}$: integrated emittance

$S_{1.5}(\lambda)$: solar irradiance spectrum AM1.5

L(λ): spectral radiance

M(λ): spectral radiant excitance

Activity

This thesis has been conducted at the National Institute of Optics of CNR (INO-CNR) in collaboration with the Industrial Engineering Department.

The fundamental part of the 3 PhD years has involved the construction of the new SOLAR-LAB laboratory, aimed at the characterization of materials, especially regarding the solar energy exploitation.

The laboratory realization has been funded by “Ente cassa di risparmio di Firenze” (SOLE Project) and the Italian Ministry of University and Research (FIRB project).

The aim of the new laboratory is to study the optical properties of new materials: solid, liquid, thin films and nanostructures, mainly aimed to applications in solar energy. Transmittance, reflectance, spectral fluorescence, thermal emissivity and absorption are the main physical quantities that can be investigated. The available scientific instruments allow spectral analysis of materials over an extremely wide range of wavelengths, in the ultraviolet, visible, near, mid and far infrared, corresponding to a spectral range from 200 to 50000 nm (50000-200 cm-1).

During the PhD years I took part in the three lines of research followed by the laboratory, especially the design and development of a new apparatus aimed to measure the spectral emissivity of materials as a function of temperature up to 1000 °C.

The three lines of research are:

1) **Solar absorbers for high-temperature thermal power generation**
2) **Innovative fluids as direct solar absorbers in Concentrating Solar Power**
3) **Wavelength converters for photovoltaic cells**

1) Solar absorbers for high-temperature thermal power generation: Absorption characteristics and spectral emissivity of bulk absorbers in Solar Power Tower Plants

CSP-T consist of a series of mobile mirrors (heliostats), which concentrate the solar radiation on the top of a tower where a receiver is placed [Ref. (1)]. This latter accumulates the solar radiation in the form of thermal energy. Then the heat stored by the receiver is converted into electrical energy by a proper system of energy conversion.

One of the main problems associated with a large-scale development of such systems is related to their low efficiency, mainly due to the receiver. In fact, at present the temperature reached by the receiver is not higher than 400 °C ~ 600 °C, because of problems of mechanical strength and chemical stability at higher temperature.

Thus to increase the efficiency of this kind of systems, finding new and better materials for the receiver is mandatory. They have to show high refractoriness to be able to operate at very high temperatures and a series of favorable characteristics such as high mechanical strength, good chemical stability, high thermal conductivity and a good spectral selectivity. This latter property

allows the receiver to absorb most of sunlight, showing at the same time low heat losses due to re-radiation at the operating temperature.

Therefore, the development of potential materials to be used as solar absorbers critically depends on a careful characterization of their surface optical properties and on the study of the thermal emittance at the operating temperature.

Materials belonging to the family of UHTCs, e.g. carbides, nitrides and borides of zirconium, hafnium and tantalum, have better characteristics than those of the materials currently used for solar absorbers, as i.e. Silicon Carbide.

2) Innovative fluids as direct solar absorbers in Concentrating Solar Power: Nanofluids for Solar Parabolic Troughs

The optimization of the characteristics of fluids used in CSP-PT [Ref. (1)] is one of the main activities of the Laboratory.

CSP-PT is formed by linear parabolic mirrors oriented north-south, which rotate from east to west depending on the position of the sun. In conventional systems, mirrors concentrate the solar radiation on a blackened tube, which absorbs the sunlight and transfers the heat to a heat exchange fluid flowing within the tube.

To overcome some efficiency and cost limitations of this kind of architectures, it has been proposed to use a direct solar absorber fluid [Ref.(2)(3)(4)(5)(6)]. It is a dark fluid which flows inside a transparent tube and, at the same time, works as solar absorber and heat exchange medium.

This fluid receiver must have a high absorption of solar radiation and a high thermal capacity and thermal conductivity to help heat exchange at the following stages of the solar plant.

Solids typically have thermal conductivity which is orders of magnitude higher than that of liquids. Thus the idea is to add a certain amount of solid particles to a liquid base, to improve thermal conductivity and thermal capacity of fluid, as well as to give good sunlight absorption properties to the resulting suspension.

The literature reports on the study in the past of organic inks. However, these had serious drawbacks due to thermal degradation at operating temperatures. Recently, the laboratory has been studying the so-called "nanofluids" (i.e. fluids with nanosized particles in suspension); in particular, the activity has been mainly focused on a new type of carbon nanoparticles, i.e. carbon nanohorns, which roughly are spheroidal agglomerates of nanometer-sized cones made by wrapped graphene sheets. Carbon nanohorns belong to the family of better-known carbon nanotubes, and they have very favorable characteristics over them. Recently, the activity of the Lab has been extended also to nanofluids containing metallic nanoparticles [Ref.(7)], and magnetic nanoparticles [Ref.(8)].

3) "Wavelenght Converters" for photovoltaic cells

In PV, one of the current areas of research is the study of systems that can increase the efficiency of cells.

Indeed, some inherent limitations limit the maximum efficiency that solar cells can reach (transparency at wavelengths below the band-gap of the semiconducting material, lattice thermalization, etc.) [Ref.(9)]. It has been calculated that for monocrystalline silicon cells, theoretical maximum efficiency is only around 30% (Shockley limit).

Some methods to overcome this problem consist in adapting the cell to the solar spectrum (for example as in multi-junction cells) or modifying the spectrum of incident light so that it is almost completely absorbed by the cell. Among the various techniques presented over the years, an economical solution for that consists of coupling the cell with another material (typically a ceramic matrix doped with rare earths, organic dyes or Quantum-Dots), able to absorb the wavelengths otherwise unused and to convert them into light having wavelengths corresponding to those of the maximum yield for the semiconducting substrate [Ref.(9)].

The solar spectrum can be modified in two ways: by phenomena of "up-conversion" and "down-conversion". In the case of "up-conversion" two low energy (infrared) photons are transformed into a photon of higher energy. Therefore, it can be possible converting sub-bandgap photons, which would otherwise be lost, in above-bandgap photons, which can be absorbed.

The reverse process, "down-conversion" is defined as the "cutting" of a high-energy photon (UV-visible) in two low-energy photons. This process can reduce the energy loss on the lattice thermalization that dominates at high energy photons (Blue-UV). The laboratory has been investigating the characteristics of materials that can be used for this purpose.

Very recently, the laboratory is gearing up to the characterization of Perovskite solar cells. This technology is considered one of the most promising solar photovoltaic technology of the future and is attracting many investments both by public institutions and by private companies. Indeed, Perovskite solar cells have very low production costs and the solar efficiency has improved a lot, reaching in early 2016 almost 23%.

Introduction

During the 3 PhD years much of the work in Solar-laboratory has regarded the design and development of a new apparatus aimed to measure the spectral emissivity of materials as a function of temperature up to 1000 °C. This thesis will focus on the characterization of some UHTCs, especially the optical properties, and the study of high-temperature emission characteristics, in order to assess the performance of these innovative materials for possible use as receivers in solar thermal power plants.

Among all the renewable Energy sources, CSP [Ref.(1)], and especially CSP-T [Ref.(10)], is considered the most promising for the future.

This is for different reasons: mainly it has an intrinsically higher efficiency than solar photovoltaic and allows exploiting mature technologies of conventional fossil fuel plants and, for this reason, CSP-T is attracting important investments both from private and from public companies.

However, the key for a more efficient operation of thermodynamics cycles is reaching the highest temperature as possible, because it is a general rule that the efficiency of solar thermal systems rapidly increases with increasing working temperature.

For CSP-T, a key issue for the overall plant efficiency is the choice of **receiver material**, namely the **absorber**, where the heliostat field concentrates the collected sunlight.

The sunlight absorber material must satisfied several requirements [Ref.(11), (12)], mainly:

- a *high solar absorbance*, to be able to efficiently absorb the sunlight collected by the mirrored field,
- a *low thermal emittance*, so that thermal re-radiation losses by the heated absorber are kept low,
- *good thermal properties*, for efficiently transferring the thermal energy to a thermal fluid (steam, air, molten salt, etc.) with minimal losses [Ref.(13), (14)].
- *good chemical stability*, to resist to oxydation and degradation.

Summarizing, the main challenge for increasing the operating temperature of thermal plants is the development of novel receiver materials able to resist to damage at very high temperatures while keeping good spectral selectivity, good thermal conductivity and favorable radiative properties at the operating temperatures.

Carbides, borides and nitrides of zirconium, hafnium and tantalum of early transition metals, well known as UHTCs, have properties like chemical and structural stability at extremely high operating temperatures, thanks to their solid state stability, good thermochemical and thermomechanical properties, high hardness, high electrical and thermal conductivities, and high melting points above 3200K [Ref.(15)]. Those materials have been used since the sixties especially for thermal protection systems, and aerospace.

Recently our group has been proposing UHTCs, such as HfC, TaC, ZrC and borides like HfB_2 and ZrB_2 for solar receiver applications [Ref.(16),(17),(18)], because of their favorable optical and radiative properties. In fact, the characterization of optical properties, like solar absorbance and

thermal emittance, is particularly important as they are strictly connected to the thermal behavior and thus to the material suitability as solar radiation receiver and, definitely to the overall system efficiency.

This thesis is part of a research project aimed at developing various advanced ceramic materials and at studying their basic properties in order to evaluate their possible use in solar receiver construction.

In the **first chapter,** it will be shown a brief introduction on industrial implications and the importance of high-temperature measurements, in particular in the field of solar absorbers.

In the **second chapter,** it will be shown some quantities and radiometric techniques useful in dissertation.

In the **third chapter,** it will be explained the experimental techniques that have been used for UHTCs materials characterization.

In the **fourth chapter,** it will be introduced the studied materials and the main uses in industry.

In the **fifth chapter,** it will be shown the results obtained.

1. Materials characterization at high temperature

Materials characterization at high-temperature is useful in a wide variety of technology areas. In particular, the analysis of the optical properties at high temperature is useful in the fields of energy, electronics, photonics, and chemical applications.

The new apparatus built at INO-CNR allows studying optical properties of materials at high temperature for use in various technological areas, with emphasis on solar absorbers.

This chapter shows some industrial attractiveness of the new INO apparatus and of the high temperature measurements in general [Ref.(19)].

1.1 Industrial attractiveness

The assessment of spectral emittance is of fundamental importance for many applications:

The new apparatus allows studying the optical properties of emitting materials for use in thermo-photovoltaic technology (TPV), through a direct measurement of the emitted radiation, in order to examine the effect of temperature on the absorption properties and thermal emission.

In TPV, thermal energy is directly converted into electrical energy by means of a thermally heated radiation emitter and proper photovoltaic cells [Ref.(20)]. As only photons with energy above that of band gap of the cell (E_g) can be converted into electricity and, moreover, only for those with energy slightly above E_g the conversion is efficient, there is a large effort in optimizing the thermal spectrum of the emitter by developing different solutions [Ref. (20), (21), (22), (23)]. For all these applications, the knowledge of spectral emittance at the high operating temperature is a key parameter.

Another industrial application is in the field of High Temperature Fuel Cells. In particular, Solid oxide fuel cells (SOFCs) use a hard, non-porous ceramic compound as the electrolyte, and the ceramic material, used at high temperature, must satisfied some optical requirements [Ref.(24)].

The INO experimental apparatus has been designed primarily to study solid solar absorbers in CSP-T. In fact, the good candidate for a solar receiver in solar power tower plants should have [Ref.(25)]:

1) High absorbance in the sunlight spectral region to absorb efficiently the sunlight collected by the mirrored field

2) Minimal emission losses when it gets heated, i.e. a low emittance at thermal infrared wavelengths [Ref.(12), (26)]

3) Good thermal properties, for efficiently transferring the thermal energy to the exchange medium.

Thus, the main challenge for increasing the operating temperature of thermal plants is the development of novel receiver materials able to satisfy the above properties. Therefore, a spectral analysis of the material as a function of the temperature is of great interest to understand its behavior and to identify the best operating conditions.

1.2 Solar Absorbers: state of art

In this section, there is a brief introduction on the current solar absorbers. There are various types of solar receivers, different in shape, structure and composition.

Typically, a receiver is composed of a substrate coated with other materials that have the purpose to protect it from degradation phenomena (oxidation, hydrolysis or corrosion by atmospheric dust) and to improve the optical characteristics [Ref.(11)].

The receiver structure depends on the type of concentrator associated to it (parabolic, heliostat, etc.), from the heat transfer fluid working temperature and, the solar radiation flux.

Shape of solar absorbers:

The receiver must also possess a form and a suitable composition to support thermal stress. Moreover, this shape must allow a good heat exchange with the heat transfer fluid.

The receiver shape varies mainly according to the type of concentrator used.

In case of CSP-PT are used predominantly receivers *tube-shaped* while in case of CSP-T, are mainly used *volumetric* receivers.

The volumetric receiver can be formed by a porous structure, which can be obtained using [Ref.(27)]:

- Dense nano-structured materials
- Structured wire materials mesh to form a plan
- Foam materials
- Intrinsic porosity materials.

The porous structure created within the material and the interstices, which is present on the surface, do so that the solar radiation penetrates to the bottom inside of the receiver, because the porous surface has a large equivalent area. Consequently, the volume of the material, rather than the surface, absorbs the solar radiation, and this is the reason why this type of absorbers is called volumetric.

Subsequently, the accumulated heat is transferred from the receiver to a fluid, which is forced to pass through the material using a pump; therefore, a heat exchange is realized by forced convection between fluid and receiver. The most common heat exchange fluid is air, but may be steam or another gas. The main volumetric receiver structures are [Ref. (28), (29), (30), (31)]:

- *Foil Receiver*: consists of a thin metal wires network, which absorb the solar radiation and through which the cold air pass. This class of volumetric receivers are the first that have been built. A receiver of this type was tested for the first time in the Swiss Alps in 1985.

- *Honeycomb Receiver*: It is formed by hexagonal blocks of highly refractory material wedged between them.

Volumetric VS Tube Receiver:

In a volumetric receiver Air-type, cool air enters the material from the front, where it comes solar radiation (Figure 1B), and exits at high temperature on the back [Ref.(32)].

In the volumetric case, the temperature distribution of the material and air have a pattern as shown in Figure 1B at the bottom. The air temperature increases going towards the receiver, until the difference in temperature between air and solid tends to be the same. Usually, this happens after a few diameters of the cells of the porous structure that is after distances of the order of 1-2 millimeters. This distance is called *extinction length*.

On the contrary, in case of a *tube receiver*, as we can see in the graph at the bottom of Figure 1A, the temperature is higher in the air-side than in the material-side where the heat transfer fluid is placed.

The temperature distribution of a tube receiver is disadvantageous compared to that of a volumetric receiver, because, as the warmer outside than the inside, it has a greater loss by radiation. Indeed, in case of receiver tube, the heat exchange fluid flows inside the tube itself. The solar radiation heats the tube that in turn heats the fluid. The temperature at the outer surface of the tube is significantly higher than the inside, with higher radiation losses.

Another disadvantage of this type of receiver is that the temperature on the outer surface of the tube is limited by the thermal resistance of the material used and therefore, to avoid the destruction of the receiver, the intensity of the focused radiation must be kept quite low compared to that the volumetric one. Typical concentration values are 200 kW/m^2 in tube receiver case and up to 1000 kW/m^2 in the volumetric one.

Other advantages offered by a volumetric structure comprise thin walls and, due to the porosity of the material, a high equivalent geometric surface area that consequently leads to a good air-receiver contact.

Moreover, the air (or whoever it) that passes through the volumetric receiver can be maintained at high flow rates with little pressure loss during the crossing [Ref.(32)].

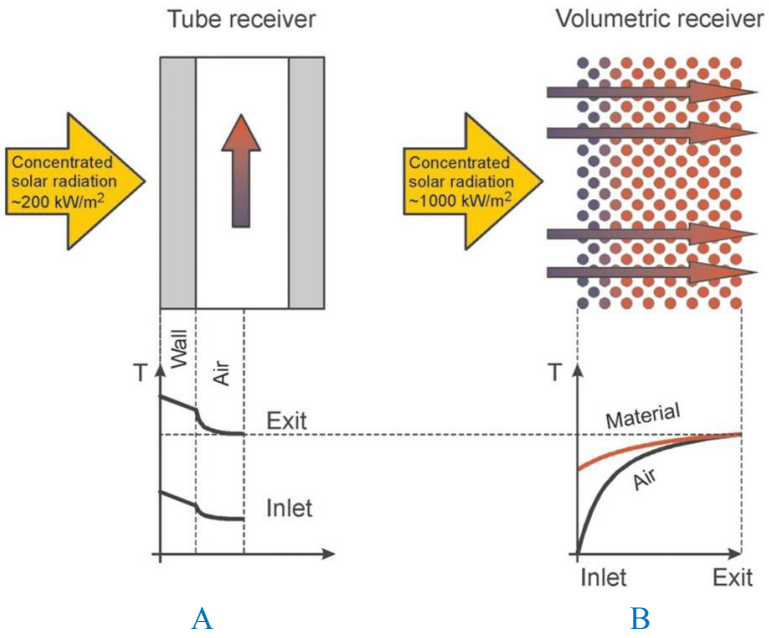

Figure 1 : The volumetric receiver principle compared to a tube receiver

The requirements that the volumetric absorber materials must have are: resistance to temperatures above 1000 °C, a high degree of roughness necessary to allow to maximize the penetration of solar radiation inside the material, a high graininess to obtain large surfaces required to transfer heat from the material to the gaseous fluid that flows through the pores, and a high thermal conductivity.

Although the extinction volume, which is the volume of the receiver in which the solar radiation is absorbed or rather the extinction length multiplied by the surface, decreases as the size of the cells increases, it is preferable to have a structure formed of cells as small as possible. Indeed, this leads to increase the surface absorption and heat exchange.

The air flow through the porous material is defined by the pressure difference between the two sides of the receiver. Problems of instability of the air flow through the receiver leads to local overheating and therefore to melting and local cracking with consequent loss of performance and irreversible damage to the receiver itself.

The spectral selectivity improves: 1) by using coatings formed from other materials or combinations of materials, 2) by chemically or physically modifying the surface of the material itself. Among the main types of coatings used for solar absorbers [Ref.(12),(33)]:

Optical characterization of solar absorbers:

Currently, the solar absorbers are characterized using the Kirchhoff's law (experimental procedure reported in paragraph 3.1). This method does not provide the real performance of the material, as the measurements are carried out at room temperature. The new system allows measuring the emissivity of solar absorbers at operating temperature, testing the real performance.

1.3 High temperature measurements: State of art

Unfortunately, spectral measurements at high temperature are not easy to perform. Different not-spectrally resolved methods exist to radiometrically [Ref.(34)] or, more often, by heat loss measurements or calorimetric techniques measure the emittance of different systems (see for instance [Ref.(35), (36),(37), (38)] for various metals [Ref.(39)] for films and [Ref.(40)] for solar collector tube architectures). The most common techniques for emissivity measurements are shown in paragraph 2.3.

If the spectral information for emittance is concerned, a radiometric approach is required and, for an opaque material, two basic ways can be explored: a) a direct measurement of the radiation emitted from the surface, b) an indirect method, namely the measurement of the radiation of a source reflected from the surface and the use of the Kirchhoff's and energy conservation laws [Ref.(41), (42)]. The reflection method (b) is more complex, as it requires an external radiation source with enough intensity, good stability and considerable spectral extent to cover the entire thermal spectral region. Moreover, it also requires a complex detection system with techniques able to discriminate reflected radiation from that emitted by the sample or the furnace [Ref.(42)].

The direct measurement of the emitted light (a) is conceptually simpler [Ref. (43), (44), (45), (46)], providing that some requirements are fulfilled. In particular, also the direct method suffers from spurious signal deriving from the hot furnace. This problem can be avoided keeping all the walls and objects close to the sample at a low steady temperature. Moreover, for a correct measurement, the sample should be kept in vacuum to avoid unwanted thermal exchange with the atmosphere in the furnace. In fact, it must be guaranteed that the only thermal exchange processes undergone by the investigated surface take place via radiative phenomena. In addition, the vacuum chamber also helps to minimize chemical processes like oxidation, which can distort the emittance measurement [Ref.(47), (48)].

Some recent examples of direct measurements carried out using spectrometers interfaced to heating chambers are shown, for instance, in [Ref.(49)] for temperatures up to 1050K, wavelengths in the range 2.5-22 μm and under controlled atmospheres to assess the emittance evolution during sample oxidation, in [Ref.(50)] for temperatures below 400°C and wavelengths in the range 4-40 μm and in [Ref.(44)] for (-40°C÷450°C) temperatures and (4÷100μm) wavelengths. Finally, a hybrid direct-indirect method has been recently shown [Ref.(51)], where the sample is heated by infrared radiation emitted by sources with different spectral distributions and both sample emittance and temperature are obtained as a result of a fitting procedure.

2. Radiometric measurements

This chapter introduces some quantities and radiometric techniques and has the purpose of a better understanding by the reader. It will be introduced some radiometric measurements and some useful definitions [Ref.(52)].

Radiometry is a set of techniques for measuring optical radiation. Radiometric techniques characterize the distribution of the radiation's power in space and wavelength. In radiometry, the optical radiation is modeled as a ray travelling in a straight line. Lenses and mirror redirect these rays along predictable paths. *Light Wave effect* and *quantum effect* can be neglected with this approach, so radiometry is distinct from quantum techniques.

2.1 Radiometric quantities

The main radiometric quantities are:

Radiant flux: is the energy emitted per unit of time, and is measured in watts (**W**).

Radiant intensity: is the radiant flux per unit solid angle. It is measured in (**W/sr**).

Radiance: is the radiant flux in a given direction for unit of solid angle and the emitting surface. It is measured in (**W/m^2 sr**) Figure 2.

Radiant Excitance: is the radiant flux emitted from an emitting surface in the hemispherical space. It is measured in (**W / m^2**).

Irradiance: is the radiant flux which impacts on a surface. It is measured in (**W / m^2**).

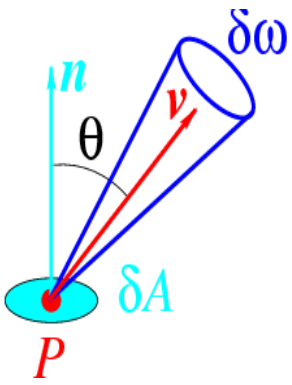

Figure 2: Representation of surface radiance.

2.2 Black Body: Planck, Wien and, Stefan-Boltzmann laws

A black body is an idealized physical body that absorbs all incident electromagnetic radiation, regardless of wavelength or angle of incidence. A widely used model of a blackbody is a small hole in a cavity with walls that are opaque to radiation Figure 3:

Suppose the cavity is held at a fixed temperature T and the radiation, trapped inside the enclosure, is at thermal equilibrium with the enclosure. The hole in the enclosure will allow some radiation to escape. If the hole is small, radiation passing in and out of the hole has negligible effect upon the equilibrium of the radiation inside the cavity. This escaping radiation will approximate blackbody radiation that exhibits a distribution in energy characteristic of the temperature T and does not depend upon the properties of the cavity or the hole, at least for wavelengths smaller than the size of the hole.

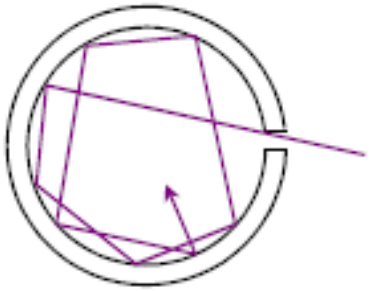

Figure 3: A blackbody cavity: An incident ray on the hole will pass into the cavity, and it is completely absorbed by the enclosure of the cavity.

2.2.1 Planck law

Planck's law identifies the blackbody spectrum, or rather the energy distribution. More precisely, the radiance (W/sr m^2) of the black body is represented as:

$$L(\lambda;T)_{bb}\,d\lambda\,d\Omega = \frac{2hc^2}{\lambda^5}\frac{1}{\exp[\frac{hc}{kT\lambda}-1]}d\lambda\,d\Omega$$

Where $\boldsymbol{L(\lambda;T;)_{bb}}$ is the black body radiance, or rather the amount of energy radiated per unit area, per unit time, per unit solid angle **dΩ**, in the range of wavelengths between **λ** and **λ + dλ**, **h** is Planck's constant, **c** is the speed of light, **k** is the Boltzmann constant. By definition, the black body radiance is isotropic.

2.2.2 Wien Law

Wien's law states that the blackbody radiance spectrum shows peak at a wavelength inversely proportional to the temperature, and derives from Planck's law:

$$\lambda_{max} = \frac{b}{T}$$

where **T** is the absolute temperature (in K), and **b** is the Wien's displacement constant, equal to 2.89777 x 10^6 nm K.

2.2.3 Stefan-Boltzmann law

The *Stefan Boltzmann law* describe the radiant excitance (W/m^2) of a black body $\boldsymbol{M(T)_{bb}}$, in terms of its temperature, per unit surface area, across all wavelengths, per unit of time:

$$M(T)_{bb} = \sigma T^4$$

Where σ is Stefan-Boltzmann constant (5.670×10^{-8} W m^{-2})

2.3 Emissivity: definition and measurements techniques

By definition *emissivity* or *emittance* is the ratio between the *radiance* of the real body and that of the ideal body (blackbody) at the same temperature T, and therefore emittance is between 0 and 1. The emittance is a function of wavelength λ, temperature T, and solid angle of emission Ω:

$$\mathcal{E}(\lambda; T; \Omega) = \frac{L(\lambda; T; \Omega)_{sample}}{L(\lambda; T)_{bb}}$$

The emissivity depends on several factors; those that affect the most are the chemical composition of the material, its electrical properties (metal, dielectric, semiconductor), homogeneity or heterogeneity of the material, and the surface characteristics such as roughness, oxidation layers, etc.

In general, we can take into consideration the angular emissivity distribution (i.e. in a solid angle or in a hemispheric angle) or the energy distribution considering particular spectral bands. Therefore, it is useful to consider the following specific emissivity:

Name	Definition
Monochromatic directional emissivity	$$\varepsilon(\lambda;T;\Omega)=\frac{L(\lambda;T;\Omega)_{sample}}{L(\lambda;T)_{bb}}$$
Band directional emissivity	It is obtained by integrating in a certain range of wavelengths, the monochromatic directional emissivity: $$\varepsilon(T;\Omega)=\frac{\int_{\lambda_1}^{\lambda_2}\varepsilon(\lambda;T;\Omega)*L(\lambda;T)_{bb}\ d\lambda}{\int_{\lambda_1}^{\lambda_2}L(\lambda;T)_{bb}\ d\lambda}$$ **If $\lambda_1\rightarrow 0$ and $\lambda_2\rightarrow\infty$ it is said Total directional emissivity and it takes the following expression: $$\varepsilon(T;\Omega)=\frac{\int_0^{\infty}\varepsilon(\lambda;T;\Omega)*L(\lambda;T)_{bb}\ d\lambda}{\int_0^{\infty}L(\lambda;T)_{bb}\ d\lambda}=\frac{\int_0^{\infty}\varepsilon(\lambda;T;\Omega)*L(\lambda;T)_{bb}\ d\lambda}{\sigma T^4/_{2\pi}}$$
Monochromatic hemispherical emissivity	It is obtained by integrating over a half-space the monochromatic directional emissivity:
Band hemispherical emissivity	It is obtained by integrating over a half-space, and in a certain wavelengths band, the monochromatic directional emissivity: $$\varepsilon=\frac{\int_{\lambda_1}^{\lambda_2}d\lambda\ \int_{2\pi}d\Omega\,\varepsilon(\lambda;T;\Omega)*L(\lambda;T)_{bb}}{\int_{\lambda_1}^{\lambda_2}d\lambda\ \int_{2\pi}d\Omega\ L(\lambda;T)_{bb}}$$ **If $\lambda_1\rightarrow 0$ and $\lambda_2\rightarrow\infty$ it is said Total hemisferical emissivity and it takes the following expression: $$\varepsilon=\frac{\int_0^{\infty}d\lambda\int_{2\pi}d\Omega\,\varepsilon(\lambda;T;\Omega)*L(\lambda;T)_{bb}}{\sigma T^4}$$

The most common experimental techniques used for emittance measurements are based on direct or indirect approaches [Ref.(53)(54)]:

Among the **direct** methods, the main ones used are the following:

A1) Method utilizing a black body as a reference source: This method follows directly the emittance definition. The radiance of the sample is divided with that of a blackbody brought to the same temperature.

A2) Absolute method in polarized light: This method allows deriving the *normal emissivity* (monochromatic directional emissivity in the direction perpendicular to the sample's surface)

through three direct radiance measurements and does not require a blackbody as external reference. In particular, by measuring the *normal directional radiance*, the *directional radiance at 45° in S polarization,* and the *directional radiance at 45° in P polarization,* it is possible to obtain the normal directional monochromatic emissivity of the surface.

The **indirect** emissivity measurement techniques are based on the following methods:

B1) Measurement of reflectance: The procedure consists in measuring the hemispherical reflectance of the material and deriving the emittance using the Kirchhoff law, considering completely opaque material (spectral transmittance = 0), thermodynamic equilibrium of the sample, and no energy transfers between the atomic species that make up the material.

B2) Complex refractive index measurement: The emissivity is derived from a measurement of complex refractive index, on condition that to consider pretty smooth surfaces and that the diffuse reflection effects are small. The complex refractive index can be determined from emission or reflection parameters. *Ellipsometry* is the most usual method and consist in measuring the reflectance relationship, at a certain fixed angle, between the reflected light S polarized and the reflected light P polarized. The applicability of the method is restricted to a perfectly smooth surface and thus without diffusive effects.

B3) Calorimetric method: This technique is based on the measurement of the heat flow exchanged between two surfaces. The specimen is immersed in a vacuum cavity, to avoid convection and conduction processes. The surfaces of the cavity have known emissivity and are maintained at a fixed temperature. From the measurement of the power required to maintain the sample at the temperature T it is obtained the hemispherical emissivity [Ref.(55)]. This technique does not allow directional emissivity measurements, and does not allow spectral measurements.

2.4 Surface properties: Specular and Lambertian Surface

The optical surface properties are one of the main parameter that influences the performances of a material for solar applications. Considering a beam incident on a surface, and analyze the reflected radiation.

The reflectance is *specular* if the incident radiation reflects according to Snell and Fresnel laws Figure 4.

The reflectance is *lambertian* if a beam of light, that hits the surface with any angle of incidence, is reflected in random directions following the *Lambert law* of the diffuse reflection $\boldsymbol{I(\theta) = I_0 \cos \theta.}$

In a similar way, we can introduce the specular and lambertian transmittance. A generic surface acts as a combination of both, lambertianity and mirroring.

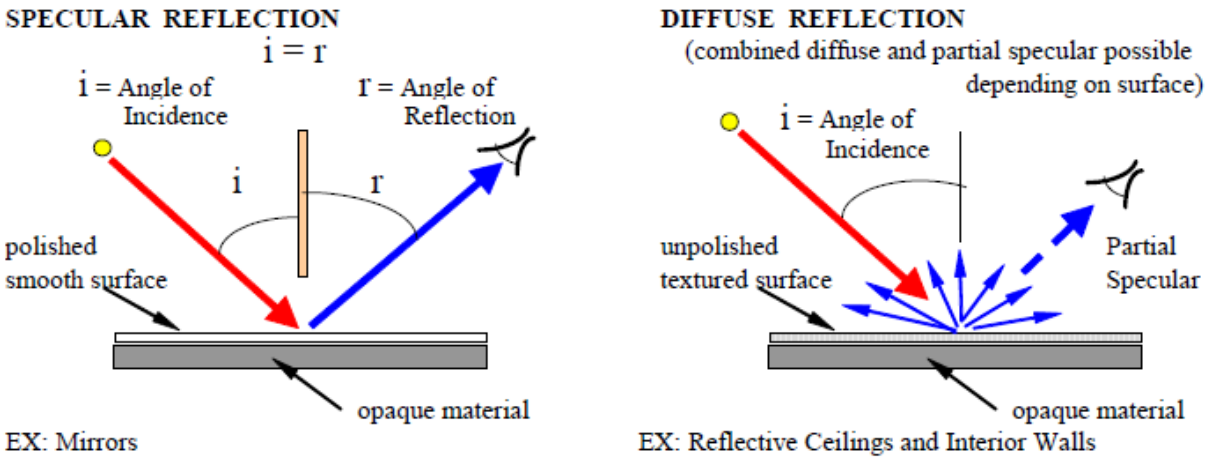

Figure 4: Specular reflectance (left) and lambertian reflectance (right)

3. Experimental techniques used

This chapter shows the experimental techniques used to characterize the UHTCs materials, as regards the optical properties.

3.1 Optical Spectroscopy

The experimental procedure consists in measuring the *hemispherical spectral reflectance* of the material, and derive the spectral emissivity. For the conservation of energy law we have:

$$\tau(\lambda) + \alpha(\lambda) + \rho(\lambda) = 1$$

Where **τ**, **α,** and **ρ** are respectively the transmittance, the absorptance and the hemispherical reflectance. If we consider a completely opaque material, as in our case, the transmittance is none.

If the following conditions are satisfied [Ref.(56)]:

- Thermodynamic equilibrium of the sample
- No energy transfer between atomic species (eg. fluorescence)
- No dielectrics multilayer.
- No surfaces with metal particles.

we can consider the *Kirchhoff's law*, and the spectral emittance Ɛ (λ; T) is equal to the spectral absorptance α (λ; T). So combining the previous laws, we obtain:

$$\mathcal{E}(\lambda) = \alpha(\lambda) = 1 - \rho(\lambda)$$

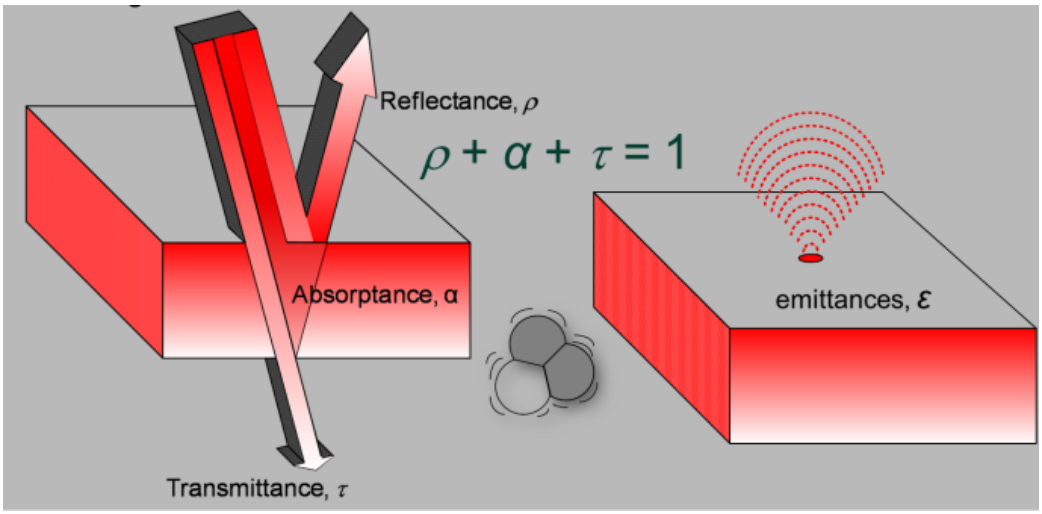

Figure 5: Kirchhoff and energy conservation laws

To measure the hemispherical reflectance you need an integrating sphere that surrounds the sample in order to collect all the rays reflected and diffused at any angle by the sample surface.

This method has been abundantly used in literature since many years to estimate the spectral emissivity at high temperature from measurements at room temperature, especially in case of solar absorbers [Ref.(13)(57)(58)].

The main limitation associated with this approach is due to the fact that the reflectance (and hence the emissivity) is measured at room temperature, although this may differ from that at high temperature. Furthermore, the requirements above of validity of the Kirchhoff's law not always are completely satisfied.

Despite this limitation, this is a very important method of investigation, as it allows a first comparative analysis of the properties of absorption and emission of the materials.

3.1.1 Instrumentation used

The hemispherical reflectance was performed using a scanning spectrophotometer (Lambda900, Perkin Elmer) for the spectral range 0.3-2.5 μm and a FTIR spectrophotometer (Excalibur, BioRad) for the range from 1.6 to 17 μm , both equipped with appropriate integrating sphere for measuring the hemispherical reflectance.

Perkin Elmer Lambda900

Spectrophotometer Perkin Elmer Lambda 900 has a spectral range covering NIR, VIS, UVA, UVB and a little of UVC. The accuracy in wavelength is ± 0.08 nm in the UV / VIS and ± 0.32 nm in the NIR; the photometric accuracy is 2%. Since the reflectance measurements are referred to a primary sample (Calibrated white Spectralon), also the error on the reflectance of the latter must be considered. This is 2% so the overall error on the spectra measurement is 4%.

The structure of the Lambda 900 spectrophotometer is characterized by the optical system reproduced schematically in Figure 6 .

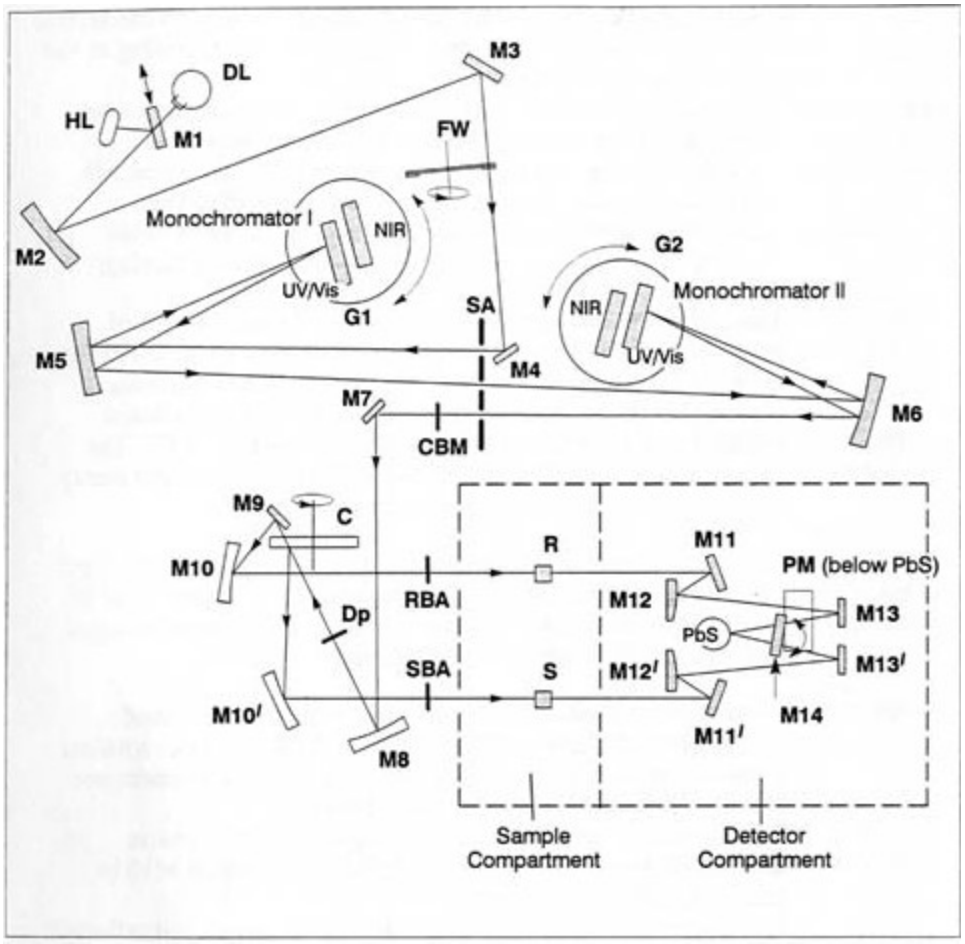

Figure 6 : Lambda900 spectrometer, optical system

As sources of radiation, the spectrometer has: a deuterium lamp (in the figure indicated by DL) that emits broadband radiation in the VIS / UV range and a halogen lamp (shown HL) that covers the spectral band NIR / VIS.

When NIR / VIS has selected, the M1 mirror reflects the radiation coming from the halogen lamp on the mirror M2, and M1 at the same time blocks the radiation from the deuterium lamp.

When VIS / UV has selected, the M1 mirror allows the radiation from the deuterium lamp to hit the mirror M2. The change of the source has been set to 315 nm.

Among the mirrors M3 and M4 there is a filter holder wheel (FW), which possesses different band pass filters selected according to the wavelength that it must be produced. This allows pre-screening the radiation before it enters the first monochromator and thereby, it allows avoiding diffraction orders higher than the first.

Between M4 and M5 mirrors there is the double monochromator entrance slit (SA). There are two sets of gratings (G1 + G2): 1200 lines / mm for the UV / VIS / NIR and 600lines / mm for IR. The change between gratings was selected to 860nm.

The rotation of G1, G2 gratings and the input wheel FW filters are synchronized with each other to maximize the signal/noise ratio and the spectral purity of the output signal from the last slit. The

mirrors M7 and M8 reflect the output beam, once passed through an adjustable common beam mask (CBM) useful to reduce dimensions of the beam spot.

Subsequently, there is a shutter (D_p). If the shutter is closed, no signal arrives to the detector allowing taking the dark signal. A rotating chopper (C), formed by an alternation mirror-hole, deflects the beam in two different directions:

- If the beam encounters the hole, it passes through the chopper, it is reflected by the mirrors M9 and M10, and creates the so-called reference beam R.
- If the beam meets the mirror, it is reflected towards M10' mirror and creates the so-called sample beam S.

The instrument software performs the spectrum measurements automatically as the ratio between the two signals explained in the above issues.

It is possible to extract and change the final part of the instrument (in Figure 6 the part between the dashed lines) according to the different usages. For our experiment the final part is equipped with an integrating sphere, 150mm diameter, coated of Spectralon (highly reflective and lambertian material), as shown in Figure 7.

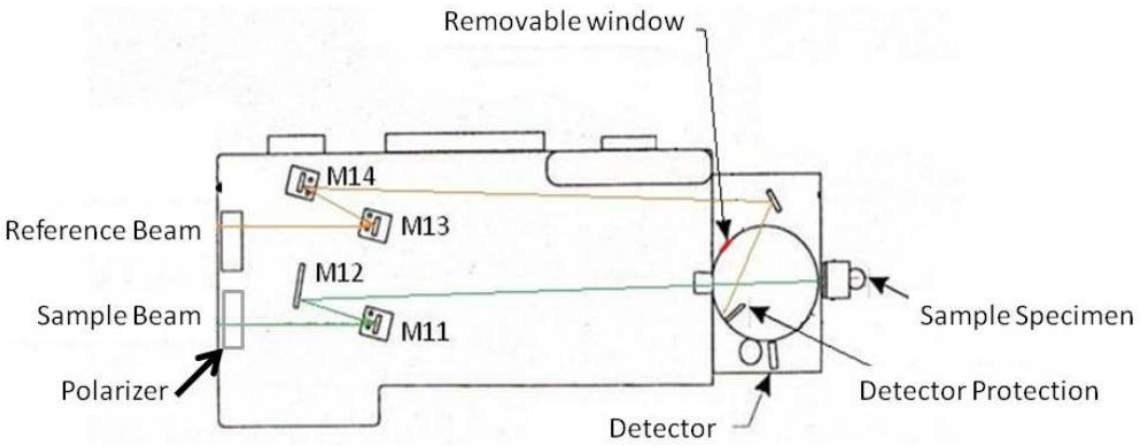

Figure 7 : Final part of L900 instrument equipped with integrating sphere

In the final part of the spectrometer occurs as following:

- When the beam passes from M13 and M14, the radiation hits the integrating sphere at one point and the light rays diffuse in the surrounding space. In this situation, the detector makes a reference measurement.
- When passing from M11 and M12, the radiation hits the sample surface at an angle of 8° with respect to the normal, and the detector measures the diffuse radiation in the integrating sphere.

The ratio between these two measurements is the hemispherical reflectance.

Initially, the sample holder is equipped with Spectralon as calibration target, and all the subsequent reflectance measurements referred to this one.

The integrating sphere is equipped with two detectors: a photomultiplier for UV / VIS / NIR band and a PbS photodiode for the IR band. The detector change was set at 860nm.

FTIR Biorad Excalibur

The spectrophotometer Biorad Excalibur has a spectral range covering from 1.6 to 25μm. The instrument was equipped with special integrating gold-coated sphere Pike technologies [Ref.(59)] as to permit diffuse reflectance measurements. The instrument is based on a Michelson interferometer (Figure 8).

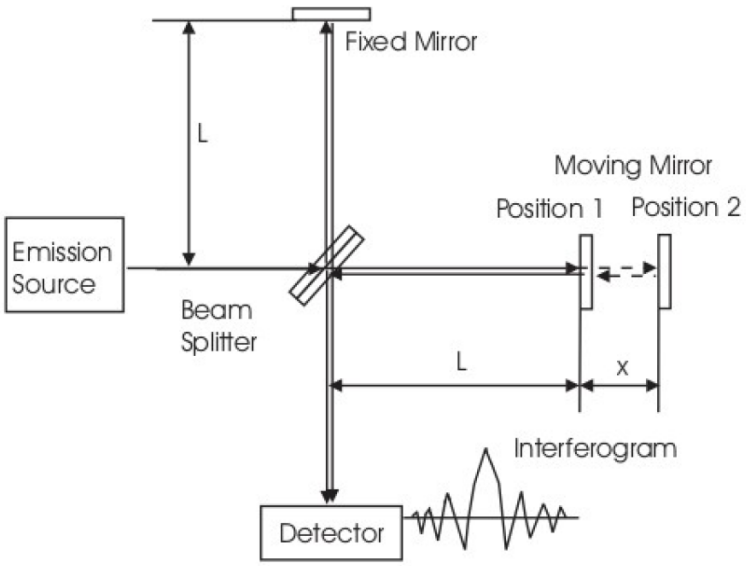

Figure 8: FTIR spectrometer, working principle

As sources of radiation, the spectrometer has a 900°C blackbody internal source. Unlike Lambda900, Excalibur is based on a single beam. Therefore, the reflectance measurements refer to the reflectance of the integrating sphere coating surface.

The beam hits the sample at an angle of about 10 ° (differently from Lambda900, which has an angle of 8°). Via a removable mirror, it is possible to hit the integrating sphere, for the reference measurement, or the sample, for the sample measurement. The instrument software automatically calculate the spectra as the ratio between the two signals.

The signal is indicated as an interferogram. The execution of a Fourier transform of this signal it gives the spectrum of reflectance as with a conventional dispersive spectrometer, but the results are much faster with scan times much lower. The detector is a Mercury cadmium telluride and needs to be cooled to the melting temperature of liquid nitrogen (-210 ° C).

3.1.2 Considerations and data analysis

The spectra has been exported in ASCII format and then reworked with *OriginPro-8 software*. The reflectance spectra, measured with the two instruments, showed a positive shift in the range of wavelengths common to the two spectrometers (2-3%). This difference depends on the surface

roughness, the observed area of the sample, the angle of the incident beam (8° in case of Lambda900, 10° in case of Excalibur) and, the fact that spectra are referred to different calibration standards (*Spectralon* in case of Lambda900 and *gold coating* in case of Excalibur).

Therefore, the spectra have been linked, keeping fixed that one measured with Lambda900 and multiplying spectra obtained with Excalibur. This is justified by the fact that Lambda900 spectra are referred to calibrated *Spectralon*, traceable at the National Institute of Standards and Technology (NIST).

All the information about the optical characteristics of the materials is then included in the hemispherical reflectance spectrum. However, for a better interpretation of the characteristic of the solar absorbers, it could be useful to introduce the *integrated absorptance* and *integrated emittance*, widely used in literature, defined as:

$$\alpha_{int} = \frac{\int_{\lambda_1}^{\lambda_2}[1-\rho(\lambda)] \ * \ S_{1.5}(\lambda) * d\lambda}{\int_{\lambda_1}^{\lambda_2} S_{1.5}(\lambda) * d\lambda}$$

$$\varepsilon_{int} = \frac{\int_{\lambda_1}^{\lambda_2}[1-\rho(\lambda)] * L(\lambda;T)_{bb} * d\lambda}{\int_{\lambda_1}^{\lambda_2} L(\lambda;T)_{bb} * d\lambda}$$

Where **ρ(λ)** is the spectral hemispherical reflectance (so [1-ρ(λ)] represents the spectral absorptance / emittance in case of validity of the *Kirchhoff's law)*, $\mathbf{S_{1.5}(\lambda)}$ is the solar irradiance spectrum AM1.5 [Ref.(60)], $\mathbf{L_{bb}(\lambda;T)}$ is the blackbody spectral radiance calculated with *Planck's law* at temperature T. α_{int} and ε_{int} give an assessment of the amount of absorbed solar radiation and the amount of re-emitted thermal radiation.

Considering the spectral emissivity [1-ρ(λ)], measured at ambient temperature, valid at high temperature is a heavy approximation. Anyway, this is a method widely used in literature to characterize solar absorbers, and it is very useful to compare samples among them.

A parameter used to express the goodness of a material as a selective solar absorber is the *selectivity index*, widely used in the literature. This is defined as the ratio between *integrated absorptance* and *integrated emittance:*

$$Selectivity\ Index = \frac{\alpha_{int}}{\varepsilon_{int}}$$

The spectra of materials that possess high *Selectivity Index* have the characteristic step shown in Figure 9. They have low reflectance [ρ(λ)→0] at wavelenghts λ ≤ 1400nm, corresponding to almost all of the solar spectrum energy, and high reflectance [ρ(λ)→1] at λ ≥ 1400nm, corresponding to the emission spectrum of the receiver at that temperature. The cut-off at 1400nm refers to a receiver temperature of 1000°C; this value have to be at wavelengths greater or smaller depending on the

temperature of the receiver. In fact, in accordance with *Wien's law*, the emission peak, and consequently the whole blackbody emission spectrum, shifts to wavelength smaller with increasing temperature and vice versa. As cut-off, it is considered the value of the wavelength at which the blackbody curve reaches half of the maximum.

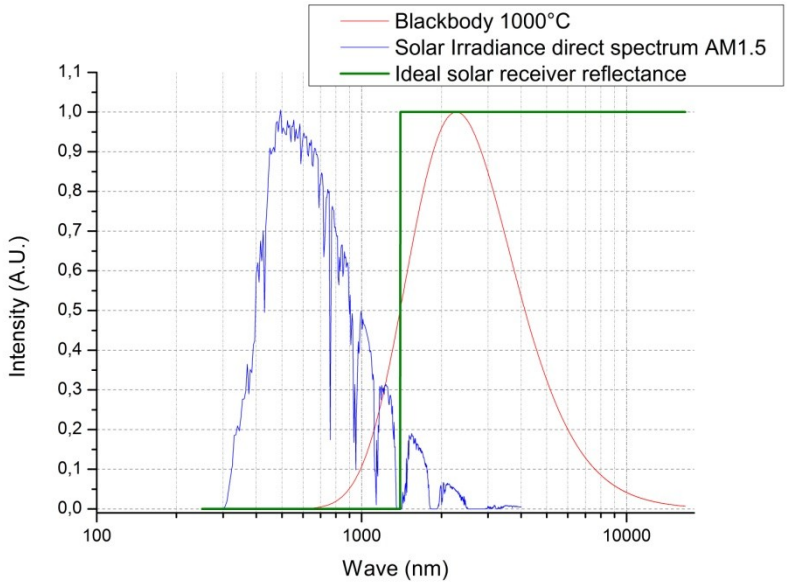

Figure 9: Ideal high selectivity solar absorber for a solar receiver that operates at a temperature of 1000°C.

3.2 New INO-CNR apparatus

3.2.1 Purpose of the new apparatus

The most diffuse approach used in literature to measure the spectral emittance/absorbance is to measure the hemispherical reflectance at room temperature and to use the *Kirchhoff's law*.

This method is not very effective, as the absorbance/emissivity may change with temperature and *Kirchhoff's law* is not always valid. For example, this method is not valid in characterization of TPV emitters; since, in this case, energy transfers occur between atoms that make up the material (usually a ceramic material enriched with rare earths), and the requirements of the *Kirchhoff's law* are not satisfied. In addition, this method does not characterize the real performances of a material as solar absorbers, as the emittance may change with temperature.

Although this approach is a useful method for a first screening of materials, it was necessary the realization of an experimental apparatus that will have allowed radiative property measurements of a material at the temperature of use.

3.2.2 Experimental apparatus

The set-up and the method chosen permit to perform the direct spectral emittance of opaque solid materials. The set-up is optimized to study UHTCs samples at temperature from 500 to 1200 K in high vacuum.

The experimental method used is directly connected to the emittance definition, that is the ratio between the *radiance* emitted by the sample surface at a given temperature and that emitted by a blackbody at the same temperature. Therefore, a calibrated blackbody source is used as a reference.

Fixed the following parameters: temperature T, wavelength λ, observation direction (normal to the sample surface or the blackbody exit port respectively) and detection solid angle Ω, the spectral emittance ε is calculated as the ratio between the radiance of the sample L(Ω,T,λ) and the radiance of the reference blackbody L_{bb} (Ω,T,λ):

$$\varepsilon(\lambda;T;\Omega) = \frac{L_{sample}(\lambda;T;\Omega)}{L_{bb}(\lambda;T;\Omega)}$$

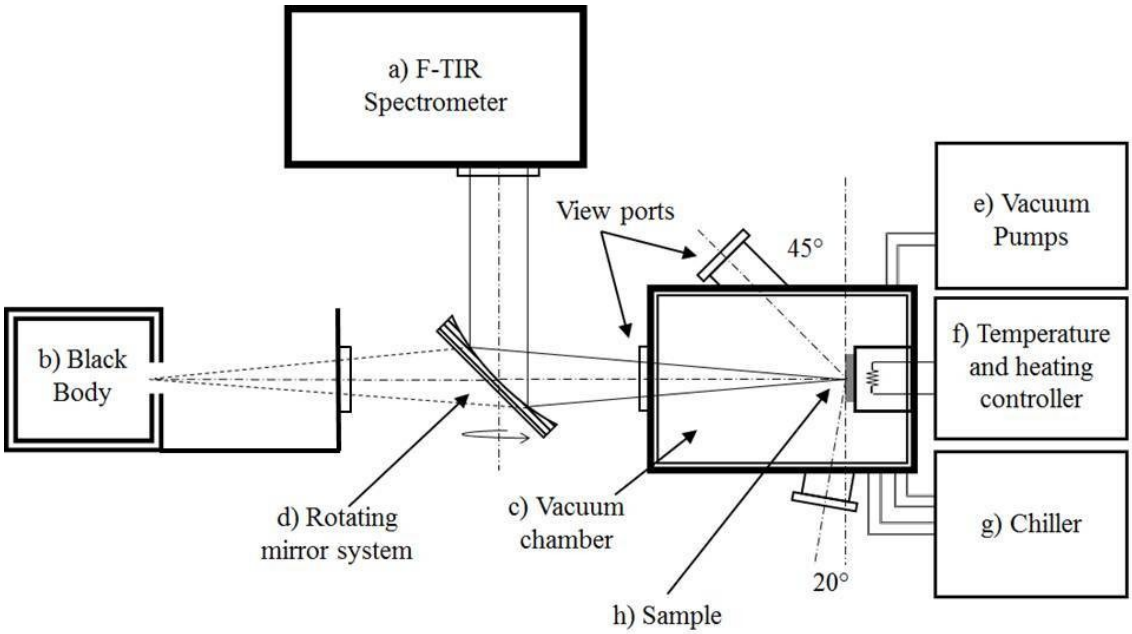

Figure 10: Scheme of INO vacuum electric furnace. Signal from sample and from reference source at high temperature are directed alternately to a Fourier-Transform InfraRed (FTIR) spectrophotometer for spectrally resolved measurement.

Three main blocks compose the experimental setup (Figure 10):

a) the spectral measurement system,
b) the reference blackbody (C.I. Systems SR-2) and
c) the homemade vacuum furnace with electric heating, where the sample can be heated up to 1200 K in a completely controlled environment.

In Figure 11 the view of the vacuum chamber and in Figure 12 the splitting optical system.

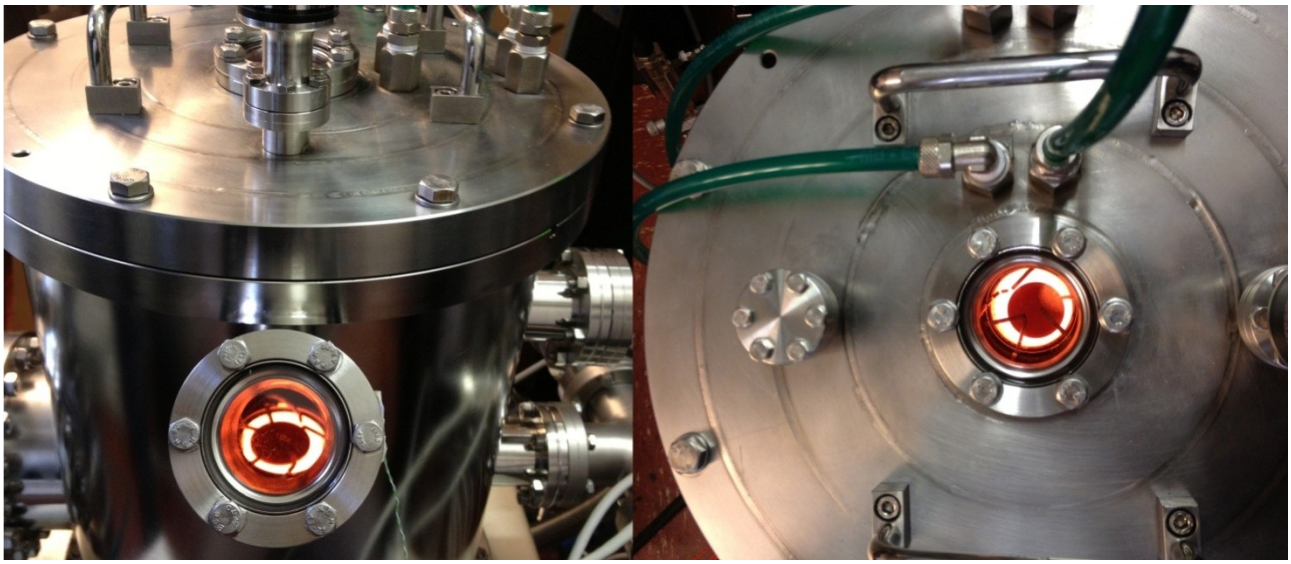

Figure 11: The vacuum chamber

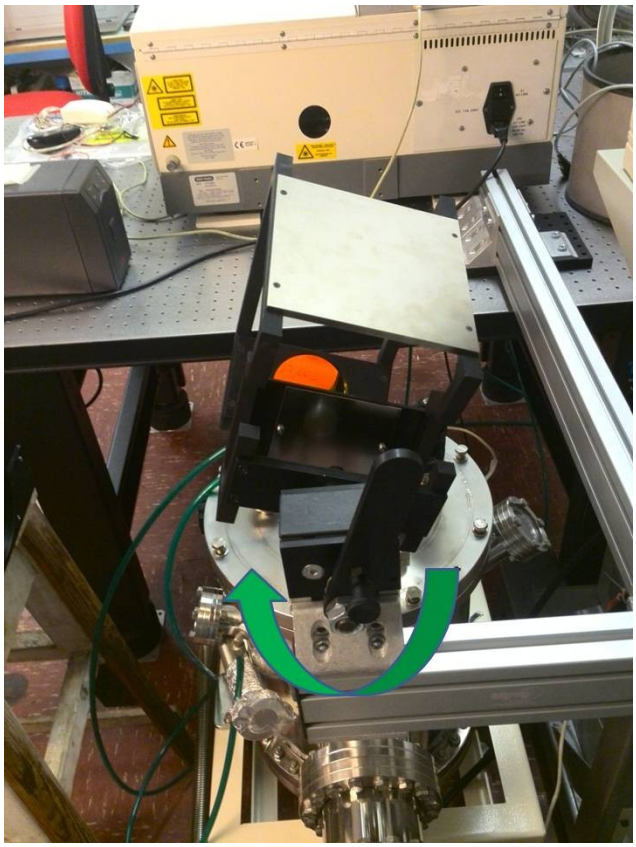

Figure 12: the splitting optical system allows interfacing the spectrometer with blackbody or sample.

3.2.3 Optical system

Referring to Figure 10, a specifically designed and realized optical system interfaces either blocks (a) or (b) to (c). The optical system consist of three gold mirrors, that collect the signal from the center of the sample and directs it into the detection system (Figure 12). The optical system acts as an objective, reproducing the real image of the sample, or the blackbody, on the front port of a FTIR spectrometer (Biorad, Excalibur), with a full acceptance angle < 3°. This highly directional system allows minimizing spurious radiation back-reflected on the sample itself by the chamber walls. Moreover, as the walls are kept at near room temperature, their thermal irradiance is very low, making negligible their contamination of the signal.

The mirror mounting can be rotated in a second fixed position to collect the radiation emitted by the blackbody. Sample and blackbody aperture are located at same distance with respect to the entrance port of the detection system. According to the characteristics of the optical system, the viewport acts as a stop, fixing the solid angle of detection. Thus, there is an identical viewport in front of the blackbody source in order to allow observing blackbody and sample within the same solid angle.

The optical apparatus is constituted by a spherical mirror, with a radius of curvature of 779.5 mm, and two plans mirrors, and generates on the external input port of the spectrometer a real image of the sample under test (technically combines the planes of the sample, or of black body, with the spectrometer entrance window). In other words, it alternately produces the image of the sample surface and the output aperture of the blackbody in correspondence of the entrance window of the FTIR spectrometer with a magnification of about 1.7.

A circular diaphragm located on the image plane (field aperture) selects the observation area of the image. As both, sample and blackbody radiation, have the same optical path (identical path length, windows, observation solid angle and thus observed emitting area), the measurement of the *transfer function* of the overall system is not needed.

In Figure 13 there is a drawing of the optical system (considering the figure on the left, at the bottom is placed the output window of the furnace and on the left the entrance window of the spectrometer; the spherical mirror is placed on the top of the picture, in orange).

The main viewport allows acquiring the radiation emitted by the sample in the direction normal to the surface. Additional viewports, not operative at this moment, have been made to observe the sample emission at a 45° and 70°, after that ad-hoc optical systems will be designed and realized in the future. The main viewport is equipped with a ZnSe window (transmittance range 0.5-21 μm) whereas side viewports now are equipped with silica windows (transparent up to 3.5 μm) and will be replaced with ZnSe windows in the next future.

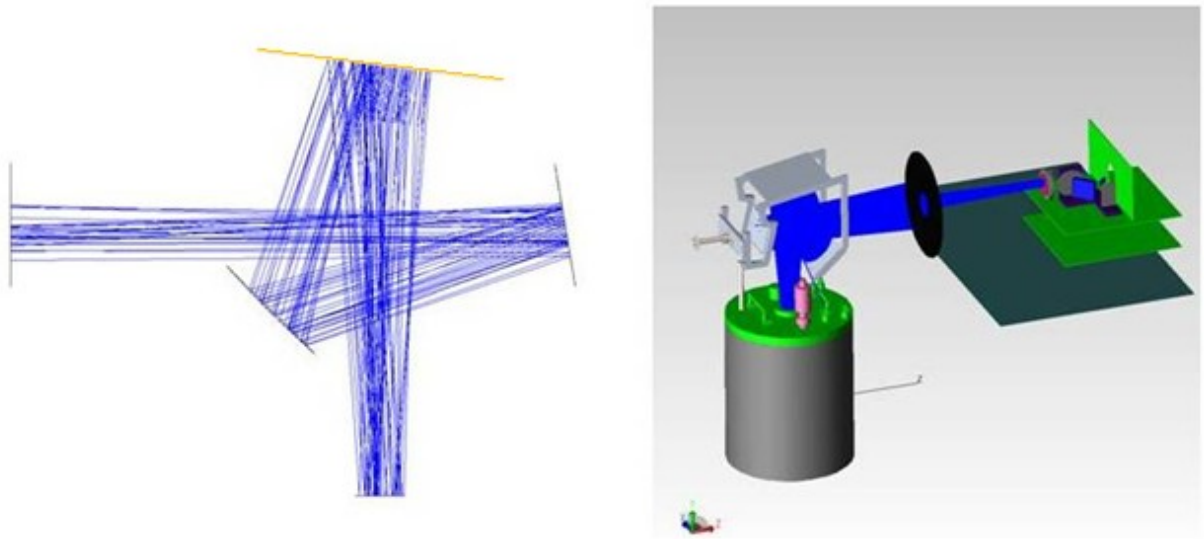

Figure 13: Ray tracing (left) and ¾ view (right) of the optical system

3.2.4 Criticality in temperature measurement

The disc shaped sample is put in the vacuum chamber on the upper horizontal plate of the cylindrical heating support (HeatWave Labs, Inc.) and locked with three clips. The sample surface temperature is read by three S-type thermocouples. The temperature of the heater is controlled via an internal K-type thermocouple, which provides the feedback to the power controller. Vacuum in the furnace is provided by a rotary (OME 25S, Adixen) and a turbo molecular (Turbovac 361, Leybold) pumps, with ultimate pressure limit of few 10^{-6} mbar. A closed-cycle water circuit with chiller steadily maintains furnace walls and cover at nearly room temperature.

It should be noticed that the maximum temperature, which has been reached at this moment, is around 1000 K, due to losses at thermal contact between sample and heater.

A market survey led to the conclusion that there are no thermal pastes operating at these temperatures, and then the only way to facilitate the heater-sample thermal contact is mirror polishing of the specimen so as to increase the effective surface area in contact with the heater. Moreover, it must be emphasized that, since the vacuum system, the heat exchange is about 30 lower than in the air.

The largest component of the emissivity measurement uncertainty is the temperature measurement of the sample, which is not easily assessable since the sample does not act as a black (or gray) body.

The uncertainty on the temperature measurement affects the correct interpretation of the radiance of the black body, and bring to an incorrect assess of emittance.

To overcome this, the s-type thermocouples have been replaced with a more efficient system of temperature measurement based on a spring K-thermocouple, which is squashed directly on the sample.

Another system used is a system based on bichromatic pirometry. Unlike the traditional pyrometer, it does not require as input parameter the value of emissivity at working wavelength, but the ratio between the emissivity at the two working wavelengths.

The two working wavelengths are given by two optical bandpass filters, with partially overlapping spectral bands and close together. Therefore, the ratio between the two emittances will be very close to unity and, for a wide range of materials, will be in any case between 0.9 and 1.1. Consequently, the temperature evaluation is more precise than that with the traditional pyrometer.

The use of both measuring systems, spring K-Thermocouple and bichromatic pyrometry, assures an excellent precision and repeatability in temperature measurement.

3.2.5 Detection system

The detection and spectrally resolving block is composed by a commercial Fourier-transform infrared spectrometer (Excalibur by BioRad) sensitive into the 1.6-25 μm spectral range. The spectrometer has been modified, allowing accepting an external source. The external radiation enters the spectrometer through a KBr window and, inside the spectrometer, there is an optical system that has the following functions:

• It must allow matching the radiation coming from the front entrance window of the spectrometer to the interferometer.

• It must be able to rotate and permit the use of the spectrometer both in “furnace mode” and in “traditional mode”.

The designed system is formed by a movable mirror, an electric motor (Minimotor SA swiss made 15 / s 485: 1 99 1 323 219) supplied with a circuit to 2.5V and an appropriate ON OFF ON switch, that allows the direction inversion of the electric motor.

3.3 Promes CNRS (France)

The high temperature optical characterization was performed using, as experimental apparatus, the MEDIASE. This apparatus is located at the solar furnace of Odeillo (french Pyrenees). The equipment is owned by PROMES-CNRS laboratories (Figure 14).

Heliostat mirrors, placed on the ground, and a large parabolic mirror that constitutes the north facade of the CNRS building, form the furnace. The solar radiation, intercepted by the heliostats mirrors, focuses on the parabolic mirror and subsequently on the point of focus, where there is the MEDIASE apparatus (Figure 15).

Figure 14 : The solar furnace of Odeillo (Promes-Cnrs)

The temperature of the sample can be controlled by regulating the flow of solar radiation through an opening (maximum flux 1MW) and, under optimum conditions, it can be reached temperatures above 3500 °C. The furnace is used both for industrial applications and for basic research applications.

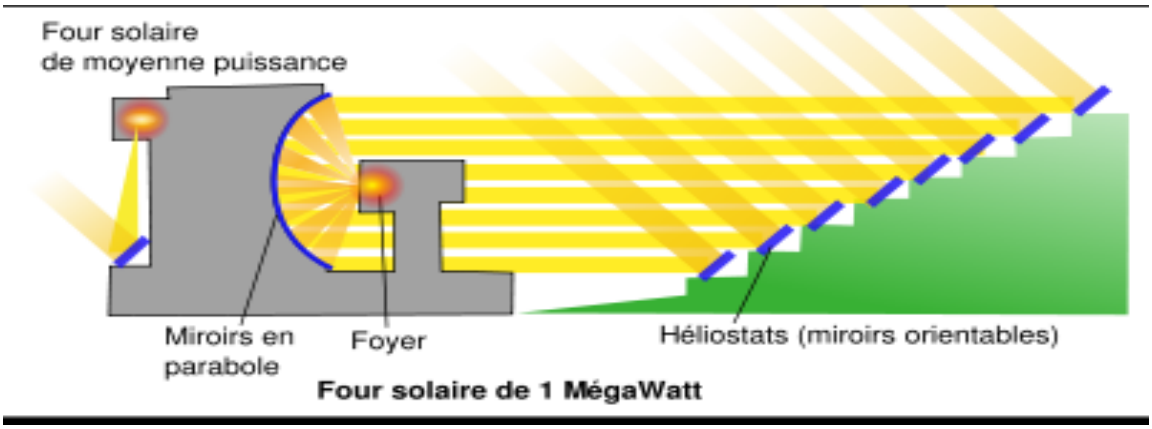

Figure 15 : Drawing of the solar furnace of Odeillo

3.3.1 MEDIASE [Moyen d'Essai et Diagnostic en Ambiance Spatiale Extreme].

In Figure 16 there is the MEDIASE setup. The following points are numbered:

1) Silica hemispherical glass window, 35 cm diameter.
2) Cooler system of the front shield.
3) Sample holder.
4) Mobile probe.
5) Optical Fiber.
6) Temperature detection device, by bicolor *pyroreflectometry* and *pyrometer*.
7) Mirrors.
8) Output window.
9) Radiometer equipped with a specific filter.
10) Solar radiation.
11) Connection to a vacuum pump.

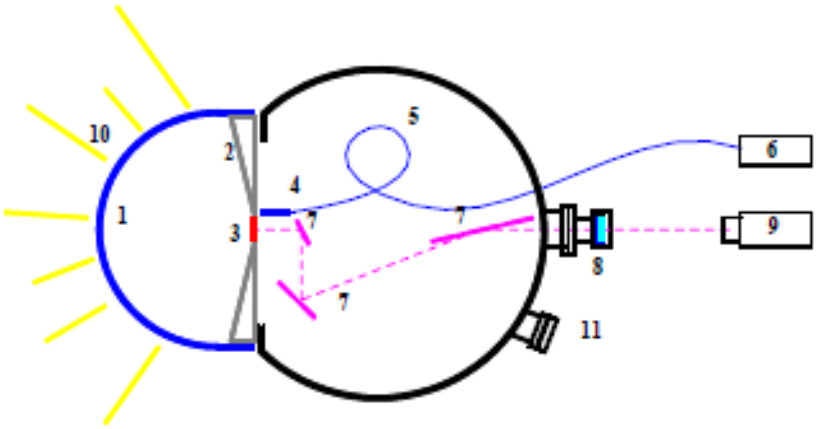

Figure 16 : MEDIASE Set-Up

The solar radiation flux (10) heats the sample (3) on its front face, whereas the instrumentation analyzes the radiation coming from the rear face (Figure 17 e Figure 18).

A movable probe (4) is placed in proximity of the rear face of the sample and is equipped with some optical fibers (5) connected to an optical temperature measuring system (Bycolor-pyroreflectometry) and to a pyrometer (6).

The sample radiation reaches the radiometer (9), passes through the mirrors (7), and reaches one of the output ports (8). The MEDIASE have remaining output ports, which are not yet used and are not shown in the figure.

The bandwidth of the radiometer (9) is between **0.6-40µm**. The radiometer has 2 spectral filters, **0.6-2.8µm** and **8-14µm** bandwidth, and 3 monochromatic filters (FWHM: 0.1µm) at wavelengths of **4.5µm**, **5µm** and **5.5µm**.

Through the mirrors (7) it is possible to measure the directional emissivity at various angles. A controlling software moves the mirrors and calculates the hemispherical emissivity through integration of directional emissivity measurements.

A high vacuum pumping system (11) keeps the pressure inside the chamber lower than 10^{-5} mbar.

The sample is maintained exactly where the solar rays converge and a water cooling system chills the hemispherical cap (Figure 18).

Care must be taken mounting the specimen, so as to minimize the thermal losses toward the door sample holder. In this manner, the only relevant channel of energy loss is the heat radiation.

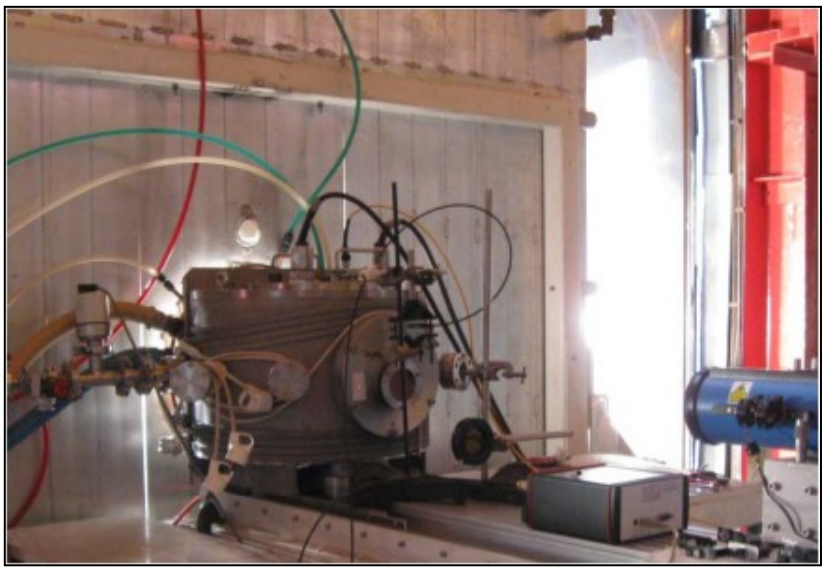

Figure 17 : MEDIASE back-side

Figure 18 : MEDIASE front-side

3.3.2 Measuring procedure

Calibration:
The spectral response of the optical system was obtained using as a reference a black body. This operation was carried out in all spectral bands of the radiometer available listed previously.

Optical System and emittance:

The radiometer measures the directional radiance of the sample, integrated in the band of wavelengths considered. To avoid effects due to the non-uniform distribution of temperature on the sample (the edges are colder than the central part), the radiance is measured in a small region of the sample of about 7 mm in diameter around the center using a suitable optical system (Cassegrain) in front of the radiometer.

The emittance was calculated as the ratio between the measured directional spectral radiance, at given angle θ and given temperature T, and the blackbody directional spectral radiance at the same condition. Hemispherical emittance values were obtained by integration of the angular values over a half space, assuming hemispherical symmetry of the emission lobe.

Temperature:
The surface temperature was carried out using two techniques:

- The first makes use of a *pyrometer* that measures the color temperature of the object (ColorT), so the sample is assumed to behave as a gray body.
- The second, *bicolor pyroreflectometry BP,* was developed by PROMES CNRS laboratories. This technique makes two measurements of reflectance at two different wavelengths and a complex algorithm returns the value of the surface temperature (CrossT) [Ref.(61),(62)].

Because UHTCs possess spectral emissivity spectra very different from that of a gray body, the temperature measured with the two systems does not coincide.

CrossT is a more reliable temperature but it is sometimes not possible to measure it, because of problems linked to the degeneration of the equations that are at the basis of the algorithm.

When CrossT was not available, ColorT was used. Although this is not the real temperature, this is still useful to observe trend as a function of temperature.

4. Materials: UHTCs

For some years, the laboratory has been studying the possibility of using innovative materials such UHTCs (Ultra High Temperature Ceramics) in the construction of solar receivers; this thanks to their physical properties such as high refractoriness, high mechanical strength, high thermal conductivity and good chemical stability. Among these the most important, are borides, carbides and nitrides of Hf, Ta and Zr. They have been used since the 60s mainly in aerospace industry by Russian and U.S. laboratories during the Cold War [Ref.(63)].

Those materials have the highest melting temperatures of any known materials (exceeding 3200K), physical properties of ceramics, and the electronic properties of metals [Ref.(15)]. They show also spectral selectivity with high α_{int} and low ε_{int}.

4.1 Industrial applications of UHTCs

Ultra High Temperature Ceramics (UHTCs) are a good choice for several extreme applications: thermal protection materials on hypersonic aerospace vehicles or re-usable atmospheric re-entry vehicles, specific components for propulsion, furnace elements, refractory crucibles, missile defense, automotive, coatings of reactors for nuclear fission and fusion.

Hypersonic flights, re-entry vehicles, and propulsion applications all require materials that can perform in oxidizing or corrosive atmospheres at temperatures above 2000°C and sometimes they must have a long working life. Ultra High Temperature Ceramics (UHTCs) are good candidates to fulfill these requirements [Ref.(64)].

Regarding hypersonic flight [Ref.(63),(65)], the airfoils generally have a thin section formed of either angled planes or opposed arcs (called "double wedge airfoils" and "biconvex airfoils" respectively), with very sharp leading and trailing edges. The sharp edges prevent the formation of a detached bow shock in front of the airfoil as it moves through the air.

UHTCs are also useful in thermal protection systems [Ref.(66)]. For example, vehicles re-entering the atmosphere at orbiting velocities reach Mach numbers of at least 25. Flows at these Mach numbers result in very high vehicle surface temperatures due to air friction.

The high thermal conductivity makes the UHTCs useful in the construction of rocket nozzles [Ref.(67)]. In fact, during the instants following power-on, the temperature on the inner surface of the nozzle can reach 2000°C in less than 0.15s whereas the external surface is just the ambient temperature. This temperature gradient generates tensions between the inner surface (hot) and external (cold). Thickness, thermal conductivity and hardness are the parameters that determine the resistance or breakage of the nozzle. Some UHTCs, having high thermal conductivity, can easily transfer the heat through the two nozzle parts in order to balance the temperature, thus reducing the thermal stress.

Another application of UHTCs is in the construction of Diesel Particulate Filters [Ref.(68)]. Indeed, they need to be periodically regenerated in order to achieve efficient and safe vehicle operation. Under typical diesel exhaust conditions, this invariably requires the raising of the exhaust gas

temperature by active means, up to the point that particulate oxidation (soot) can be self-sustained in the filter.

Future nuclear applications [Ref. (69)] will potentially include UHTCs, for example, as non-oxide fuels (U/Pu carbides and nitrides) and fuel cladding (TaC, ZrC, HfC). MAX phases may also find application as fuel cladding. Oxide and non-oxide composite (e.g., SiC/SiC) and inert matrix fuel systems are under development for future fission reactors whereas uses of ceramics in fusion reactor systems will be both functional (such as the ceramic superconductors in the magnet systems for controlling the plasma) and structural in various locations outside of the first wall in magnetic confinement fusion.

4.2 Manufacturing process of UHTCs

The materials studied in this work have been produced by ISTEC and UNICA, partners in the project. The UHTCs production process can be schematized as following [Ref.(70),(67)]:

It starts from raw materials reduced to powder so as to increase the specific surface area. The powders are produced from highly selected and pure raw materials mainly including oxides, carbides, nitrides, silicides and borides.

Very high quality powders have to be used. Those are obtainable only through artificial synthesis processes. One of this technique is Self-propagating high-temperature synthesis (SHS) [Ref.(71)].

SHS is a method for producing inorganic compounds by exothermic reactions, usually involving salts or pure metals. SHS is conducted starting from finely powdered reactants that are intimately mixed. They are sintered to minimize their surface area and prevent uninitiated exothermic reactions, which can be dangerous. After reactant preparation, synthesis is initiated by point-heating of a small part (usually the top) of the sample. Once started, a wave of exothermic reaction sweeps through the remaining material. SHS has also been conducted with thin films, liquids, gases, powder–liquid systems, gas suspensions, layered systems, gas-gas systems, and others. Reactions have been conducted in a vacuum and under both inert or reactive gases. The temperature of the reaction can be moderated by the addition of inert salt that absorbs heat in the process of melting or evaporation.

Artificial synthesis processes allow a greater control of both the impurities and the micro structural defects. It is also possible to control different parameters such as the diameter, the shape and the distribution of particle size, which results in a high purity of the obtained powders and the maximum performance of the final material.

The most difficult point is relative to the densification of the material. Typically, this may involve one of the following processes:

- Hot pressing (HP) or hot isostatic pressing (HIP)
- Pressureless sintering (PS)
- Spark plasma sintering (SPS)
- Reactive spark plasma sintering (RSPS)

- Reaction sintering (RS)
- Plasma or vapor deposition technique (PVD)
- Chemical vapor deposition (CVD)
- Microwave Sintering (MS)

HP and **HIP** involve the simultaneous application of pressure and high temperature to promote sintering and densification of the UHTCs at temperatures much lower than it would be in case of ambient pressure. The faster rate of densification has also the advantage of maintaining a smaller grain size of the UHTC material, which enhances its high-temperature mechanical and thermal properties. Another advantage is the using of a smaller quantity of sintering additive respect to PS.

PS is the sintering of compact powders (sometimes at very high temperatures, depending on the powders) without applied pressure. This avoids density variations in the final component, which occurs with HP method. This technique involves significant quantities of sintering additives, coupled with control of the atmosphere to strip the powders of inhibiting oxides prior to either liquid phase or solid state sintering. With careful selection of additives and the processing of raw materials, densities close to theoretical can be achieved.

SPS is a technique in which external pressure and an electric current are applied simultaneously to enhance the densification of the metallic/ceramic powder compacts. It has been found to play a dominant role in the densification of powder compacts, which results in achieving near theoretical density at lower sintering temperature compared to other conventional sintering techniques. The heat generation is internal, in contrast to the conventional HP, where the heat is provided by external heating elements. This facilitates a very high heating or cooling rate (up to 1000 K/min). This allows even faster sintering. Both SPS and HP techniques are currently able to produce a limited range of simple shapes, hence expensive machining processes are required to generate complex engineering components. The same technology can be also used to make reaction synthesis and densification in one single processing step, by the so-called Reactive SPS (**RSPS**), starting from appropriate elemental reactants [Ref.(72)].

RS and **PVD** rely on the in situ formation of the UHTC via chemical reaction. In RS, a solid compact is converted into the UHTC via either solid state or vapor phase reaction. The material formed in this way is often limited in density. PVD and RS techniques both produce coatings on a substrate and offer an efficient way to concentrate the UHTC material on the component surface where it is needed. Plasma coating involves melting the material in a gas plasma before propelling it at high velocity onto a substrate where it cools and solidifies. Plasma sprayed coatings are characterized by a high concentration of defects, which can serve to enhance thermal insulation resistance to rapid temperature changes.

CVD, on the other hand, uses chemical reactions between gases to directly deposit material onto a substrate. In this case, the coating is generally dense and defect-free and potentially more resistant to corrosion and oxidation than a sprayed coating.

MS. In microwave sintering, heat is generated internally within the material, as in SPS, rather than via radiative heat transfer from an external heat source. Other benefits of MS are a better heat diffusion, less time needed to reach the sintering temperature, less heating energy required and improvements in the product properties.

Each technique has its pros and cons. The key to the success of UHTCs lies in the ability to generate denser materials with high quality microstructures. Toward this end, several development programs are currently under way. They are focused not only on the materials, but also on the fabrication technologies required to produce high quality, cost-effective components.

The sintering allows transforming the material into a very dense compound with a high packing factor, or, depending on the duration of this process, it is possible to control the density of the material that will form, in the range 60-100% of the theoretical density [Ref.(73)].

In UHTCs materials the atoms or ions are arranged in such a way as to form a crystalline or amorphous structure and the type of bonds that form between them, whether ionic or covalent, affect the physical parameters of the final product.

4.3 UHTCs as Solar absorbers

There are various types of solar absorbers, different in shape, structure and composition. Typically, a receiver is composed of a substrate coated with other materials that have the purpose to protect it from phenomena of degradation (oxidation, hydrolysis or corrosion by atmospheric dust) and to improve the optical characteristics of absorptance and spectral selection.

In this thesis, it has been studied "intrinsic materials" (bulk), without any type of coating. The latter may increase the performance in view of a possible industrial application.

The structure of a receiver depends on the type of concentrator associated to it (parabolic, heliostat, etc.), from the working temperature, and the heat transfer fluid. In CSP-T and CSP-D, the concentration factor reaches about 100-1000 times the normal solar flux and consequently the receiver must have shape and composition suitable to support such thermal stress. Moreover, this shape must allow a good heat exchange with the heat transfer fluid.

To date, the research on CSP-T receivers has been mainly focused on silicon carbide (SiC) [Ref.(74),(75)] and alumina (Al_2O_3) [Ref.(31)]. However, both these materials show serious drawbacks. SiC is a grey semiconductor with good solar absorbance and high oxidation resistance, but also high thermal emittance arising in large thermal losses at high temperature. On the other hand, Al_2O_3 is characterized by high refractoriness, high thermal stability and oxidation resistance, but, being white, also by very poor sunlight absorption properties. Thus, grey low-emissive and intrinsically spectrally selective UHTCs have a great potential for solar applications, once their properties would be carefully characterized and weaknesses addressed.

It should be reveal in advance that UHTCs in general are typically characterized by absorptance values lower than those of SiC, even if significantly higher than those of white absorbers e.g. alumina. However, it has been recently demonstrated, for the case of HfC [Ref.(76)], that proper surface treatments or surface texturing can significantly increase solar absorptance.

4.4 Studied Materials

Some of UHTCs samples have been studied, for different compositions and structural parameters, at room temperature and at high temperature, following the experimental procedures described in Chapter 3.

ISTEC and UNICA have produced the materials, disk shape, 40 mm diameter and 2 mm thickness, in order to be able to perform the optical and thermo-mechanical characterization measurements. Figure 19 shows one of the samples.

Figure 19 : Example of studied UHTC sample

The samples studied are carbides and borides and were obtained with different sintering techniques, grade of porosity, secondary phases, etc. The main characteristics of the materials studied are the following:

4.4.1 Borides

Zirconium diboride (ZrB_2). It is a highly refractory material with a type of hexagonal crystalline structure. It has a melting point of 3246 °C and its maximum density is about 6.09 g/cm^3. Various ceramic samples made from this material have been produced at different degrees of porosity and quantity of the sintering aid. During the sintering process of ZrB_2 the covalent nature of the material and the presence of surface oxides increase the size of the grains hindering consequently the spread of these. For this reason, generally the ZrB_2 is obtained by HP and then worked to shape it. The PS sintering of ZrB_2 is still possible using sintering additives that react with the oxides formed on the surface of the grains, preventing the increase in size. The ZrB_2 samples created by ISTEC were produced using particles of diameter 5-9 μm, with $MoSi_2$ as sintering additive.

Hafnium diboride (HfB_2). It has a melting temperature of about 3250°C. It has high thermal and electrical conductivities, properties it shares with ZrB_2. HfB_2 has a hexagonal crystal structure, a molar mass of 200.11 gr/mol, and a density of 10.5 g/cm^3. HP technique commonly forms it.

Tantalum diboride (TaB_2). It is a highly refractory material with a type of hexagonal crystalline structure. It has a melting point >3000°C and its maximum density is about 11.15 g/cm^3. This material are stable to oxidation below 700 °C and to acid corrosion.

Most of the properties of borides, such as hardness, depend on the manufacturing process and the microstructure, whereas the thermal conductivity is an intrinsic property of the material and for example, in the case of ZrB_2 and HfB_2 is close to that of copper at room temperature with little variation up to 2500 °C. The high thermal conductivity and the high melting points make borides promising materials for the construction of solar receivers.

Oxidation resistance of Borides

The primary research interest on borides by INO-CNR, UNICA and ISTEC was primarily focused on improving the oxidation resistance at high temperatures, especially regarding ZrB_2 and HfB_2, keeping good optical performances.

The oxidation depends on temperature and pressure. For example, at temperature 1500 °C and pressure 1atm, in HfB_2 it forms a layer of various types of oxides on the surface.

When the temperature exceeds 1600 °C and the pressure drops below 1atm, the oxidation resistance of HfB_2 and ZrB_2 is drastically reduced [Ref.(15)].

The presence of a silica-based sintering additive does greatly increase their oxidation resistance due to the formation of a borosilicate glass on the surface of the material, which prevents the diffusion of oxygen in the bulk material. It has been found that an optimal composition of ZrB_2 + 10%vol $MoSi_2$, produces a good oxidation resistance up to 2000 °C [Ref.(77)].

4.4.2 Carbides

Zirconium Carbide (ZrC). Zirconium carbide is made by carbothermic reduction of zirconia by graphite. Densified ZrC is made by sintering powder of ZrC at upwards of 2000 °C. HP of ZrC can bring down the sintering temperature consequently helps in producing fine grained fully densified ZrC. SPS also has been used to produce fully densified ZrC.

Poor oxidation resistance over 800 °C limits the applications of ZrC. One way to improve the oxidation resistance of ZrC is to make composites. Important composites proposed are ZrC-ZrB_2 and ZrC-ZrB_2-SiC composite. These composites can work up to 1800 °C.

Due to the presence of metallic bonding, ZrC has a thermal conductivity of 20.5 W/m·K and an electrical conductivity (resistivity ~43 μΩ·cm), both of which are similar to that for zirconium metal. The strong covalent Zr-C bond gives this material a very high melting point (~3530 °C), high modulus (~440 GPa) and hardness (25 GPa). ZrC has a lower density (6.73 g/cm^3) compared to other carbides like WC (15.8 g/cm^3), TaC (14.5 g/cm^3) or HfC (12.67 g/cm^3)

Hafnium Carbide (HfC). Hafnium carbide is usually carbon deficient and therefore its composition is often expressed as HfC_x (x = 0.5 to 1.0). It has a cubic (rock-salt) crystal structure at any value of x. Hafnium carbide powder is obtained by the reduction of hafnium (IV) oxide with carbon at 1800 to 2000 °C. A long processing time is required to remove all oxygen. Alternatively, high-purity HfC coatings can be obtained by CVD from a gas mixture of methane, hydrogen, and vaporized hafnium (IV) chloride. HfC has a melting point of about 3900°C. However, it has a low oxidation resistance, with the oxidation starting at temperatures as low as 430 °C.

Tantalum Carbide (TaC). TaC_x powders of desired composition are prepared by heating a mixture of tantalum and graphite powders in vacuum or inert gas atmosphere (argon). TaC_x compounds have a cubic (rock-salt) crystal structure, as HfC, for x = 0.7–1.0. TaC_x has a melting point about 3800°C and its maximum density is about 14.50 g/cm^3. This material are stable to oxidation below 700 °C and to acid corrosion.

Oxidation resistance of Carbides

The main weakness of carbides in general is their poor resistance to oxidation, so they are primarily proposed, as solar absorbers, for operation under inert atmosphere or in vacuum, like in the device described in [Ref.(78)].

However, it should be emphasized that the introduction of secondary phases able to produce silica-based glass (like SiC, $MoSi_2$, $TaSi_2$, and all transition-metal silicides) greatly improves their oxidation resistance [Ref.(79),(80)].

5. Results

The spectral emissivity curves, obtained at room temperature, have been interpreted by putting them in relation with the characteristics of the material such as: composition, porosity, surface finish, and other, in order to choose the most advantageous combination of parameters and to understand any dependencies of these curves from these parameters.

Some samples have also been studied at high temperature with the experimental technique explained in paragraphs 3.2, 3.3. In these conditions the measurements allow an assessment of the actual performance of the materials at the operating temperatures, above 1000 °C, of new generations of solar concentration plants.

5.1 Dense Zirconium, Hafnium and Tantalum borides

Purpose

In this section, it is reported a comparative characterization of ZrB_2, HfB_2 and TaB_2, produced by HP and PS techniques. It is investigated how sintering technique and starting powders composition affect the optical properties of final materials. Additional characterization of the materials such as microstructure, roughness, secondary phases and mechanical properties can be found on [Ref.(81)].

Studied Materials

Commercial powders were used for the preparation of the materials:

- hexagonal **ZrB_2** (H. C. Starck, Germany. Grade B). Mean particle size: 1.5 μm, impurities (wt%): C 0.25, O 2.0, N 0.25, Fe 0.1, Hf 0.2;
- hexagonal **HfB_2** (Cerac Inc., Milwaukee, USA). Mean particle size: 2.2 μm, impurities (wt%): Al 0.001, Fe 0.002, Zr < 0.5;
- hexagonal **TaB_2** (Materion Adv. Chemicals, Milwaukee, USA). Mean particle size: 0.9 μm, impurities (wt%): Al 0.04, Cd < 0.0007, Cr < 0.0005, Fe 0.07, Nb 0.02, Pb < 0.0004;
- tetragonal **$MoSi_2$** (Aldrich, Milwaukee, USA). Mean particle size: 2.8 μm, impurities (wt%): O 1.0.

Some samples have been sintered through HP with 10 vol% of $MoSi_2$, and other samples have been densified by PS with 20 vol% of $MoSi_2$ (samples listed in Table 1).

Label	Matrix	$MoSi_2$ (vol%)	Sintering	T, t, P (°C,min,MPa)	Final ρ (g/cm^3)	Rel. ρ (%)	Pores (%)	m.g.s. (µm)	Max g.s. (µm)	Min g.s. (µm)	Secondary phases by SEM-EDS (vol%)
ZBM10	ZrB_2	10	HP	1850, 10, 20	6.1	98.3	3.7	2.4±0.6	3.9	1.4	10 $MoSi_2$, 1.4 SiO_2, 0.7 SiC
ZBM20		20	PS	1950, 60, -	6.1	99.0	0.8	2.6±0.7	4.1	1.3	18 $MoSi_2$, 2 MoB, 0.5 SiO_2
HBM10	HfB_2	10	HP	1900, 8, 30	10.1	96.4	0	0.8±0.3	0.3	2.3	5 $MoSi_2$, 3 HfO_2, 2 SiO_2
HBM20		20	PS	1950, 60, -	10.0	98.0	1.4	1.4±0.8	4.9	0.4	15 $MoSi_2$, 2 Mo_5Si_3, 0.5 HfO_2
TBM10	TaB_2	10	HP	1690, 10, 30-40	10.2	95.4	1.3	3.8±1.1	6.7	1.7	3 $MoSi_2$, 9 SiO_2/SiC
TBM20		20	PS	2100, 180, -	9.2	(90.4) 97.0	3.0	38.4±13.6	84.2	13.6	10 $MoSi_2$, 8 Si, 4 SiC

*Table 1: Composition, sintering parameters (**T**: maximum temperature, **t**:dwell at T, **P**:applied pressure), final and relative densities (**ρ**), mean grain size (**m.g.s.**), smallest (**Min g.s.**) and largest (**Max g.s.**) grain size and secondary phases of the borides sintered with $MoSi_2$.*

Optical characterization

Figure 20 compares the hemispherical reflectance spectra of the different materials as a function of the sintering technique.

For ZrB_2 (Figure 20a) the two investigated samples have very similar spectra, with absolute reflectance differences lower than 3%. ZBM10 has a slightly higher reflectance than ZBM20 in the infrared above 2µm, while the reflectance value of ZBM20 is the highest at shorter wavelengths.

Also in the case of HfB_2 (Figure 20b) the samples show similar curves. The largest difference among them lies in the region about 2.8µm (about 10% difference in hemispherical reflectance), where HBM20 shows a minimum due to higher amount of residual $MoSi_2$, as it can be easily recognized by comparing the boride spectra to that of a reference $MoSi_2$ specimen.

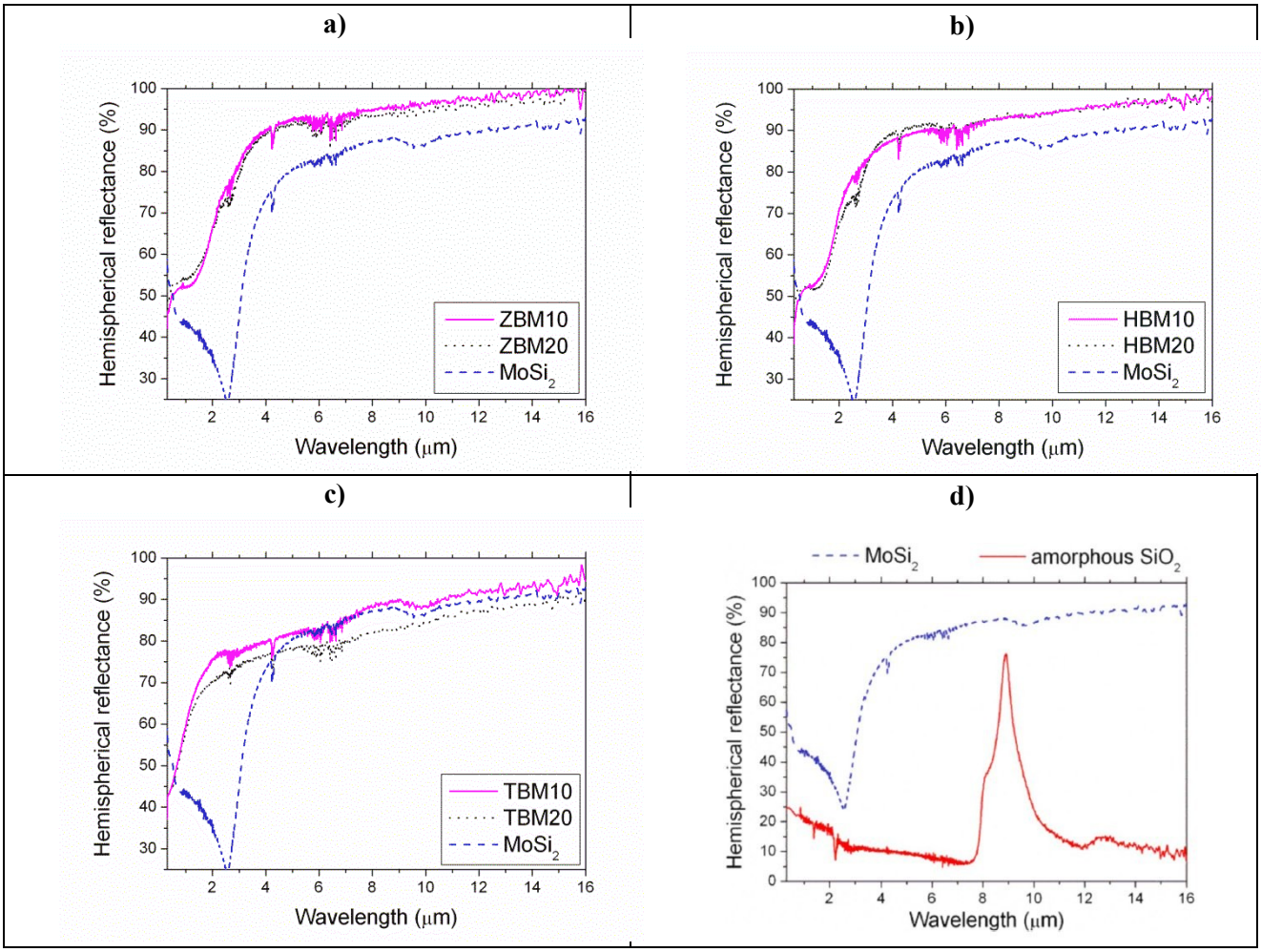

Figure 20: Comparison of hemispherical reflectance spectra of different borides as a function of additive amount. The spectra of $MoSi_2$ and SiO_2 are also shown for reference. a)ZrB_2, b)HfB_2, c)TaB_2, d)$MoSi_2$ and SiO_2 reflectance spectra

As for spectral signatures of secondary phases, we should notice that $MoSi_2$ itself shows SiO_2 impurities. If we compare the spectrum of $MoSi_2$/ SiO_2 with that of pure SiO_2, we can tentatively assign to SiO_2 secondary phase the small feature in the $MoSi_2$ spectrum at around 9μm (Figure 20d).

As we will detail in the following, this attribution allows fairly well explaining the spectra of borides.

If we consider TaB_2 (Figure 20c), the two samples show larger differences among them, likely due to the considerable difference in their roughness values (57 vs 257 μm Ra for TBM10 and TBM20, respectively [Ref.(81)]). If we compared the acquired curves for borides and pure $MoSi_2$, (the small slope change at around 2.8μm, likely connected to the minimum in the $MoSi_2$ spectrum).

The shoulder at around 9μm in TBM10, which appears to be more pronounced than the $MoSi_2$ dip at 2.8μm and is absent in TBM20, can thus be ascribed to SiO_2 rather than to the $MoSi_2$. In fact, compositional analysis reveals SiO_2 in TBM10 (9 vol% SiO_2, Table 1).

Coherently to microstructural analysis, SiO_2 peak is not shown in the spectrum of TBM20. However, for PS TaB_2 (TBM20), the spectral signature of $MoSi_2$ is more pronounced. Indeed, according to microstructural analysis, it has a higher $MoSi_2$ content than the corresponding HP specimen (10 vol% VS 3 vol%).

Spectral signals coming from other secondary phases like SiC, which should be recognized by a feature at around 12μm [Ref.(82)], cannot be detected. This could be likely due to the notably higher roughness of this sample, arising in a generally lower reflectance hiding small spectral features.

Figure 21 compares the spectra of different materials for fixed processing technique, i.e. for fixed $MoSi_2$ amount. We can appreciate that the spectral shapes of ZrB_2 and HfB_2 curves are very similar and TaB_2 always has the lowest reflectance for wavelengths longer than about 2μm and shorter than about 1μm, while in the intermediate region 1-2μm its reflectance is by far the highest.

The feature at around 9μm is significant only in HP TaB_2 (TBM10), in agreement with its much higher SiO_2 content than the other HP materials. As for HfB_2 and ZrB_2, the more pronounced shoulder at around 2.8μm of PS samples, with respect to HP specimens, agrees with their higher $MoSi_2$ content, see Table 1.

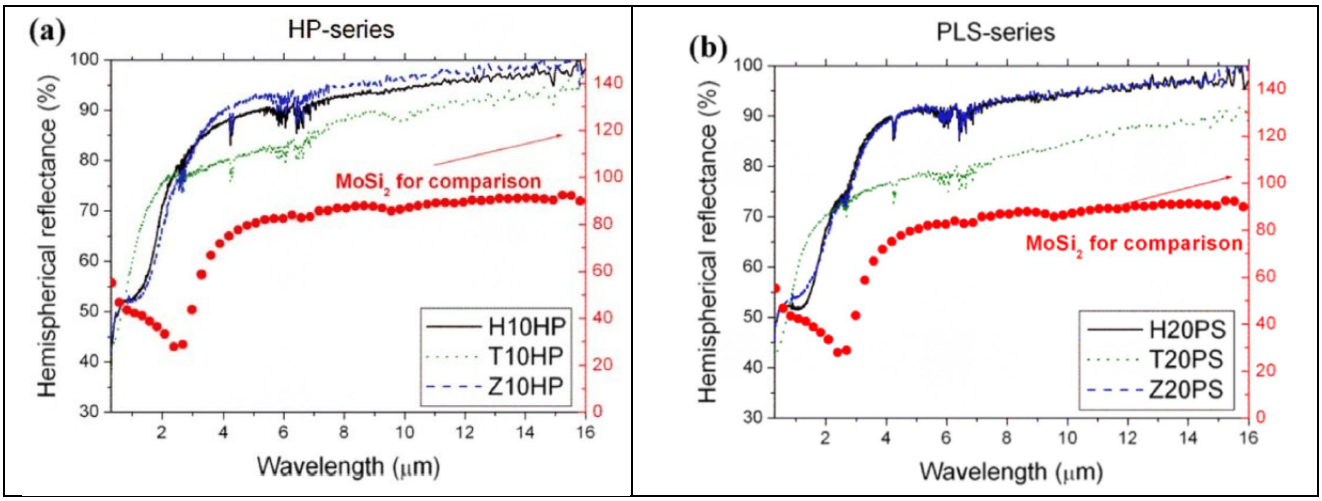

Figure 21: Comparison of hemispherical reflectance spectra of different borides for fixed sintering aid content. The spectrum of $MoSi_2$ is also shown for reference and referred to a different scale (right axis, where physically meaningless labels higher than 100% are shown only for visualization purposes)

Performance evaluation as solar absorbers

From the experimental hemispherical reflectance ε_{int} and α_{int} (paragraph 3.1.2) have been calculated (Parameters used: T=1200K, λ_1=0.3μm, λ_2=16.0μm).

Figure 22 compares the calculated *selectivity Index* as a function of processing technique. The variability range lies between 1.9 and 2.6. For a given material, HP samples (10vol% $MoSi_2$) always show a slightly higher *selectivity index* value than PS ones (20 vol% $MoSi_2$). ZrB_2 and HfB_2 are similarly performing, while *selectivity Index* for TaB_2 is generally lower.

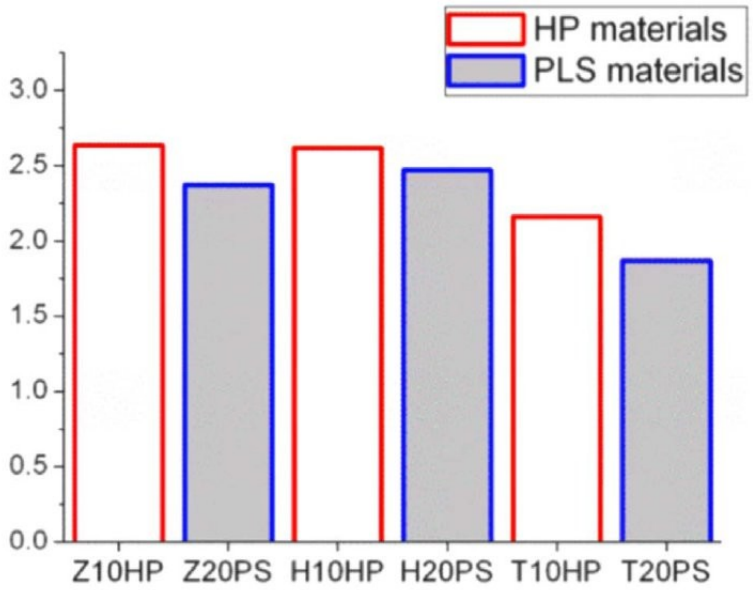

Figure 22: Calculated Selectivity Index for materials produced with different processing techniques.

Summarizing

PS specimens typically display larger grain size, rougher surface, lower fracture strength [Ref.(81)] and slightly worse optical performances (lower *selectivity index*) than the corresponding HP samples, but the high temperature strength is generally better, thanks to elimination of residual SiO_2 in the as-sintered microstructure.

5.2 Dense ZrB_2: Effect of amount of sintering aid

Purpose

This section reports on a comparative characterization of ZrB_2 obtained with different amounts of $MoSi_2$ sintering aid, investigating how sintering technique affects the optical properties of final materials. Additional characterization of the materials such as microstructure, roughness, secondary phases and mechanical properties can be found on [Ref.(81)].

Studied Materials

A series of ZrB_2 samples containing $MoSi_2$ from 5 to 50 vol% were prepared by HP (samples listed in Table 2). The powers used are the same listed in the previous paragraph. All the samples have been densified to the maximum obtainable density.

Label	Matrix	$MoSi_2$ vol%	T,t,P (°C,min,MPa)	Final ρ (g/cm^3)	Rel. ρ (%)	Pores (%)	m.g.s. (µm)	Max g.s. (µm)	Min g.s. (µm)	Secondary phases by SEM-EDS (vol%)
Z5HP	ZrB_2	5	1900, 10, 30	5.96	97.5	0.2	1.9±0.7	3.6	0.9	1.4 $MoSi_2$, 1.5 SiO_2/SiC
Z10HP		10	1850, 10, 30	6.1	98.3	3.7	2.4±0.6	3.9	1.4	10 $MoSi_2$, 1.4 SiO_2, 0.7 SiC
Z20HP		20	1800, 4, 30	5.89	95.8	0.1	2.4±0.9	5.4	0.6	13 $MoSi_2$, 2.5 SiO_2, 2.0 SiC, 0.7 $ZrO_2$2, 0.6 MoB
Z30HP		30	1850, 3, 30	5.95	96.5	0.2	1.7±0.6	3.6	0.6	28.4 $MoSi_2$, 3.4 SiO_2/SiC
Z50HP		50	1750, 13, 30	5.89	94.9	0.3	1.9±0.8	4.3	0.7	39 $MoSi_2$, 6.5 SiO_2, 2 MoB, 1 ZrO_2, 1 SiC

*Table 2: Composition, sintering parameters (**T**: maximum temperature, **t**:dwell at T, **P**:applied pressure), final and relative densities (**ρ**), mean, maximum and minimum grain size (**m.g.s.**) and secondary phases of the ZrB_2 based composites sintered by HP with increasing amount of $MoSi_2$*

Optical characterization

Figure 23a shows the spectra of the various hot pressed ZrB_2 samples as a function of the sintering aid amount, ranging from 5 to 50 vol% in the nominal composition. In the sample with the lowest $MoSi_2$ amount, no $MoSi_2$ or SiO_2 signals are detected, in agreement with the very low content proved by microstructural analysis (Table 2). As the original composition is enriched in $MoSi_2$, $MoSi_2$ signature starts to appear in the spectra and progressively increases proportionally. Similarly, the peak attributed to SiO_2 increases in intensity, in agreement with the increasing of SiO_2 phase content from Z20HP to Z50HP.

It is interesting to notice (Figure 23b) that the reflectance curve of Z50HP can be fairly reproduced by a linear combination of almost pure ZrB_2 (Z5HP) and reference $MoSi_2$ (with SiO_2 impurities) in a rough 1:1 ratio.

Finally, in Figure 23c there are the spectra of two ZrB_2 samples with the same nominal composition, but produced with different techniques. It can be appreciate that both curves show the $MoSi_2$ dip and that the sample produced by the HP technique (Z20HP) is characterized by a lower reflectance in the whole spectral region. For wavelengths shorter than 6µm, the two curves are roughly parallel. This behavior cannot be explained neither by the different roughness, as the sample with the (even slightly) higher roughness also shows the highest reflectance, neither by the different $MoSi_2$ content, as the impact of the $MoSi_2$ dip on the spectra is similar and, again, the sample containing a higher amount of $MoSi_2$ (18% VS 13%) shows the highest reflectance, neither, finally, by different grain size, because grain sizes are also similar. The parameter most significantly changing from Z20PS and Z20HP samples is the SiO_2 content (0.5% vs 2.5%) and allows explaining the experimental curves. In fact, the reflectance is lower in the sample containing

a larger amount of SiO_2, because SiO_2 (whose shoulder at 9μm can be clearly recognized in Z20HP) is characterized by very low reflectance values in spectral regions outside its vibrational peaks (Figure 20d).

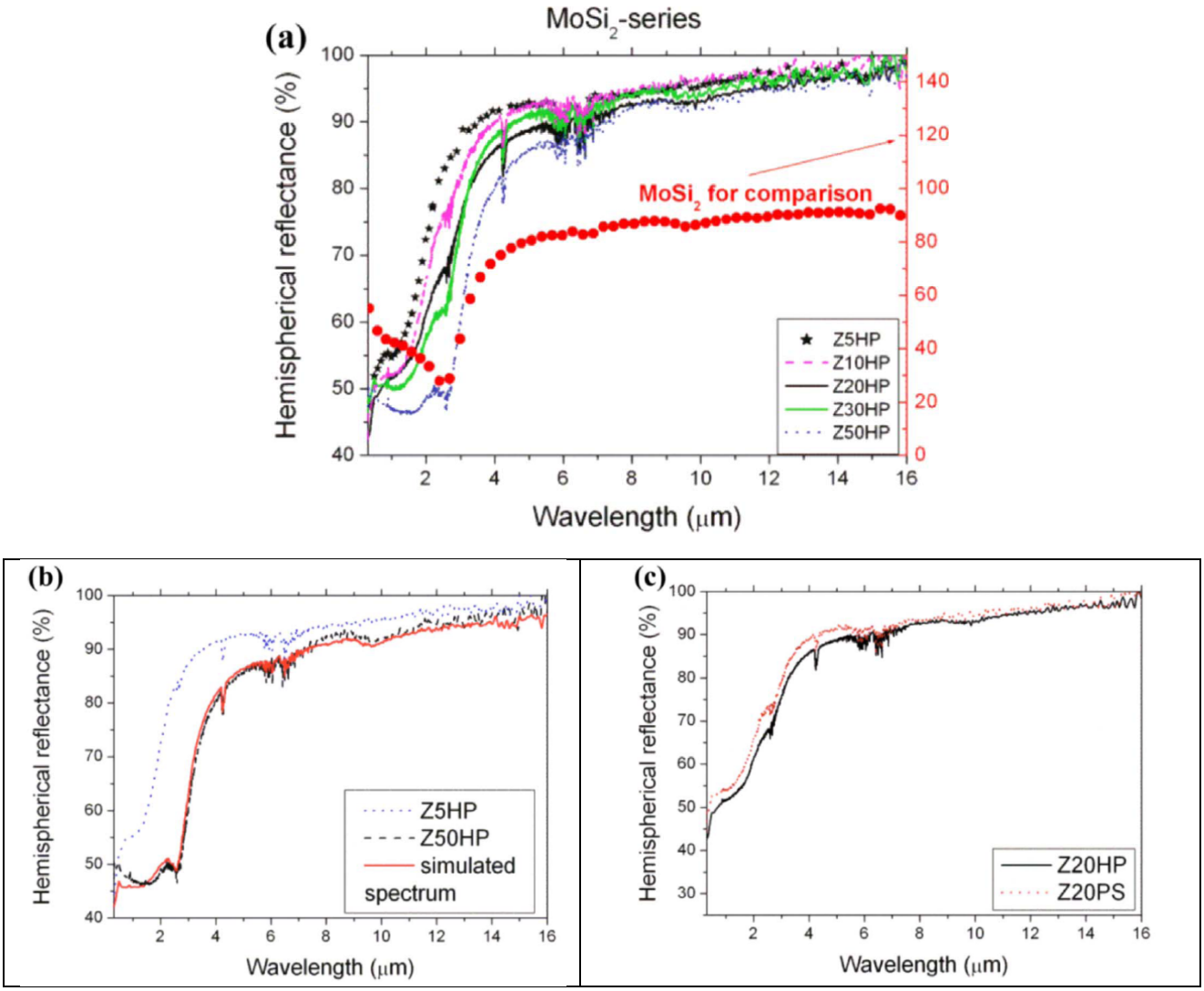

Figure 23: a) Hemispherical reflectance spectra of hot pressed ZrB_2 as a function of increasing $MoSi_2$ content. b) Tentative simulation of the sample spectrum Z50HP, demonstrating the impact of $MoSi_2$ on its surface. c) Spectra of ZrB_2 samples containing 20 vol% of $MoSi_2$ produced with different processing techniques.

Performance evaluation as solar absorbers

From the experimental hemispherical reflectance ε_{int} and α_{int} (paragraph 3.1.2) have been calculated (Parameters used: T=1200K, λ_1=0.3μm, λ_2=16.0μm).

Figure 24 shows the calculated *selectivity Index* values for hot pressed ZrB_2 as a function of the nominal $MoSi_2$ content.

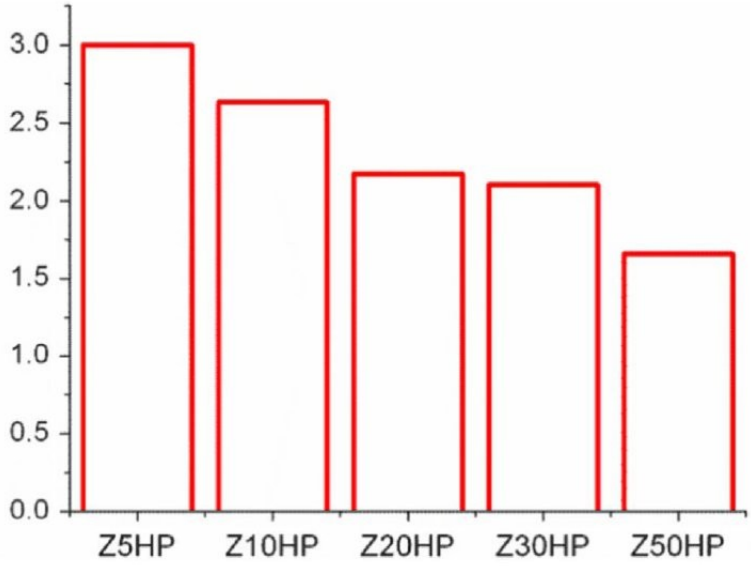

Figure 24: Calculated Selectivity Index for HP ZrB_2 samples.

The trend in Figure 24 is immediately evident, suggesting that, at least for the investigated boride matrix, the worsening of spectral selectivity it is due to the increasing content of $MoSi_2$ and related secondary phases.

Summarizing

For ZrB_2 produced through high-pressure method, it is studied the effect of the $MoSi_2$ nominal content, ranging from 5 to 50vol%, on the optical properties. Effects in the microstructural, roughness, and mechanical properties are reported on [Ref.(81)].

Thus, for future solar absorber applications, the addition of $MoSi_2$ sintering aid should be not higher than 10vol% in order to ensure good sinterability and oxidation protection at high temperature.

5.3 Dense Zirconium and Hafnium borides VS Silicon Carbide

Purpose

The aim is to compare two samples of dense ZrB_2 and HfB_2 with a sample of SiC, the material currently used in the development of solar absorbers at high temperature.

Studied Materials

Dense ZrB_2 and HfB_2 samples were prepared with $MoSi_2$ as sintering aid, with a typical content of 5 to 10 vol% starting from commercial powders listed in paragraph 5.1. For reference, a SiC sample was also obtained by sintering at 1800°C, with a small percentage of alumina and yttria as sintering aids.

Optical characterization

The room-temperature hemispherical reflectance spectra of dense ZrB_2 and HfB_2 samples are shown in Figure 25, for polished samples. Borides are characterized by a high reflectance plateau, for this reason it is expected a low thermal emittance, as confirmed by the high-temperature experiments described below.

On the contrary, SiC shows a reflectance lower than 20% for wavelengths shorter than 10.5μm and a single high-reflectance peak in the range 11-13μm (about 90% reflectance), with a quickly decreasing reflectance for longer wavelengths (the reflectance is already dropped to about 40% at 14μm).

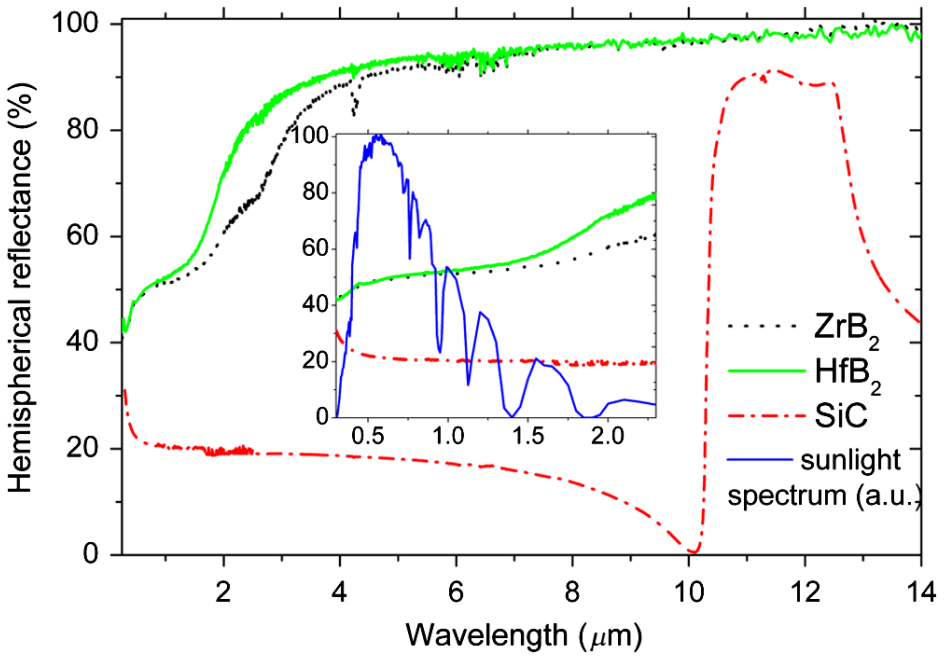

Figure 25: Reflectance curves of almost fully dense ZrB_2, HfB_2, and SiC samples

Performance evaluation as solar absorbers

In the wavelength region of the solar spectrum (see inset of Figure 25), SiC has a higher solar absorbance, but the boride samples still are good absorbers (reflectance about 50% in the range 500 to 900 nm, where the sunlight spectral irradiance is maximum). The measured hemispherical reflectance allows the calculation of the α_{int} and ε_{int}.

The obtained values of α_{int} for the two borides are very similar (0.49 for ZrB_2 and 0.48 for HfB_2, while α_{int} for SiC is 0.78.

The obtained values of the calculated *selectivity index* is about 2 for ZrB_2, about 2.5 for HfB_2, and about 1 for SiC.

High Temperature characterization

The measured total hemispherical emittance at high temperature (MEDIASE) is shown in Figure 26. The two investigated borides show similar emittance values and the favorable emittance characteristics of borides over SiC are immediately evident. Indeed, it is about a half of that of SiC. A similar temperature dependence of emittance between ZrB_2 and HfB_2 can be inferred in the temperature region where the measurement ranges on the two samples are superimposed. Moreover for HfB_2, which has been investigated up to 1636K temperature, the maximum measured emittance value is as low as 0.47. The obtained results show that boride UHTCs are promising for novel solar absorbers especially after a treatment aimed at increasing the absorbance.

The hemispherical emittance of samples has been investigated also in the different spectral bands available: 0.6-40µm, 0.6-2.8µm, 8-14µm, 2.7µm, 5µm, 5.5µm.

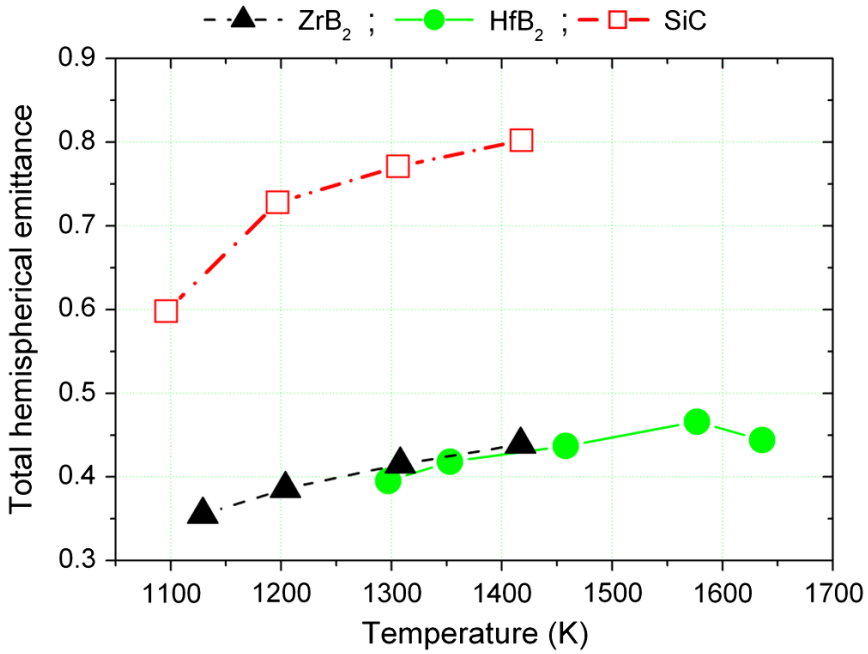

Figure 26: Total hemispherical emittance of dense samples as a function of the temperature

Figure 27 shows the temperature dependence of the emittance in the considered bands as a function of the temperature. For a visual evaluation of the relative weight of the different contributions of the various spectral bands to the whole wavelength range, Figure 28 and Figure 29 show the histogram of the hemispherical emissivity of the boride samples measured in the considered spectral bands.

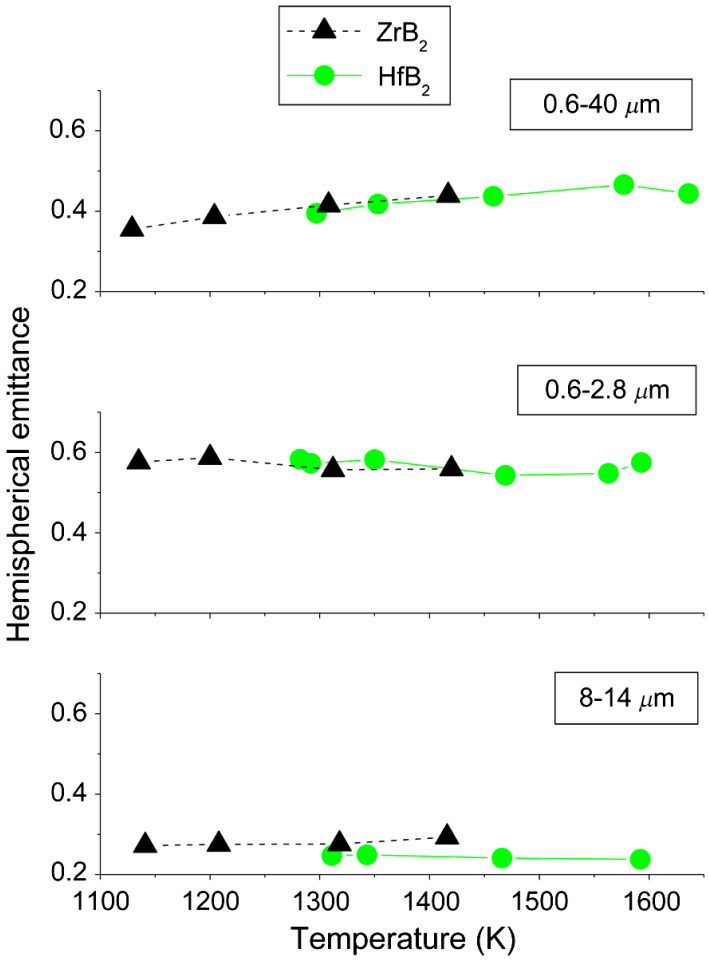

Figure 27: Temperature dependence of the hemispherical emittance measured in the various spectral bands

Abscissas in Figure 28 and Figure 29 correspond to the width of the spectral range relative to each measurement. From the definition of emittance [paragraph 2.3], the measured emittance in the range (λ_1; λ_2) represents the mean emittance value in the considered range. Therefore, by comparing the relative values measured in the different spectral bands, information about the spectral dependence of the emittance curve can be obtained.

From Figure 27 to Figure 29, the main contribution to the emittance is given by radiation emitted by the samples at wavelengths shorter than 2.8 μm, whereas at longer wavelengths, in the range 8 to 14 μm, the emittance is very low and considerably lower than the "total" 0.6-40μm value. Therefore, as a general consideration, we can infer that borides have a spectral distribution of emitted light more peaked toward shorter wavelengths and with a lower long wavelength tail with respect to a blackbody at the same temperature.

Comparing ZrB_2 and HfB_2, the emittance of the two samples are similar in all the investigated bands, with HfB_2 having a slightly lower emittance in the 8-14μm wavelength range.

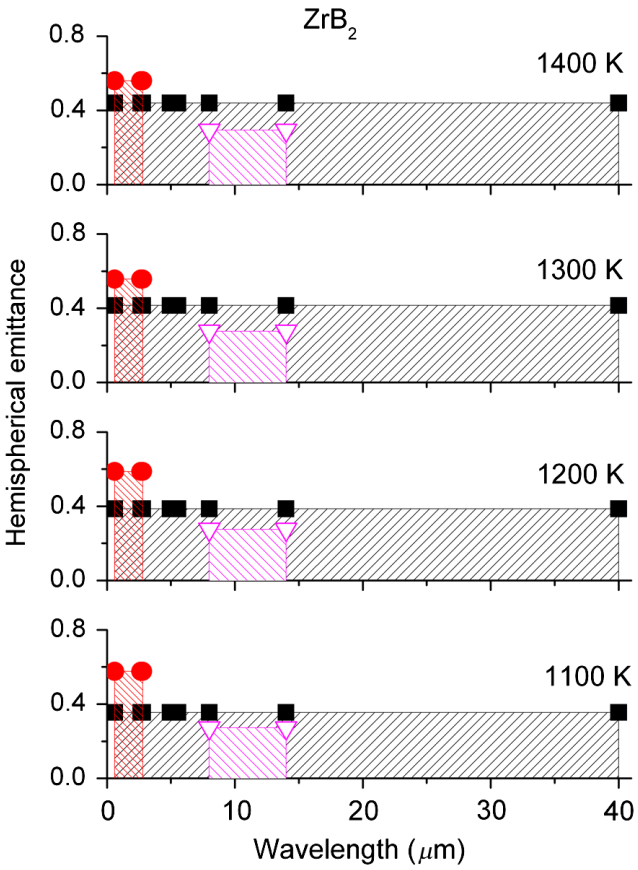

Figure 28: Histogram of the measured emittance in the various bands for ZrB_2

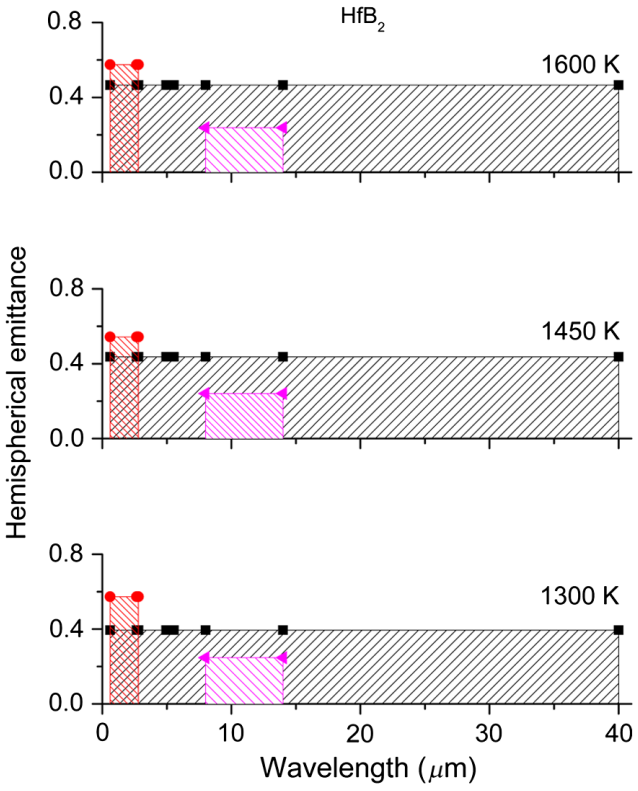

Figure 29: Histogram of the measured emittance in the various bands for HfB_2

As for the temperature dependence of the spectral band emission for both borides, as the temperature increases the emittance in the whole 0.6-40μm range increases as well, while that in the bands 0.6-2.8 and 8-14μm remains almost constant.

This seems to suggest, as the temperature increases, a corresponding increase of the emission spectrum of samples in the 14-40μm wavelength range, with an expected slightly larger increase for HfB_2 with respect to ZrB_2.

Summarizing

Both the considered borides show good spectral selectivity properties and a thermal emittance considerably lower than that of silicon carbide, which is a material currently under development as solar absorber. High temperature emittance measurements in different spectral bands allow to infer, for both borides, similar high-temperature spectra, with a blue shifted thermally emitted light with respect to the blackbody emission.

5.4 Dense Zirconium, Hafnium and Tantalum carbides

Purpose

This section reports on a comparative characterization of ZrC, HfC and TaC, produced by HP and PS techniques and with different amounts of $MoSi_2$ sintering aid, investigating how sintering technique and starting powders composition affect the optical properties of final materials. Additional characterization of the materials such as microstructure, roughness, secondary phases, and mechanical properties can be found on [Ref.(83)].

Studied Materials

Commercial powders were used for the preparation of the materials listed in Table 3:

- cubic **ZrC** (Grade B, H.C. Starck, Germany). Mean grain size 3.8 μm, impurities (wt%) C:1.5, O:0.6, N:0.8, Fe:0.05, Hf:2.0;
- cubic **HfC** (Cerac Inc., USA). Mean grain size 1.04 μm, impurities (wt%) Zr:<0.6, O:0.35, Cd:0.002;
- cubic **TaC** (Cerac Inc., USA). Mean grain size 1.21 μm, impurities (wt%) Ti:0.04, Nb:0.03, Na:0.03, Fe:0.02, Ca:0.01;
- tetragonal MoSi2 (Aldrich, USA). Mean grain size 2.8 μm, impurities (wt%) O:1.

Samples to be sintered by HP contained 10vol% of $MoSi_2$, whilst those densified by PS contained 20 vol% of $MoSi_2$.

Label	Matrix	$MoSi_2$ vol%	Sintering	T, t, P (°C,min,MPa)	Final ρ (g/cm^3)	Rel. ρ (%)	m.g.s. (µm)	Secondary phases by SEM-EDS (vol%)
ZCM10	ZrC	10	HP	1930, 14, 35	6.6	> 99.5	5.1±1.4	1.5 $MoSi_2$, 5 SiC
ZCM20		20	PS	1950, 60, - Ar	6.4	> 97	7.6±2.1	11 $MoSi_2$, 5 SiC, 3 Zr_xSi_y
HCM10	HfC	10	HP	1900, 10, 35	11.79	> 99.5	1.5±0.4	5 SiC, 6 HfO2, 3 $MoSi_2$, 1 Mo_5Si_3
HCM20		20	PS	1950, 60, - Ar	10.36	94	1.9±0.4	5 $MoSi_2$, 1 Hf-Si-C
TCM10	TaC	10	HP	1850, 10, 30	13.28	> 99.5	1.5±0.4	6 $MoSi_2$, 3 SiC/SiO_2
TCM20		20	PS	1950, 60, - Ar	12.66	98.5	5.1±1.5	13 $MoSi_2$, 2 SiC/SiO_2, 1 Ta_xSi_y

*Table 3: Composition, sintering parameters (**T**: temperature, **t**: dwell at T, **P**: applied pressure), final and relative densities (**ρ**), carbide mean grain size (**m.g.s.**), and secondary phases of the carbides sintered with $MoSi_2$.*

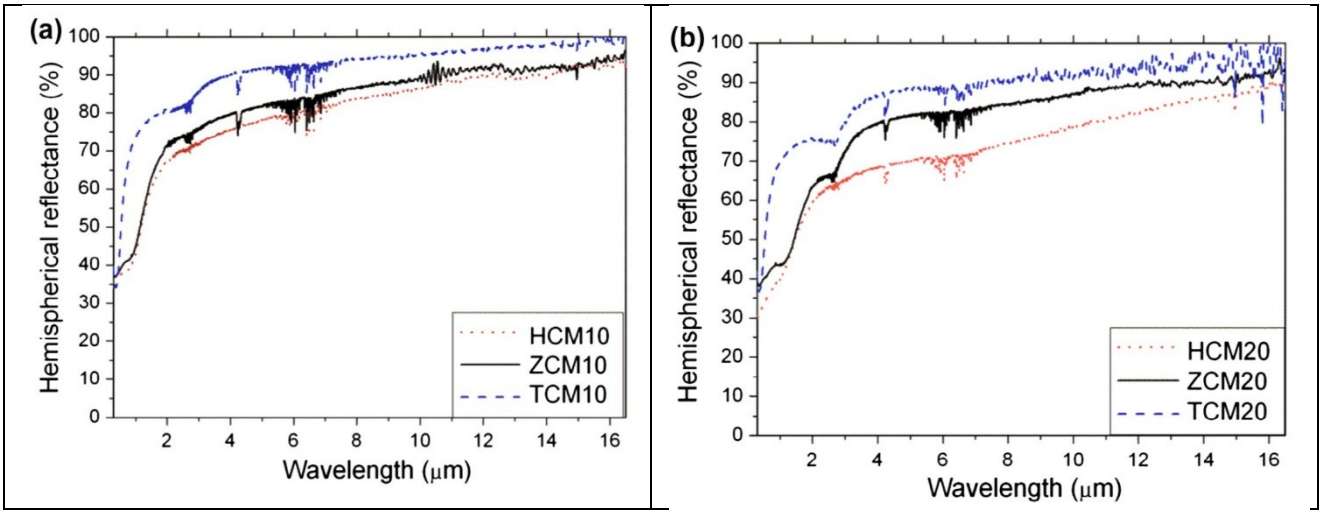

Figure 30: Comparison of hemispherical reflectance spectra of different materials. a) for fixed sintering aid content 10 vol%, b) 20 vol%.

Optical characterization

Figure 30 compares the 10 vol% $MoSi_2$ and 20 vol% $MoSi_2$ samples for the different materials. For both investigated classes (10 and 20 vol% containing $MoSi_2$, corresponding to HP and PS fabrication processes, respectively) reflectance decreases from TaC to ZrC to HfC.

This trend is in agreement with previous studies and is related to the intrinsic radiative properties of the three carbides. For instance, the higher reflectance of ZrC compared to HfC is consistent with lower emissivity of the former measured at higher temperature.

Even if the detailed theoretical interpretation of optical features is out of the scope of this thesis, some basics comments can be made. In fact, the electronic band structure of carbides allows explaining the main characteristics of the observed optical spectra (e.g. the effects of the sample primary phase). However, it should be emphasized that these considerations are forced to be only

qualitative, as defect states due to deviations from stoichiometry and grain boundaries strongly affect the resulting density of states [Ref.(84), (85)]. For instance, the observed high reflectance plateau at long wavelengths is connected to intra-band transitions and described by the Drude model in metal-like materials, while inter-band transitions effects account for the dip in the reflectivity curves [Ref.(85)] and are typically located at lower energies for ZrC and HfC than for TaC [Ref.(84)], thus explaining the relatively better radiative properties of the latter.

The similarity between the electronic density of states of hafnium and zirconium compounds [Ref.(85)] explains the similarity between the spectra of pure ZrC and HfC [Ref.(86)]. In the samples this can be recognized in 10 vol% doped specimens, while, in the 20 vol% ones, it is lost because of roughness/porosity and composition effects.

As regards the effects of surface roughness, it can be observed that the lower Ra (roughness arithmetic average), found for TaC-based materials, is an additional factor explaining the higher reflectance of these ceramics compared to HfC and ZrC. Again, the effect of surface roughness can be observed in the spectra of PS samples, for HfC. In this case, the superficial porosity (12%) notably increased Ra and decreased the reflectance with respect to the corresponding HP samples.

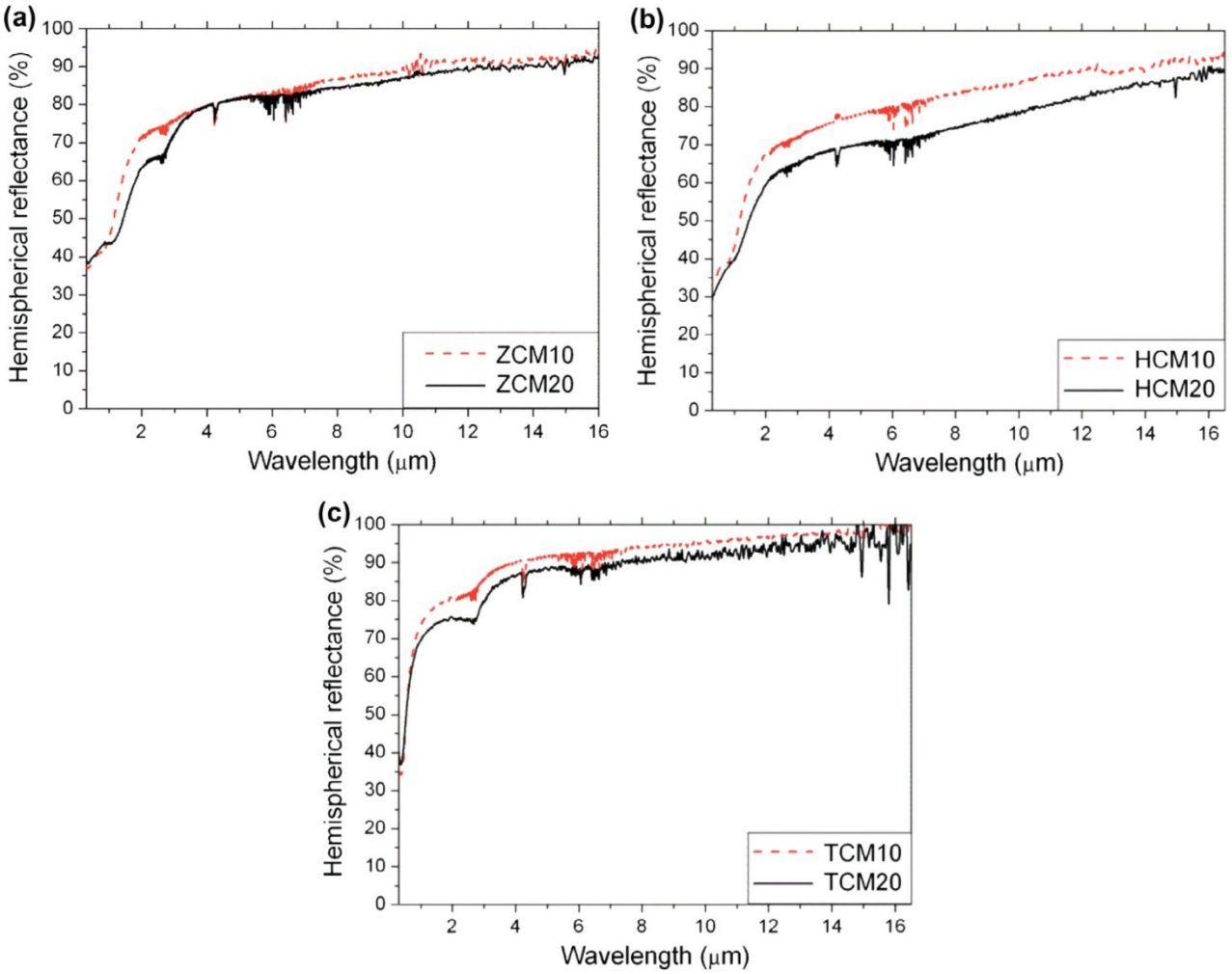

Figure 31: Comparison of hemispherical reflectance spectra of different materials as a function of additive amount

From peculiar features of the spectra, it is possible to infer some compositional information of investigated surfaces. For instance, the presence of $MoSi_2$ in the samples can be recognized from the reflectivity minimum at around 2.7μm, as confirmed by previous studies [Ref.(86)].

This minimum is obviously more pronounced for compositions with 20vol%, rather than for 10 vol% (Figure 31) and it is more evident for TaC-based composites. Indeed, the initial nominal content of $MoSi_2$ is strongly changed after sintering, due to partial conversion of $MoSi_2$ to SiC. In this respect, according to Table 3, TaC-based compositions are those containing the highest amount of residual $MoSi_2$ and PS TCM20 has the highest content.

For HfC-based ceramics, the presence of the 2.7μm shoulder is not very visible due to removal of $MoSi_2$ phase on the surface. On the other hand, the spectral signature of SiC can be often, but not always, recognized by a feature at around 12μm, corresponding to its known Reststrahlen peak [Ref.(82)] and it has been evidenced mainly in ZCM10 and HCM10, in agreement with microstructural analysis [Ref.(83)]. The identification of this peak is not always possible, and a content of 5 vol% seems to be the minimum detectable level in these ceramics. For instance, despite the presence of 5 vol% SiC in ZCM20, the corresponding peak in the spectrum was not recorded.

This could be due to several reasons including the fact that, in this sample, SiC particles had bigger size, but were dispersed discontinuously, compared to ZCM10 where SiC was much finer and homogeneously scattered throughout the surface.

Summarising

To sum up, although the present study deals with three types of carbides where different variables are changing (mean grain size, secondary phase, surface roughness), a general trend is observed: optical spectra are chiefly affected by the intrinsic radiative properties of the ceramics.

The second fundamental parameter affecting the optical spectrum seems to be the surface roughness, even though it does not influence the hierarchy of reflectance among different materials.

Surface roughness is mainly related to the surface porosity, which in turn is determined by the kind of process used. HP materials are always denser than PS ones, thus having a lower roughness and a higher reflectance.

The amount of $MoSi_2$ is also expected to affect reflectance significantly. Ongoing studies on HP materials with increasing amounts of $MoSi_2$ have shown that reflectance has the tendency to increase with decreasing the $MoSi_2$ amount. Thus, for HP samples with 10 vol% $MoSi_2$, the reflectance is always higher than PS samples with 20 vol% $MoSi_2$ due to both decrease of surface roughness and less residual $MoSi_2$ content after sintering (see Table 3).

Other parameters, such as secondary phases in amounts lower than 5-8% and mean grain size do not seem to have an appreciable effect.

Compared to the ideal behavior of a solar absorber (e.g. reflectance is 0 below 1.5μm and 100% at longer wavelengths) considering for instance a working temperature of 1200 K, TaC-based composites are the best amongst the composition investigated, being intrinsically selective in a higher extent compared to HfC and ZrC (see below).

Additional factors to consider for increasing the reflectance are both a minimization of the final porosity and a reduction of the surface roughness as much as possible. As for the secondary phase, the addition of $MoSi_2$ sintering aid should be minimized to avoid the formation of the 2.7μm shoulder.

Figure 31 compares, for each fixed material, the hemispherical reflectance spectra as a function of the amount of sintering aid. Notice that HP specimens (10 vol% $MoSi_2$), which always have the highest density, the lowest roughness and the smallest grains always show also the highest reflectance when compared to PS samples. The reflectance hierarchy is clear for wavelength above about 1μm. The slightly higher reflectance at shorter wavelengths of TCM20 and ZCM20 samples compared to TCM10 and ZCM10, respectively, is not significant as it lies within the instrumental uncertainty (1-2% in absolute reflectance). As mentioned above, the small curve feature at around 12μm in ZCM10 and HCM10 can be assigned to the detection of SiC secondary phase, as it is confirmed by microstructural analysis, while the shoulder at around 2.5μm in ZrC and TaC-based

samples can be explained in terms of $MoSi_2$ residuals. In agreement with the microstructural observations, $MoSi_2$ signal is not detected in HfC-based materials, Figure 31b.

Performance evaluation as solar absorbers

From the experimental hemispherical reflectance ε_{int} and α_{int} (paragraph 3.1.2) have been calculated (Parameters used: T=1200K, λ_1=0.3μm, λ_2=15.0μm).

Sample	Matrix	α_{int}	ε_{int}	Selectivity index
ZCM10	ZrC	0.57	0.26	2.2
ZCM20		0.61	0.34	1.8
HCM10	HfC	0.37	0.13	2.8
HCM20		0.39	0.18	2.2
TCM10	TaC	0.55	0.23	2.4
TCM20		0.56	0.27	2.1

Table 4: Calculated solar absorbance, thermal emittance and selectivity index

Table 4 compares the calculated ε_{int}, α_{int} and *selectivity Index*. While the absorbance value remains in all cases to be improved, for instance using femtosecond laser writing as described in [Ref.(76)], or chemical attack techniques similar to those used for black silicon [Ref.(87)], the absorbance is higher for 20 vol% $MoSi_2$ specimens and for HfC-based material (0.61).

As for spectral selectivity, 10 vol% $MoSi_2$-containing specimens (i.e. HP materials) are more performing among all the three investigated carbides, while, for fixed sintering aid amount, the best performing material is always TaC and the worse is HfC. However, three samples (HCM10, TCM20 and ZCM20) share similar *selectivity index* values (2.2, 2.2 and 2.1, respectively). The lowest obtained value is for HCM20 (1.8), but it is not an unfavorable result, as, in any case, it is nearly twice that of the reference SiC (1.0) [Ref.(17)].

5.5 Dense ZrB_2 e TaB_2 obtained by SPS/SHS and RSPS

Purpose

The purpose is to compare the optical properties of dense samples of ZrB_2 and TaB_2 obtained through two different techniques. Additional characterization of the materials such as microstructure, roughness and machining details can be found on [Ref.(88)].

Studied Materials

SPS equipment (515 model, Sumitomo Coal Mining Co Ltd, Japan) was used under mild vacuum conditions (20 Pa) to obtain TaB_2 and ZrB_2 dense samples by RSPS or non-reactive sintering. In the non-reacting sintering, transition metal diborides were preliminarily synthesized by SHS and the

obtained powders consolidated by SPS. Such two steps processing route will hereafter indicated as SHS/SPS.

Powders used for the preparation of the materials were:

- **B** (SigmaeAldrich, amorphous, particle size < 1 mm, 95% purity),

and:

- **Zr** (Alfa Aesar, particle size < 44 mm, 98.5% purity)
- **Ta** (Alfa-Aesar, particle size < 44 mm, 99.6% purity)

combined according to the reaction Me + (2 + x) B→ MeB_2, where Me = Zr or Ta. The samples studied are reported in Table 5.

Matrix	Method	Relative Density (%)	Grain Size (µm)	Pore Size (µm)
ZrB_2	RSPS	96.0 ± 0.4	50	6-8
	SHS/SPS	98.3 ± 0.8	20-30	3-4
TaB_2	RSPS	95.4 ± 0.7	10	1.5-3.5
	SHS/SPS	94.0 ± 0.4	10	0.5-3.0

Table 5: Main characteristics of obtained samples

Optical characterization

Figure 32 shows the room-temperature hemispherical reflectance spectra. No significant differences have been found in both TaB_2 and ZrB_2 systems when comparing the utilized production methods.

Therefore, the small discrepancies in surface roughness values and pore size, particularly when considering the ZrB_2 system, appear to entail a minor effect on optical spectra.

As for the influence of roughness, this can be mainly ascribed to differences in the R_t values (which, in turn, are connected to the pore depth) as, in any case, typical R_a ranges for the samples studied are much lower than the investigated optical wavelengths.

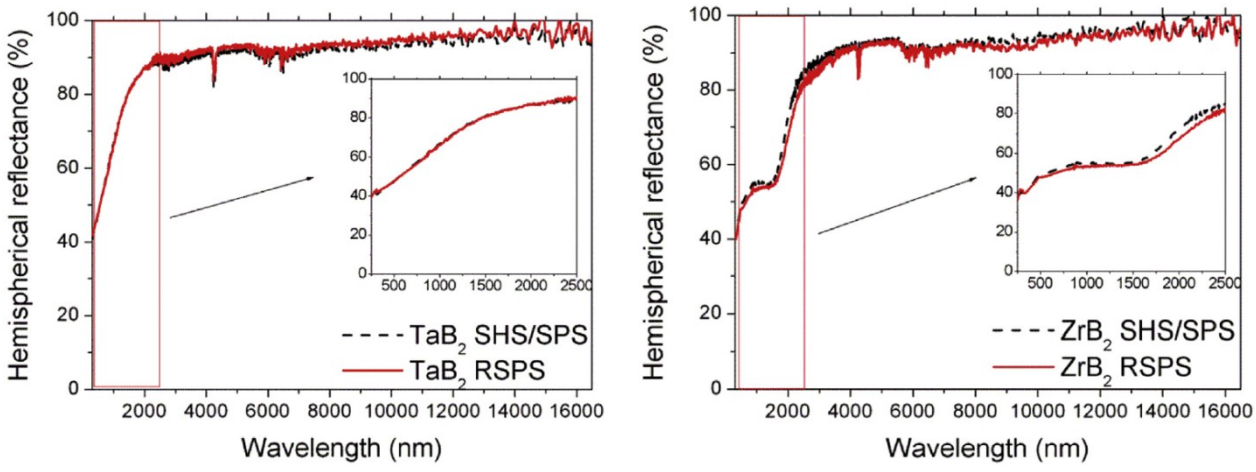

Figure 32: Hemispherical reflectance spectra of TaB_2 and ZrB_2 samples. The inset shows in detail the 250-2500 nm region.

To evaluate spectral differences between the two considered borides, Figure 33 compares the spectra of TaB_2 and ZrB_2 for fixed SHS/SPS processing technique. Both borides show step-like reflection curves characterized by a quick reflectance increase for wavelengths up to about 3000 nm and nearly constant high reflectance plateau at longer wavelengths. The TaB_2 and ZrB_2 spectra can be nearly superimposed each other for wavelengths below 550 nm and above 2600 nm. In the intermediate spectral region 550-2600 nm the reflectance of TaB_2 is higher, being its curve monotonically increasing, than that of ZrB_2, which is characterized by a nearly constant reflectance in the range 850-1400 nm and a monotonic increase from 1400 to 2600 nm.

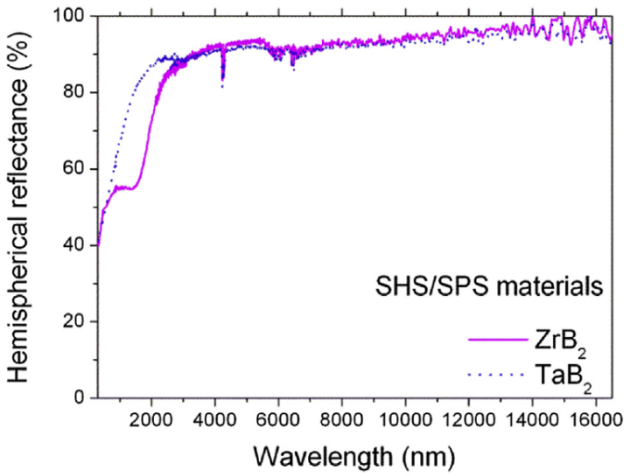

Figure 33: ZrB_2 and TaB_2 spectra (SHS/SPS method)

Performance evaluation as solar absorbers

From the experimental hemispherical reflectance ε_{int} and α_{int} (paragraph 3.1.2) have been calculated (Parameters used: T=1400K, λ_1=0.3μm, λ_2=15.0μm).

Considering an operating temperature T=1400 K, it results α_{int} = 0.47 for ZrB_2 and 0.40 for TaB_2 and ε_{int} = 0.18 for ZrB_2 and ε_{int} =0.12 for TaB_2. In other words, the low-reflectance shoulder evidenced in the ZrB_2 spectrum makes such ceramic a better solar absorber with respect to the TaB_2 sample.

On the other hand, the zirconium diboride product results to be a more emissive material. Finally, if the *selectivity index* at 1400 K is considered (2.6 for ZrB_2 and 3.3 for TaB_2), the Ta-based specimen shows a relatively more interesting performance than the ZrB_2 one. However, it should be noted that when the required operating temperature is lower, blackbody spectrum is shifted at longer wavelengths, so that the detrimental effect of ZrB_2 shoulder on the emittance is correspondingly decreased. For instance, *selectivity index* 3.9 for ZrB_2 and 4.0 for TaB_2, respectively, when T=1000K.

Matrix	Temperature (K)	α_{int}	ε_{int}	Selectivity index
ZrB_2	1400	0.47	0.18	2.6
	1000	0.47	0.12	3.9
TaB_2	1400	0.40	0.12	3.3
	1000	0.40	0.10	4.0

Table 6: Performances of materials at two different temperature

Summarizing

This investigation shows that transition metal borides may be interesting as base matrices for solar absorber applications. However, the direct exploitation of these materials will be possible only after a careful optimization, in particular aimed to increase their solar absorbance, and if a proper choice of the plant architecture/operating temperature is adopted. Anyway, the main purpose was to demonstrate no, or very small, differences in the optical properties when the two manufacturing processes were adopted for the fabrication of dense TaB_2 and ZrB_2.

5.6 TaB_2: effects of porosity and high temperature exposition

Purpose

In this section TaB_2 materials with different degrees of porosity have been studied. The purpose is to correlate the porosity to the microstructural and optical properties.

The optical characterization was performed considering the experimental techniques reported in paragraphs 3.1 and 3.3.

Emittance tests were carried out in the 1050-1800K range. Reflectance spectra at room temperature were acquired before and after the high temperature treatment. Then, the spectral features were correlated to surface changes and to the measured high temperature emittance.

Additional characterization of the materials such as microstructure, roughness, crystalline phases, and machining details can be found on [Ref.(73)].

Studied Materials

TaB_2-based materials doped with 10vol% of $MoSi_2$ were sintered by HP at increasing temperatures to obtain different levels of porosity. Porosity affects the surface roughness, which in turn, affects the optical properties at both room and high temperature.

Commercial powders were used to prepare the ceramic composites:

- hexagonal **TaB_2** (Materion. Milwakee, WI), purity 99.5%, 325 mesh, mean grain size 0.91 μm, impurities Al:0.04, Fe: 0.07, Nb: 0.02;
- tetragonal **$MoSi_2$** (o2 μm, Sigma-Aldrich, Steinheim, Germany), particle size range 0.3–5 μm and oxygen content 1 wt%; C (Degussa EB 158).

A mixture with 10 vol% of $MoSi_2$ and 3 vol% of carbon black were prepared. Carbon was included in the mixture to reduce residual silica in the final microstructure and promote the formation of silicon carbide during sintering. HP was conducted in low vacuum (100 Pa) using an induction-heated graphite die with a constant uniaxial pressure of 30 MPa, a heating rate of 20°C/min and free cooling. Different temperatures in the 1720–1900 °C range were adopted to obtain different levels of density [Ref.(73)]. The studied samples are reported in Table 7.

Sample	Sintering cycle (°C/min)	Bulk Density (g/cm^3)	Relative Density (%)	Mean grain size (µm)	Pore percentage (%)	Average pore dimension (µm)	Roughness (Ra)
TaB67	1600	7.31 ± 0.02	67	0.8 ± 0.4	29.6	0.24	0.25
TaB78	1750	8.48 ± 0.02	78	1.1 ± 0.4	18.8	0.17	0.16
TaB82	1780	8.95 ± 0.02	82	1.2 ± 0.5	17.9	0.13	0.2
TaB93	1850	10.11 ± 0.02	93	1.5 ± 0.5	12.2	0.09	0.15
TaB100	1900	10.86 ± 0.02	100	3.5 ± 1.0	-	-	0.1

Table 7: Investigated materials: sintering cycles, densities, pore dimensions, roughness

Optical characterization

Figure 34 shows the hemispherical reflectance spectra of borides measured at room temperature before and after the high temperature tests in the solar furnace. The same figure also shows the hemispherical reflectance spectrum of bulk SiC and the specular reflectance spectrum of bulk $MoSi_2$, for comparison. All the hemispherical reflectance spectra show absorption peaks (i.e. transmittance minima) around 4.2µm and in the range 5.8–6.8µm, which are instrumental artifacts due to molecular absorption by gas constituting the ambient air. The specular reflectance spectrum of $MoSi_2$ does not show this artifact because of the considerably shorter path length experienced by the light in the specular reflectance setup, as compared to the multiple-reflection light path length within the integrating sphere.

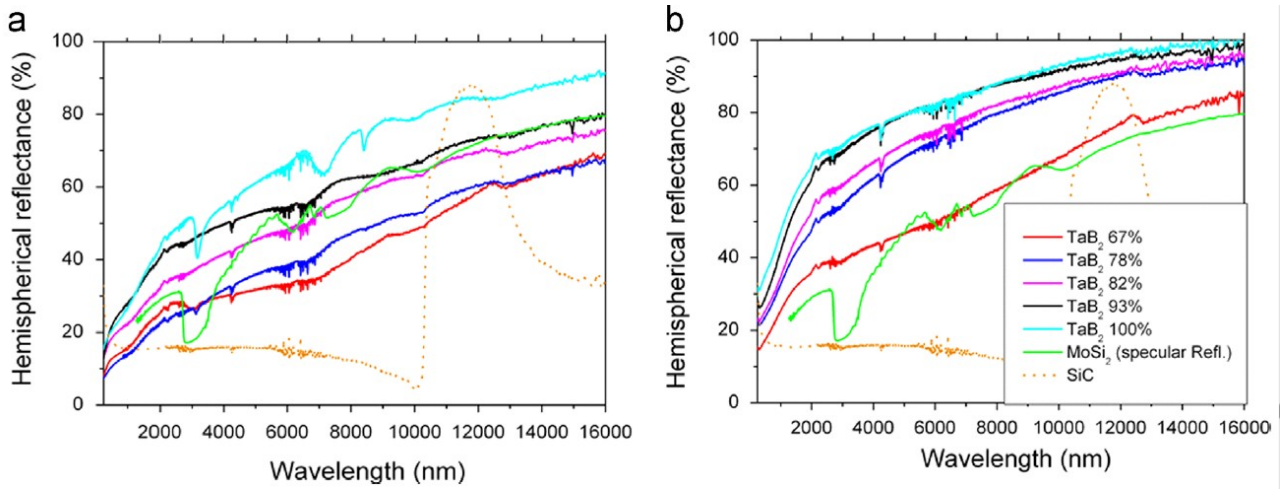

Figure 34: Hemispherical reflectance spectra of the different TaB_2 samples (a) before and (b) after the high-temperature treatment. Spectra of SiC and $MoSi_2$ are shown for comparison (specular reflectance).

All the borides seem to show some SiC impurities, as demonstrated by the shoulder on the spectra around 13μm wavelength, corresponding to the typical Reststrahlen peak of SiC and resulting from reaction of constituent $MoSi_2$ and C.

Moreover, the samples with 67%, 78% and 100% densities also show some residuals of $MoSi_2$, around 3μm, whilst for the TaB100 sample, also a feature near 7.2μm can be noticed. The samples with densities in the range 80-100% show reflectance values which increase with the density, as expected. However, the reflectance curve of TaB100 is characterized by multiple features, absent in the other samples.

Comparing the post-test optical measurements (Figure 34b) to the pre-test ones (Figure 34a), it is possible to appreciate some general trends: the common reflectance values increase and the slope increase of curves especially in the 0.5–2.5μm range. Also in this case, the reflectance monotonically increases with the sample density. All the samples appear to show small traces of SiC. Moreover, small traces of $MoSi_2$ cannot be ruled out, due to the shoulder in the curves around 3μm wavelength. In any case, the amount of $MoSi_2$ (if any) is consistently lower than in the pre-test spectra.

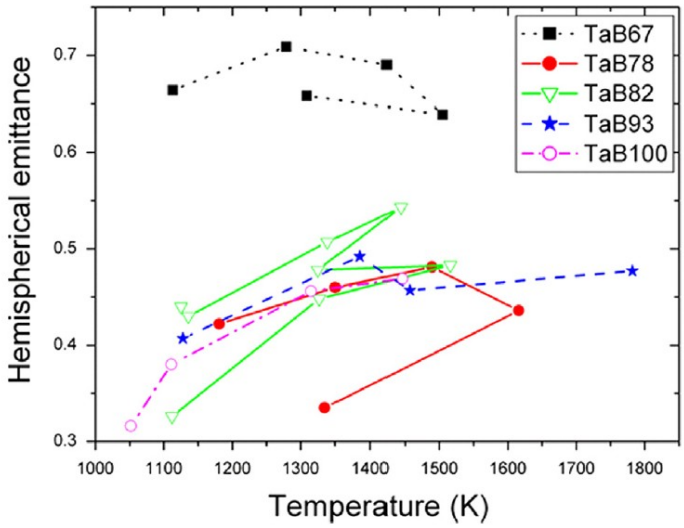

Figure 35: Measured hemispherical emittance on the various TaB_2-based ceramics.

Figure 35 shows the measured emittance at high temperature. For each sample, experimental points are connected in a chronological order, i.e. some samples have undergone one or more heating/cooling cycles (TaB67, TaB78 and TaB82). With the exception of the sample with 67% density, which has the highest emittance with values around 0.7, the other borides have values between 0.3 and 0.5. All the samples show a weak dependence of emittance on temperature.

A common trend for all the samples exposed to temperature cycling is that emittance always decreases when the measurement is repeated. This effect is particularly relevant in TaB78.

Considerations

From room-temperature spectra (Figure 34) it is apparent that TaB_2 has a step-like optical behavior as found for the other UHTCs. The analytical curve of TaB_2 reflectance shows dependence on many factors including the porosity, the surface finish and presence of secondary phases, due to either addition of sintering agents or reactions occurring during sintering or the high temperature exposure. Emittance is also affected by the presence of porosity and shows a dynamic response to changes in temperature. Furthermore, after exposure, reflectance spectra are significantly changed (Figure 34b).

As for porosity, experimental data indicate that it strongly affects the reflectance of TaB_2 samples. Looking at the optical spectra collected before the emittance tests (Figure 34a), reflectance of TaB67 is significantly lower than that of TaB82, TaB93 and TaB100, though similar to TaB78, due to the pore ability to partially trap radiation.

It is worthy to note that in the wavelength range 0-3μm, the TaB67 reflectance is higher than TaB78, becoming lower in the 3-12μm range. This can be due to several reasons. TaB67 has a quite inhomogeneous surface morphology characterized by large sintered aggregates up to 10μm wide, spaced out with voids of about the same dimensions [Ref.(73)].

After emittance tests relevant changes are observed in the optical spectra collected at room temperature (Figure 34b). It can be noticed that reflectance increased compared to pristine materials. The spectra maintain S-shaped curves, i.e. their intrinsic optical selectivity.

As for porosity, the same trend is observed as for as sintered samples. The higher the porosity, the lower the reflectance. The reflectance of TaB67 is markedly lower than for the other samples, especially in the 3-12μm range, due to the presence of large voids with the same dimensions [Ref.(73)].

As for emittance, this property is dependent on the starting porosity, as well. Some features are worthy to note: emittance is markedly higher for TaB67 but rather similar for samples with higher porosity, such as TaB78, 82, 93, and 100. This is due to the fact that in TaB67, most of the porosity is still open and this gives rise to a very rough surface.

A common trend for all the samples exposed to temperature cycling is that emittance always decreases when the measurement is repeated. This effect is particularly relevant in TaB78. The most reasonable explanation resides in the surface diffusion phenomena observed on the tested discs.

Superficial changes induced by exposure to high temperature are of extreme interest because they suggest that partially sintered materials are not stable enough for the application requirements. Moreover, even in completely dense materials, surface modifications can lead to optical properties changes, due to change of the surface roughness. This means that both density and surface finish must be carefully controlled.

Performance evaluation as solar absorbers

From the experimental hemispherical reflectance ε_{int} and α_{int} (paragraph 3.1.2) have been calculated (Parameters used: T=1300K, λ_1=0.3μm, λ_2=14.3μm).

For “rough” samples, such as TaB78 and TaB100, the reflectance spectra measured after the high-temperature treatment have been considered, as they are most representative of a solar absorber in operating conditions (especially because of removed machining residuals).

The *selectivity index* for the samples used for high-temperature experiments are 1.3, 1.7, 1.8, 2.1, 2.1, corresponding respectively to relative density 67%, 78%, 82%, 93% and 100%. Those values were calculated for the post-test spectra and for blackbody at 1300 K, appreciating that the samples become more performing as the density increases up to 90%, while there is no practical difference between 90% and 100% density samples. In fact, porous samples show a higher solar absorbance than dense specimens, but this happens at the expense of the emittance, which is also higher, entailing thus a lower *selectivity index*.

Summarizing

Compositional, structural and optical properties changes, after high temperature exposure of TaB_2-based materials at different grade of porosity have been studied.

As regards the porosity is more performing the dense material because has better radiative properties. Furthermore, superficial changes induced by exposure to high temperature of porous materials suggest that partially sintered materials are not stable enough for the application requirements in CSP-T.

5.7 ZrC prepared by SPS/SHS without sintering aid

Purpose

The purpose is to study the optical properties and the performances for solar absorber applications, of a dense ZrC sample obtained by SHS/SPS techniques. Those properties have been compared with those displayed by analogous UHTC materials, specifically monolithic ZrB_2 obtained with the same synthesis/sintering techniques and additive-containing ZrC produced by alternative methods.

Studied Material

The material has been obtained starting from Zirconium (Alfa Aesar, product code 00418, particle size < 44μm, purity > 98.5%, Karlsruhe, Germany) and graphite (Sigma-Aldrich, product code 282863, particle size < 20μm, purity > 99.99%, St. Louis, MO, USA) powders.

The powders were used as starting reactants for the synthesis of ZrC by SHS. About 98% dense monolithic ZrC samples are successfully produced by SPS after 20 min holding time at 1850°C [Ref. (89)].

The aim is to study the effects on the optical properties due to the absence of sintering additives. Indeed, the densification of UHTCs powders can be made easier by the introduction of appropriate sintering aids. However, the presence of secondary phases might not be desirable for certain high-temperature applications.

Optical Charactarization

Figure 36 shows the hemispherical reflectance of the studied ZrC specimen. It is possible to appreciate the typical step-like spectrum of UHTC carbides, characterized by a low reflectance (*i.e.*, a high optical absorption) in the visible-near infrared and a high reflectance plateau (*i.e.*, a low thermal emittance) at longer infrared wavelength.

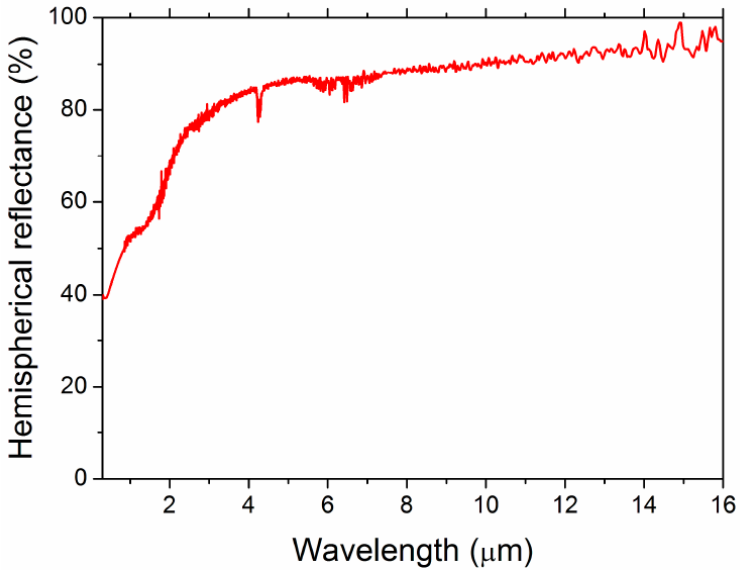

Figure 36: Hemispherical reflectance spectrum of ZrC sample obtained by SHS/SPS

Performance evaluation as solar absorbers

For solar absorbers application, α_{int} and ε_{int} have been calculated comparing them with the analogous previously investigated systems (sintering aid-doped ZrC [paragraph 5.4] and fully dense monolithic ZrB_2 obtained by SHS/SPS [paragraph 5.5]). Parameters used in calculation are: T=1200K and 1400K, λ_1=0.3μm, λ_2=15.0μm). The results are reported in Table 8.

Sample	Sintering Aid	α_{int}	ε_{int} (1200K)	ε_{int} (1400K)	Selectivity index (1200K)	Selectivity index (1400K)
ZrC	None	0.51	0.21	0.24	2.4	2.1
ZCM10 / ZCM20 [paragraph 5.4]	$MoSi_2$	0.55-0.56	0.23-0.27	-	2.4-2.1	-
ZrB_2 [paragraph 5.5]	None	0.47	-	0.18	-	2.6

Table 8: Comparison of performances as a solar absorber of ZrC and other UHTCs

Based on these results, it can be stated that the latter product is slightly less absorptive and emissive with respect to $MoSi_2$-containing ZrC samples, while spectral selectivity is similar. In addition, when the comparison is extended to the bulk additive-free ZrB_2 material processed following the same SHS/SPS route, it is found that the ZrC product appears slightly more absorptive and emissive, with a slightly higher spectral selectivity displayed by the diboride system.

Summarizing

Regarding the optical behavior, the obtained ZrC specimen displayed a step-like spectrum, typical of transition metal carbides, with absorption in the visible-near infrared area and low thermal emittance at longer infrared wavelengths. Furthermore, the resulting spectral selectivity values are sufficiently good, 2.4 and 2.1 at 1000 K and 1400 K, respectively. In summary, it is possible to conclude that the combination of the SHS and SPS routes provide highly dense ZrC products with performances for solar absorber applications comparable with those displayed by analogous UHTC materials, specifically monolithic ZrB_2 obtained with the same synthesis/sintering techniques and additive-containing ZrC produced by alternative methods.

5.8 INO-CNR apparatus, preliminary tests

Purpose

This paragraph describes the layout and first tests on the INO-CNR device, comparing the results obtained for hafnium carbide and tantalum diboride ultra-refractory ceramic samples to that obtained in the PROMES-CNRS solar furnace, obtaining a good agreement.

Furthermore, to assess the reliability of the widely used approach of estimating the spectral emittance from room temperature reflectance spectrum, the calculation in the 2.5–17 μm spectral range has been compared to the experimental high-temperature spectral emittance, obtaining that the spectral trend of calculated and measured curves is similar but the calculated emittance underestimates the measured value [Ref.(90)].

5.8.1 Comparison with PROMES-CNRS furnace

Preliminary tests on the device have been made comparing the results obtained for HfC and TaB_2 ultra-refractory ceramic samples to quasi-monochromatic measurements carried out in the PROMES-CNRS solar furnace [Ref.(90)]. More precisely we used a specimen of HfC and three specimens of TaB_2 with 70%, 80%, and 90% of relative density.

The disc-shaped pellets were set in the vacuum furnace and, once the selected temperature was stable, the sample radiance spectrum was measured by averaging on 30 consecutive recordings.

Alternately, normal radiance spectra were similarly acquired for the blackbody at the same temperatures of the sample. Thus, spectral emittance in the range of 2.5–20 μm was calculated from the ratio.

The obtained emittance values were evaluated by comparing them to the results of emittance measurements [Ref.(73), (91)] carried out with the MEDIASE apparatus at PROMES.

For the comparison to spectrally resolved data obtained with the new facility, we chose the normal emittance acquired at 2.7, 5, and 5.5 µm wavelengths (filter FWHM: 100 nm) and the integrated emittance in the band 8–14 µm.

Results and discussion

HfC emittance data for 2.7, 5, 5.5, and 8–14 µm wavelengths are shown in Figure 37. Data collected with the INO setup are plotted together with the data collected with PROMES furnace.

Although the temperature ranges of the data acquired with the two facilities did not intersect, the two datasets show comparable emittance values, without significant value jumps at the temperature of 1100 K, which separate the two ranges. The data did not intersect because of the design characteristics of the two systems (MEDIASE minimum temperature is 1100 K, while the maximum temperature obtainable on the sample by the INO setup is about 1100 K). A similar behavior is shown by the emittance data of TaB80 and TaB90, measured in the 2.7 and 8–14 µm bands (Figure 38 and Figure 39).

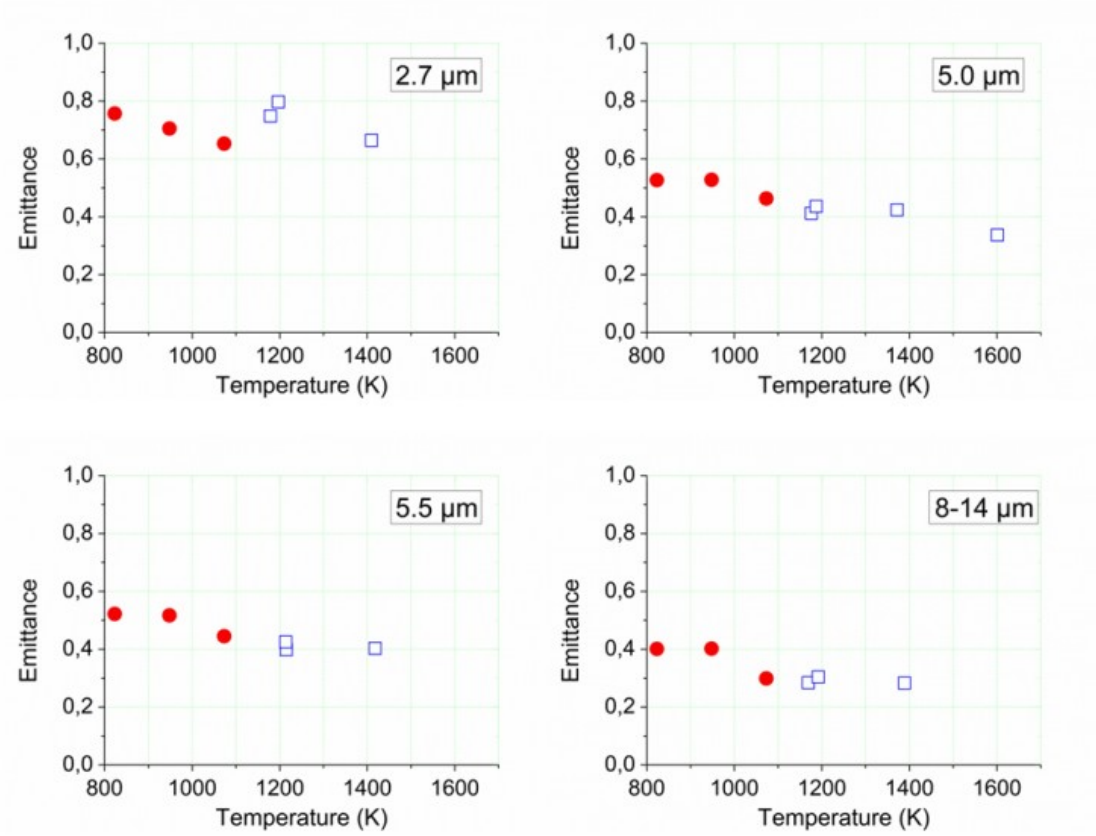

Figure 37: HfC emittance as a function of temperature. INO measurements: red dots; PROMES data: blue squares. Spectral band is indicated in legend.

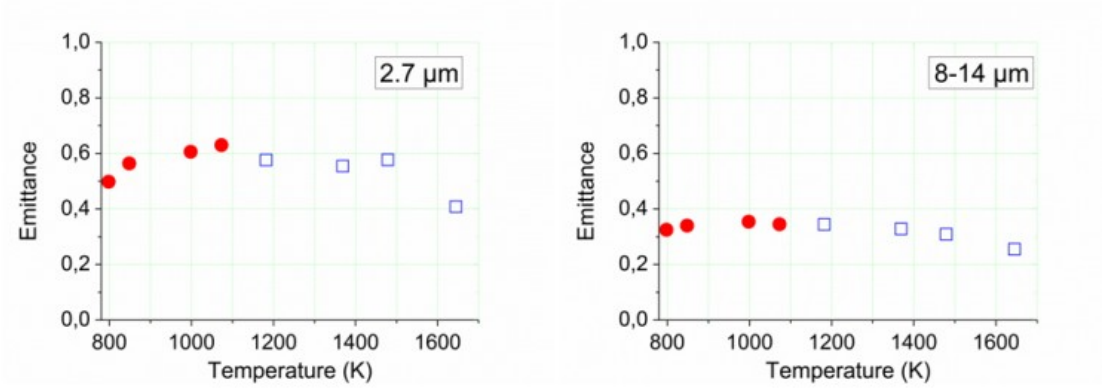

Figure 38: TaB80 emittance as a function of the temperature (circles: INO data; squares: PROMES data). Spectral band is indicated in legend.

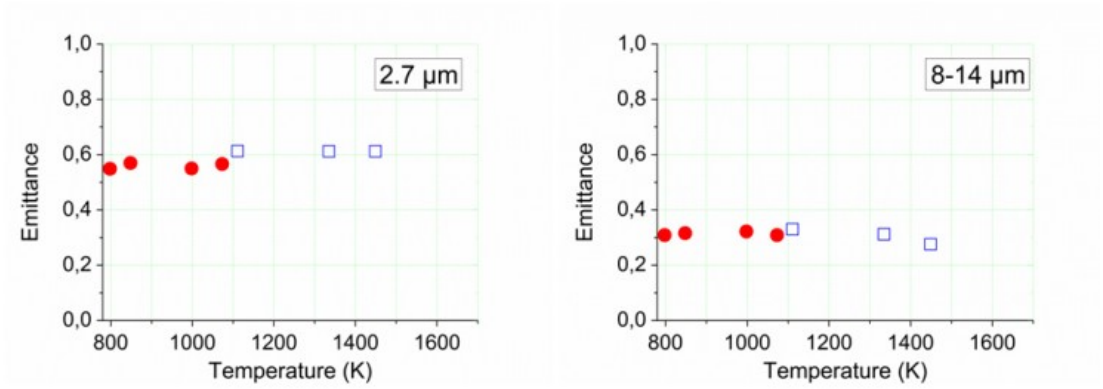

Figure 39: TaB90 emittance as a function of the temperature (circles: INO data; squares: PROMES data). Spectral band is indicated in legend.

The uncertainty on the emittance value mainly depends on the uncertainty of sample temperature read by the three thermocouples (± 50 K) and can be estimated to be ± 20% at 2 µm and ± 10% in the remaining bands (This preliminary tests have been done when it was not yet available the "spring thermocouple" and "two-color pyrometer").

5.8.2 Comparison with optical spectroscopy at room temperature

Finally, as additional evaluation, following the approach consolidated in the literature (method described in paragraph 3.1), the sample hemispherical emittance from room-temperature hemispherical reflectance spectra has been estimated.

The comparison between emittance calculated from the room-temperature spectrum and the actual emittance obtained from direct or indirect measurement techniques can be useful to estimate the reliability of considering room-temperature data. In fact, the high-temperature spectrum (either the reflectance or the radiance spectrum) is not always available, while room-temperature data are

much more accessible and thus an estimation of the error done calculating the emittance from them could be helpful.

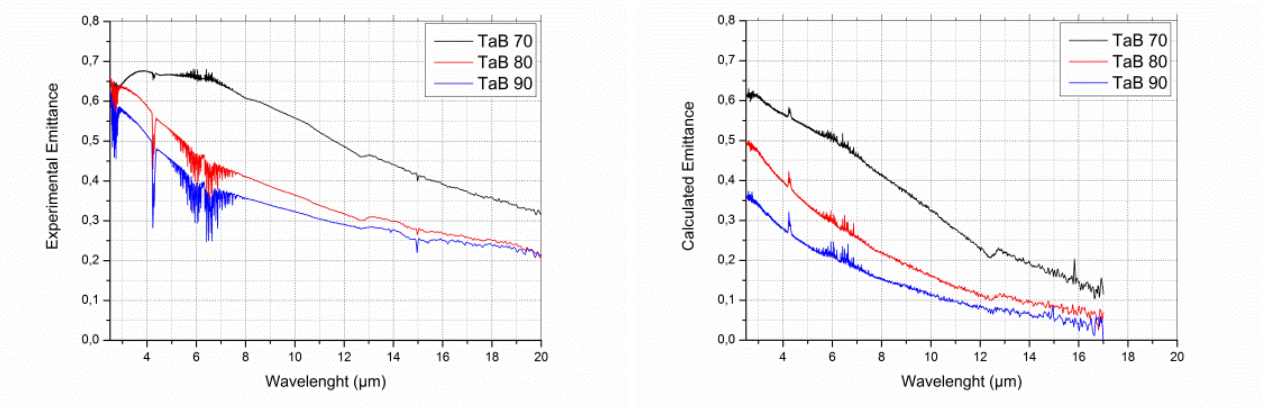

Figure 40: Direct measurement of emittance (left plot) and calculation from Eq. 5 (right plot) for boride samples.

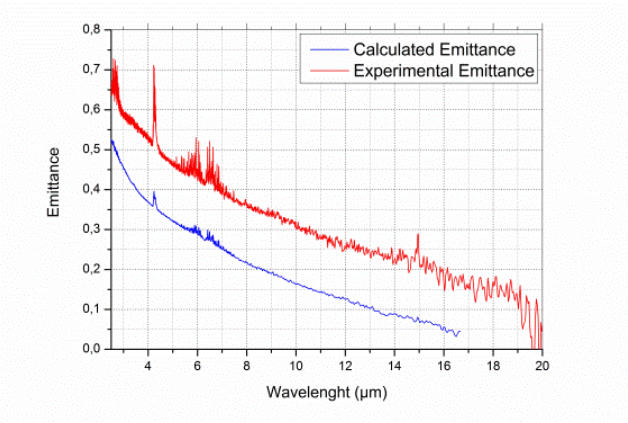

Figure 41: Directly measured (red) and calculated (blue curve) emittance for HfC.

The comparison between the results of direct high-temperature emittance measurements (paragraph 3.2) and the approximated emittance calculated from room-temperature reflectance (paragraph 3.1) is shown in Figure 40 and Figure 41 for TaB_2 and HfC samples, respectively.

The direct values have been acquired at the maximum reached temperature of 1080±50 K. The peaks observed at around 4 and 5–7μm are due to absorption by the air molecules within the optical path and can appear as positive or negative peaks. This is according to the difference in the concentration of absorbing species between the time of the background acquisition and the time of the measurement. An upgrade of the setup is foreseen in the future for the direct measurement, allowing the beam to pass through an enclosed environment under nitrogen flux.

Results and discussion

For both classes of materials, the spectral trend of experimental and calculated room-temperature curves is in good agreement. As expected, the room-temperature calculation underestimates the emittance value by about 0.2, maintaining the same spectral trend. The underestimation of emittance agrees with the literature [Ref. (92), (93), (94)] and it is because, for metal-like materials as in our case, the room temperature reflectance in this spectral range usually overestimates the high-temperature value. For TaB_2, both approaches correctly evidence the emittance increase with increasing porosity.

The obtained data bring to some conclusions about the reliability of the room-temperature approach. Indeed, when the purpose is to carry out a first screening among materials, the calculation of emittance from room temperature reflectance data gives a good method of comparison, especially if considering some parameter variation within the same material (i.e., density, porosity, roughness, etc.).

However, the emittance calculated in this case is an underestimation, useful in comparative evaluations of different samples when high-temperature data are not available. If, on the contrary, the actual value of emittance is looked for, high-temperature measurements are required.

Conclusions

During these years of doctoral studies, a laboratory for solar energy materials has been set up. The scope of the new laboratory is to study the optical properties of new materials mainly aimed to applications in solar energy field.

The present thesis has regarded the characterization of UHTCs as solar absorbers. UHTCs are ideal materials for the construction of solar receivers, as they have the ideal properties such as high refractoriness, high mechanical strength, high thermal conductivity, good chemical stability and high melting temperatures exceeding 3200K. Using the experimental techniques explained in chapter 3, precise relationships between surface roughness, microstructure, sintering aid amount and optical spectra are shown. Indeed, a precise knowledge of factors affecting optical properties of this ceramics is of great importance for material optimization in view of solar absorber industrial applications.

Much of the work in Solar Energy Laboratory has regarded the design and development of the new apparatus aimed to perform the direct spectral emissivity of opaque solid materials, in high vacuum, for temperature from 500 to 1200 K. This apparatus has been specially designed to study the characteristics of UHTCs materials, in order to assess their performance for possible use as receivers in solar thermal power plants.

The construction of the apparatus was necessary, because the method currently used in the literature to characterize the solar absorbers (Kirchhoff's law at ambient temperature) is not very effective, as the absorbance/emissivity may change with temperature and the validity requirements of Kirchhoff's law are not always satisfied. This apparatus allows characterizing materials for solar applications, in a manner never used until now, allowing the characterization of the real optical performance of the solar absorber at the operating point.

The experimental method used is directly connected to the definition of emittance as the ratio between the radiance emitted by the sample surface at a given temperature and that emitted by a blackbody at the same temperature. Initially, the system was tested by comparing it with the MEDIASE one; the obtained experimental emittance at 2.7 μm, 5 μm, 5.5 μm and in the 8-14 μm band has been compared with the results of measurements on the same samples, obtaining a similar trend and good agreement. Moreover, the spectrally resolved emittance has been compared to the common approach of calculating emittance from room-temperature reflectance, confirming that the latter approach underestimates the emittance value, while generally qualitatively maintaining the spectral trend of emittance curves.

In the future, the enlargement of the spectral range of the spectrometer up to 500nm will allow studying also the absorption properties, in addition to the emissive properties, at the operating temperature providing a complete characterization of the solar absorber material without resorting to any type of approximation.

Summarizing, studies on UHTCs have shown the following main issues:

- All the UHTCs have high intrinsic selectivity index, compared to SiC or Allumina, the materials currently used in CSP-T.

- PS specimens typically display lower *selectivity index* than the corresponding HP [paragraph 5.1].
- The presence of $MoSi_2$ sintering additive does greatly increase UHTCs oxidation resistance due to the formation of a borosilicate glass on the surface of the material, which prevents the diffusion of oxygen in the bulk material. However, the addition of $MoSi_2$ as sintering aid worsens the spectral selectivity. The addition of $MoSi_2$ sintering aid should be not higher than 10vol% in order to ensure quite good sinterability, oxidation protection at high temperature, and high selectivity index [paragraph 5.2].
- The carbides have generally minor spectral selectivity than borides and have a worse oxidation resistance [paragraph 5.4].
- As regards the study of TaB_2 at various porosity, it seems to be more performing the dense material. In fact, it has better radiative properties and selectivity index [paragraph 5.6].
- Superficial changes induced by exposure to high temperature of porous materials suggest that partially sintered materials are not stable enough for the application requirements in CSP-T [paragraph 5.6].
- Room temperature reflectance approach is an underestimation of real emittance but it is useful in comparative evaluations of different samples when high-temperature data are not available, especially if considering some parameter variation within the same material.

Finally, it should be mentioned that a possible criticism for UHTCs as solar absorbers is represented by the relatively low solar absorbance when comparing them, for instance, to SiC. However, the absorption properties may be increased, while maintaining the emissive properties. Several possibilities can be explored for this goal. At first, post-sintering surface texturing, which has already been demonstrated for HfC to be able to significantly increase solar absorbance without detrimentally affecting thermal emittance [Ref.(76)]. Other possibilities are a proper design of the material porosity and dimensions of the pores, which is known to be an important parameter affecting radiative properties, and finally the addition of a high absorbance coating, even if it requires a careful optimization of high temperature stability and thermal transfer at the interface.

Acknowledgments

This thesis was mainly conducted at the National Institute of Optics (INO-CNR), where I was as a research fellow, in collaboration with the department of industrial engineering of Florence (DIEF), the institute of science and technology of ceramic materials (ISTEC), and the department of mechanical, chemical and materials Engineering of University of Cagliari (UNICA). I remember with great joy and sweetness the moments spent here. It was a hard work and I am very pleased and proud for the work done and the results obtained.

Therefore, first, I would like to express my sincere gratitude to Dr. Luca Mercatelli (CNR-INO) and Dr. Elisa Sani (CNR-INO) for having insert myself within an interesting and challenging line of research.

Special thanks to my PhD tutor Prof. Maurizio De Lucia (DIEF) for the various suggestions received, to Dr. Stefano Pratesi (DIEF) for collaboration in the early years, to Dr. Giacomo Pierucci (DIEF) for the design of mechanical systems and for some advice on improving the temperature measurement system, and to Dr. David Jafrancesco (CNR-INO) for the design of the optical system.

I wish to thanks Dr. Lorenzo Marconi (CNR-INO), Dr. Franco Francini (CNR-INO), Dr. Daniela Fontani (CNR-INO), Dr. Paola Sansoni (CNR-INO) and Dr. Stefano Coraggia (CNR-INO), for collaboration.

I also thanks Dr. Diletta Sciti (CNR-ISTEC), Dr. Laura Silvestroni (CNR-ISTEC), and Dr. Luca Zoli (CNR-ISTEC) for providing some of the ceramic materials samples used in testing and for having carried out microstructural and thermo-mechanical characterization.

Thanks to Dr. Andrea Balbo (University of Ferrara) for performing samples surface texture measurements.

I wish to thanks Prof. Roberto Orrù (UNICA), Dr. Clara Musa (UNICA), Dr. Roberta Licheri (UNICA), Dr. Giacomo Cao (UNICA) for providing some of the ceramic materials samples and for having designed and performed SHS and SPS experiments.

I would like to thanks Dr. Jean-Louis Sans (PROMES-CNRS) for the use of MEDIASE.

I also thanks Massimo D'Uva, Sergio Acciai, Mauro Pucci, Leonardo Cirri, Roberta Parenti, Simonetta Renai, Pasqualina Pipino, for technical and logistical assistance.

Special thanks to the Italian bank foundation "Fondazione Ente Cassa di Risparmio di Firenze" and to the Italian Ministry of Research for funding the project.

References

1. **European Academic Science Advisory Council .** Concentrating solar power: its potential contribution to a sustainable energy future. 2011. ISBN: 978-3-8047-2944-5.

2. **E. Sani, S. Barison,Pagura,L. Mercatelli,P. Sansoni,D. Fontani,D. Jafrancesco, F. Francini,.** Carbon nanohorns-based nanofluids as direct sunlight absorber. *OPTICS EXPRESS.* 2010, Vol. 18, No. 5.

3. **Luca Mercatelli, Elisa Sani, Giovanni Zaccanti, Fabrizio Martelli, Paola Di Ninni, Simona Barison, Cesare Pagura, Filippo Agresti and David Jafrancesco,.** Absorption and scattering properties of carbon nanohorn-based nanofluids for direct sunlight absorbers. *Nanoscale Research Letters.* 2011, Vol. 6, 282.

4. **Moradi A., Sani E., Simonetti M., Francini F., Chiavazzo E., Asinari P.,.** Carbon-Nanohorn Based Nanofluids for a Direct Absorption Solar Collector for Civil Application. *JOURNAL OF NANOSCIENCE AND NANOTECHNOLOGY.* 2015, Vol. 15(5), 3488-95.

5. **E. Sani, P. Di Ninni, L. Colla, S. Barison, F. Agresti.** Optical properties of mixed nanofluids containing carbon nanohorns and silver nanoparticles for solar energy applications. *Journal of Nanoscience and Nanotechnology.* 2015, Vol. 15, 3568–3573.

6. **Sani E., Mercatelli L., Barison S., Pagura C., Agresti F., Colla L., Sansoni P.,.** Potential of carbon nanohorn-based suspensions for solar thermal collectors. *Solar Energy Materials and Solar Cells* . 2011, Vol. 95 (11), 2994–3000.

7. **Rosa Mondragón, Rafael Torres-Mendieta, Marco Meucci, Gladys Mínguez-Vega, J. Enrique Juliá, Elisa Sani.** Synthesis and characterization of gold/water nanofluids suitable for thermal applications produced by femtosecond laser radiation. *Journal of Photonics for Energy.* 2016, Vol. 6, 034001.

8. **Agresti. F., Zin V., Barison S., Sani E., Meucci M., Mercatelli L., Nodari L., Rossi S., Bobbo S., Fabrizio M.** NIR trasmittance tuneability under magnetic field of colloidal suspensions of Goethite (α-FeOOH) nanorods. *Soft Matter.* 2017.

9. **Luigi Torre.** Materiali convertitori di lunghezza d'onda per applicazioni fotovoltaiche. *Tesi di laurea magistrale in fisica. Università di Firenze.* 2013.

10. **Behar, et al.** A review of studies on central receiver solar thermal power plants. *Renewable Sustainable Energy Reviews.* 2013, Vols. 23, 12-39.

11. **C.E.Kennedy.** *Review of Mid- to High-Temperature Solar Selective Absorber Materials.* 2002. NREL/TP-520-31267.

12. **W.F Bogaerts, C.M. Lampert.** Review, Materials for photothermal solar energy conversion. *J. Mat. Sci.* 1983, Vol. 18, 2847-2875.

13. **S. A. Kalogirou.** Solar thermal collectors and applications. *Prog. Energy Combust. Sci.* 2004, Vols. 30, 231.

14. **T. Fend, R. Pitz-Paal, O. Reutter, J. Bauer, B. Hoffschmidt,.** Two novel high-porosity materials as volumetric receivers for concentrated solar radiation. *Sol. Energy Mater. Sol. Cells.* 2004, Vols. 84, 291.

15. **E. Wuchina, E. Opila, M. Opeka, W. Fahrenholtz, I. Talmy,.** UHTCs: Ultra-High Temperature Ceramic Materials for Extreme Environment Applications. *The Electrochemical Society Interface.* Winter 2007.

16. **E. Sani, L.Mercatelli, J.-L.Sans, L.Silvestroni, D.Sciti,.** Porous and dense hafnium and zirconium ultra-high temperature ceramics for solar receivers. *Optical Materials.* 2013, Vol. 36, 163-168.

17. **D. Sciti, L.Silvestroni, L.Mercatelli, J.-L.Sans, E.Sani.** Suitability of ultra-refractory ceramics as absorbers for solar energy applications. *Solar Energy Materials and Solar Cells.* 2013, Vol. 109, 8-16.

18. **Elisa Sani, Luca Mercatelli, Paola Sansoni, Laura Silvestroni, Diletta Sciti.** Spectrally selective ultra-high temperature ceramic absorbers for high-temperature solar plants. *J. Renew. Sustain. Energy.* 2012, Vol. 4, 033104, pp. vol. 4, 033104.

19. **Karl E. Spear, Steve Visco, Eric J. Wuchina, and Eric D. Wachsman,.** High Temperature Materials. *The Electrochemical Society Interface.* Spring 2006.

20. **S. Basu et al.** Microscale radiation in thermophotovoltaic devices-A review. *Int. J. Energy Res.* 2007, Vol. 31, 689–716.

21. **M. Garin et al.** Three-dimensional metallo-dielectric selective thermal emitters with high-temperature stability for thermophotovoltaic applications. *Solar Energy Materials & Solar Cells.* 2015, Vol. 134, 22–28.

22. **Bitnar et al.** Characterisation of rare earth selective emitters for thermophotovoltaic applications. *Solar Energy Materials & Solar Cells.* 2002, Vol. 73, 221–234.

23. **G. Torsello et al.** The origin of highly efficient selective emission in rare-earth oxides for thermophotovoltaic applications. *Nature Materials.* 2004, Vol. 3, 632-637.

24. **Ormerod, R. Mark,.** Solid oxide fuel cells. *Chem. Soc. Rev.* 2003, Vol. 32, 17-28 DOI: 10.1039/B105764M.

25. **S. Brunold, U. Frei, B. Carlsson, K. Möller, M. Köhl,.** Accelerated life testing of solar absorber coatings: testing procedure and results. *Solar Energy.* 2000, Vol. 68, 4, 313.

26. **C.M. Lampert.** Advanced optical materials for energy efficiency and solar conversion. *Sol. Wind Techn.* 1987, Vol. 4, 347.

27. **Avila-Marin, Antonio L.,.** Volumetric receivers in Solar Thermal Power Plants with Central Receiver System technology: A review. *Solar Energy.* 2011, Vol. 85, 891-910.

28. **Chaza, Manfred BiShmer and Crisfina.** The ceramic foil volumetric receiver. *Solar Energy Materials.* 1991, Vol. 24, 182-191.

29. **Pits-Paal, Robert, Morhenne, Joachim, Fiebig, Martin,.** A new concept of selective solar receiver for high temperature applications. *Solar Energy Materials.* 1991, Vol. 24, 293-306.

30. **Chaza, James M. Chavez and Cristina,.** Testing of a porous ceramic absorber for a volumetric air receiver. *Solar Energy Materials.* 1991, Vol. 24, 172-181.

31. **A. Kribus, J. Karni, R. Rubin, P. Doron.** The "Porcupine": A Novel High-Flux Absorber For Volumetric Solar Receivers. *J. Solar Energy Engineering.* 1998, Vol. 120, 85-95.

32. **Thomas Fend.** High porosity materials as volumetric receivers for solar energetics. *Optica Applicata.* 2010, Vol. XL, 2.

33. *Solar Energy Materials.* **Granqvist, Claes G.** 21, s.l. : Advanced Materials, 2003, Vol. 15.

34. **E. Sani, L. Mercatelli, F. Francini, J.-L. Sans, D. Sciti,.** Ultra-refractory ceramics for high-temperature solar absorbers. *Scripta Materialia.* 2011, Vol. 65 , 775–778.

35. **G.A. Greene et al.** Total hemispherical emissivity of oxidized Inconel 718 in the temperature range 300–1000°C. *Exp. Therm. Fluid Sci.* 2000, 22145–53.

36. **Hiromichi Watanabe and Tsuyoshi Matsumoto.** New analysis for determination of hemispherical total emissivity by feedback-controlled pulse-heating technique. *Rev. Sci. Instrum.* 2005, 76043904.

37. **Tairan Fu et al.** A steady-state measurement system for total hemispherical emissivity. *Measurement Science & Technology.* 2012, Vol. 23, 025006.

38. **Tairan Fu, Peng Tan,.** Transient Calorimetric Measurement Method for Total Hemispherical Emissivity. *J. Heat Transfer* . 2012, Vol. 134 (11), 111601.

39. **K. Fukuzawa et al.** Total hemispherical emittance of polyimide films for space use in the temperature range from 173 to 700 K. *Int. J. Thermophys.* 2002, 23319–31.

40. **D. Lei, Q. Li, Z. Wang, J. Li, J. Li,.** An experimental study of thermal characterization of parabolic trough receivers. *Energy Conversion and Management.* 2013, Vol. 69, 107–115.

41. **J. R. Markham, P. R. Solomon, and P. E. Best,.** An FTIR based instrument for measuring spectral emittance of material at high Temperature. *Rev. Sci. Instrum.* 1990, Vol. 61 (12).

42. **J. J. P. Elich and J. A. Wieringa.** Temperature Effects Influencing the Spectral and Total Emissivity of Refractories. *Exp. Therm. Fluid Sci.* 1995, Vol. 10, 318.

43. **G. Neuer and G. Jaroma-Weiland.** Spectral and Total Emissivity of High-Temperature Materials. *International Journal of Thermophysics.* 1998, Vol. 19, No. 3.

44. **A. Adibekyan, C. Monte, M. Kehrt, B. Gutschwager and J. Hollandt,.** Emissivity Measurement Under Vacuum from 4µm to 100µm and from −40 °C to 450 °C at PTB. *Int J Thermophys.* 2014, (DOI 10.1007/s10765-014-1745-7).

45. **J. Manara, M. Arduini-Schuster, M. Keller,.** Infrared-optical characteristics of ceramics at elevated temperatures. *Infrared Physics & Technology.* 2011, Vol. 54, 395–402.

46. **O. Rozenbaum, D. De Sousa Meneses et al.,.** A spectroscopic method to measure the spectral emissivity of semi-transparent materials up to high temperature. *Review of scientific instruments.* 1999, Vol. 70, 10.

47. **L. del Campo et al.** New experimental device for infrared spectral directional emissivity measurements in a controlled environment. *Rev. Sci. Instrum.* 2006, Vol. 77 , 113111.

48. **Mark J. Ballico and Trebor P. Jones.** Novel Experimental Technique for Measuring High-Temperature Spectral Emissivities. *Applied Spectroscopy.* 1995, Vols. 49, Issue 3, pp. 335-340.

49. **L. del Campo, et al.,.** New experimental device for infrared spectral directional emissivity measurements in a controlled enviroment. *Rev. Sci. Instrum.* 2006, Vol. 77, 113111.

50. **C. Monte et al.,.** The determination of the uncertainties of spectral emissivity measurements in air at the PTB. *Metrologia.* 2010, Vol. 47, S172–S181.

51. **Tairan Fu et al.,.** Measurements of the directional spectral emissivity based on a radiation heating source with alternating spectral distributions. *International Journal of Heat and Mass Transfer.* 2015, Vol. 90, 1207-1213.

52. **Ryer Alex.** Light Measurement Handbook. *International Light Inc.* 1998, ISBN 0-9658356-9-3.

53. **P. Hervé,.** Mesure de l'émissivité thermique. *Techniques de l'Ingénieur, traité Mesures et Contrôle.* 2005.

54. **P. Masclet.** Mesure de l'émissivité et de l'indice complexe des solides et des liquides dans l'infrarouge. *Thèse de docteur-ingénieur, Université Paris VI.* 1982.

55. **A. Brunotte, M. Lazarov, and R. Sizmann,.** "Calorimetric measurements of the total hemispherical emittance of selective surfaces at high temperatures,". *SPIE.* (1992), Vol. 1727, 149.

56. **Kraabel, Shiffmann, Gravisse,.** On the validity of Kirchhoff's law. *Laboratoire de Physique et du Rayonnement de la Lumière.*

57. **Wackelgard Ewa.** Characterization of black nickel solar absorber coatings electroplated. *Solar Energy Materials and Solar Cells.* 1998, Vol. 56, 35-44.

58. **Glen Mc Donald.** Spectral reflectance properties of black chrome for use as a solar selective coating. *Solar Energy.* 1975, Vol. 17, 119-122.

59. **PIKE.** Mid-IR IntegratIR™ – Integrating Sphere. [Online] http://www.piketech.com/files/pdfs/MidIRPDS611.pdf.

60. **CIE Commission Internationale de l'Eclairage.** Solar Spectral Irradiance. *Technical Report No.85.* 1989.

61. **D. Hernandez, J.L. Sans, M. Pfander,.** Pyroreflectometry to Determine the True Temperature and Optical Proprieties of Surfaces. *Journal of Solar Energy Engineering.* August 2008, Vol. 130, 031003-1.

62. **D. Hernandez, A. Netchaieff, A. Stein,.** True temperature measurement on metallic surfaces using a two color pyroreflectometer method. © *American Institute of Physics.* 2009.

63. **Ronald Loehman, Erica Corral, Hans Peter Dumm, Paul Kotula, and Raj Tandon,.** *Ultra High Temperature Ceramics for Hypersonic Vehicle Applications.* s.l. : Sandia National Laboratories Albuquerque, New Mexico 87185 and Livermore, California 94550, 2006.

64. **J.F. Justin, A. Jankowiak,.** Ultra High Temperature Ceramics: Densification, Properties and Thermal Stability. *Journal AerospaceLab.* November 2011, Vols. 3, AL03-08.

65. **T.H.Squire, J. Marschall,.** Material property requirements for analysis and design of UHTC components in hypersonic applications. *J. Eur. Ceram. Soc.* 2010, Vol. 30, 2239-2251.

66. **Raffaele Savino, Mario De Stefano Fumo, Diego Paterna, Michelangelo Serpico,.** Aerothermodynamic study of UHTC-based thermal protection systems. *Aerospace Science and Technology* . 2005 , Vol. 9, 151–160.

67. **Cotton John.** Ultra High Temperaure Ceramics. *ADVANCED MATERIALS & PROCESSES.* JUNE 2010.

68. **A.G. Konstandopoulos, E. Papaioannou, D. Zarvalis, S. Skopa, P.Baltzopoulou, E. Kladopoulou, M. Kostoglou, S. Lorentzou,.** Catalytic Filter Systems with Direct and Indirect Soot Oxidation Activity. *SAE Technical Paper.* 2005-01-0670, 2005.

69. **W.E.Lee, M.Gilbert, S.T.Murphy, R.W.Grimes,.** Opportunities for advanced ceramics and composites in the nuclear sector. *J. Am. Ceram. Soc.* . 2013, Vol. 96, 2005-2030.

70. **W.E., Lee and W.M., Rainforth,.** *Ceramic Microstructure - Propriety control by processing.* London : Chapman & Hall, 1994.

71. **J. Subrahmanyan, M. Visayakumar,.** Review: self-propagating high-temperature synthesis. *J. Mat. Sci.* 1992, Vol. 27, p. 6249-6273.

72. **Nikzad L., Orrù R., Licheri R., Cao G.,.** Influence of Mechanical and Electric Current Activation on the Mechanism of Formation and the Properties of Bulk B4C-TiB2 Composites Obtained by Reactive Sintering. *Chemical Engineering Transactions.* 2013, Vol. 32, 1669-1674, DOI:10.3303/CET1332279.

73. **D. Sciti, L. Silvestroni, J.L. Sans, L. Mercatelli, M. Meucci, E. Sani,.** Tantalum diboride-based ceramics for bulk solar absorbers. *Solar Energy Materials and Solar Cells.* 2014, Vol. 130, 208-216.

74. **Thomas Fend, Bernhard Hoffschmidt, Robert Pitz-Paal, Oliver Reutter, Peter Rietbrock,.** Porous materials as open volumetric solar receivers: Experimental determination of thermophysical and heat transfer properties. *Energy.* 2004, Vols. 29, Issues 5–6, 823-833.

75. **Christos C. Agrafiotis, Ilias Mavroidis, Athanasios G. Konstandopoulos, Bernard Hoffschmidt, Per Stobbe, Manuel Romero, Valerio Fernandez-Quero.** Evaluation of porous silicon carbide monolithic honeycombs as volumetric receivers/collectors of concentrated solar radiation. *Solar Energy Materials and Solar Cells.* 2007, Vols. 91, Issue 6, 474-488.

76. **D. Sciti, L. Silvestroni, D.M. Trucchi, E. Cappelli, S. Orlando, E. Sani,.** Femtosecond laser treatments to tailor the optical properties of hafnium carbide for solar applications . *Solar Energy Materials & Solar Cells.* 2015, Vol. 132, 460-466.

77. **K.Krnel, D. Sciti, E. Landi, A. Bellosi,.** Surface modification and oxidation kinetics of hot pressed AlN-SiC-MoSi2 electroconductive ceramic composite. *Applied Surface Science.* 2003, Vol. 210, 274-285.

78. **Alessandro Bellucci, Paolo Calvani, Emilia Cappelli, Stefano Orlando, Diletta Sciti, Ronen Yogev, Abraham Kribus, Daniele M. Trucchi,.** Preliminary characterization of STTG: Solar Thermionic-Thermoelectric Generator for concentrating systems. *Conference: NANOFORUM September 2014, At Rome, Volume: AIP Conf. Proc. 1667.* DOI: 10.1063/1.4922563.

79. **Sciti, D., Silvestroni, L., Guicciardi, S., Dalle Fabbriche, D., Bellosi, A.,.** Processing, mechanical properties and oxidation behavior of TaC and HfC composites containing 15 vol% TaSi2 or MoSi2. *J. Mater. Res.* 2009, Vol. 25 (6), 2056-2065.

80. **Silvestroni L., Sciti D.,.** Sintering behavior, microstructure, and mechanical properties: a comparison among pressureless sintered ultra-refractory carbides. *Advanced in Materials Science and Engineering.* 2010, article ID 835018.

81. **Elisa Sani, Luca Mercatelli, Marco Meucci, Laura Silvestroni, Andrea Balbo, Diletta Sciti,.** Process and composition dependence of optical properties of zirconium, hafnium and tantalum borides for solar receiver applications. *Solar Energy Materials & Solar Cells.* 2016, Vol. 155, 368-377.

82. **Bohren C.F., Huffman D.R.,.** Absorption and Scattering of Light by Small Particles. Wiley, NewYork, p. 243, 1983 , DOI: 10.1002/9783527618156 .

83. **Elisa Sani, Luca Mercatelli, Marco Meucci, Andrea Balbo, Laura Silvestroni, Diletta Sciti.** Compositional dependence of optical properties of zirconium, hafnium and tantalum carbides for solar absorber applications. *Solar Energy.* 2016, Vol. 131, 199-207.

84. **Modine A., Haywood T.W., Allison C.Y.,.** Optical and electrical properties of single-crystalline zirconium carbide. *Phys. Rev. B.* 1985, Vol. 32, 7743–7747.

85. **Delin A., Eriksson O., Ahuja R., Johansson B., Brooks M.S.S., Gasche T., Auluck S., Wills J.M.,.** Optical properties of the group-IVB refractory metal compounds. *Phys. Rev. B.* 1996, Vol. 54, 1673–1681.

86. **Sani E., Mercatelli L., Jafrancesco D., Sans J.-L., Sciti D.,.** Ultra-high temperature ceramics for solar receivers: spectral and high temperature emittance characterization. *J. Eur. Opt. Soc.: Rapid Pub.* 2012, Vol. 7, 12052.

87. **Branz H.M., Yost V.E., Ward S., Jones K.M., To B., Stradins P.,.** Nanostructured black silicon and the optical reflectance of graded-density surfaces. *Appl. Phys. Lett. 94, 231121.* 2009.

88. **Elisa Sani, Luca Mercatelli, Marco Meucci, Andrea Balbo, Clara Musa, Roberta Licheri, Roberto Orrù, Giacomo Cao.** Optical properties of dense zirconium and tantalum diborides for solar thermal absorbers. *Renewable Energy.* 2016, Vol. 91, 340-346.

89. **Clara Musa, Roberta Licheri, Roberto Orrù, Giacomo Cao, Diletta Sciti, Laura Silvestroni, Luca Zoli, Andrea Balbo, Luca Mercatelli, Marco Meucci and Elisa Sani,.** Processing, Mechanical and Optical Properties of Additive-Free ZrC Ceramics Prepared by Spark Plasma Sintering. *Materials.* 2016, Vol. 9, 489; doi:10.3390/ma9060489.

90. **Luca Mercatelli, Marco Meucci, Elisa Sani,.** Facility for assessing spectral normal emittance of solid materials at high temperature. *Applied Optics.* 2015, Vol. 54, 29.

91. **E. Sani, L. Mercatelli, D. Fontani, J.-L. Sans, D. Sciti,.** Hafnium and tantalum carbides for high temperature solar receivers. *J. Renewable Sustainable Energy.* 2011, Vol. 3, 063107 doi: 10.1063/1.3662099.

92. **P. T. B. Shaffer,.** Development of ultra refractory materials. *Progress Report No. 25, Carborundum Co., Niagara Falls, New York, 1 May-31 July 1961.* 16 August 1961, (Contract NOrd-17175) ASTIA AD-261 471.

93. **G. M. Kibler, T. F. Lyon, M. J. Linevski, and V. J. Desantis,.** Carbonization of plastics and refractory material research. *Technical Report No. WADD-TR-60-646 Part III.* 1964, Vol. 2.

94. **G. M. Kibler, T. F. Lyon, M. J. Linevski, and V. J. Desantis,.** Refractory material research. *Technical Report No. WADD-TR-60-646 Part IV*. 1964.

95. **Pratesi Stefano.** Sviluppo di un coating per assorbitore solare con tecnologie low cost. *PhD thesis, University of Florence*. 2014.